Magnetic tweezers to investigate the role of mechanics during collective cell migration

Dissertation
zur Erlangung des Grades
der Doktorin der Naturwissenschaften
der Naturwissenschaftlich-Technischen Fakultät II
- Physik und Mechatronik -
der Universität des Saarlandes

von

Ulrike Schulze

Saarbrücken

2014

Tag des Kolloquiums: 10.02.2015
Dekan: Univ.-Prof. Dr. Georg Frey

Mitglieder des Prüfungsausschusses:
Univ.-Prof. Dr. Albrecht Ott
Univ.-Prof. Dr. Karsten Kruse
Univ.-Prof. Dr. Karin Jacobs
Dr. Andreas Tschöpe

Zusammenfassung

Das Ziel dieser Doktorarbeit ist, Messungen mechanischer Eigenschaften an Zellen in vivo durchzuführen und die Rolle mechanischer Kräfte bei kollektiver Zellmigration zu erforschen. Aus diesm Grund war es noetig eine magnetischen Pinzette zur Nutzung in Zebrafischembryonen zu konstruieren. Das Seitenlinien Primordium (SLP) wurde als Modell für kollektive Zellmigration benutzt. Es besteht aus kollektiv migrierenden Zellen, welche ein Gewebe formen und eine charakteristische Zellorganisation aufweisen: die Spitze des SLP besteht aus Mesenchymzellen, während Epihelzellen im Rückteil des SLP Zellcluster bilden.

Frühere Versuche haben gezeigt, dass interzelluläre Kräfte für Zell-Zell Kommunikation von kollektiv migrierenden Zellen eine wichtige Rolle spielen. Für die Migration des SLP ist zusätzlich die Präsenz verschiedener Zelltypen notwendig. Aus diesem Grund wollten wir mechanische Kräfte auf das SLP übertragen und die Reaktion der Zellen observieren. Außerdem wollten wir messen, ob die zelluläre Organisation des SLP mit Änderungen der Materialeigenschaften der Zellen korreliert. In vitro Experimente haben gezeigt dass diese Eigenschaften bei verschiedenen Zelltypen teilweise dramatisch variieren. Es ist jedoch nicht bekannt, ob dies auch auf Zellen in Embryos zutrifft. Unsere Messungen ergaben die Existenz von Gradienten der viskoelastischen Parameter entlang der Gewebeachse, welche Einfluss auf die Koordination von Zellmigration durch mechanische Signale haben könnte.

Abstract

The aim of this thesis was to measure mechanical properties of cells in vivo and to investigate the role of mechanical forces during collective cell migration in developing zebrafish embryos by use of a magnetic tweezer set-up. The lateral line primordium (LLP) was used as a model for studying collective cell migration. The LLP consists of a group of collectively migrating cells, forming a tissue that has a characteristic cell organization: a mesenchymal-like leading region at the tip of the tissue and epithelial cell clusters at the rear.

Previous experiments have shown that intercellular forces may play a key role in cell-cell coordination within the migrating collective. Furthermore, internal tissue organization into different cell types appears to be necessary for cell migration of the LLP. For these reasons we used our magnetic tweezer to apply defined mechanical forces on the LLP and captured the reaction of the migrating tissue. Additionally, we asked whether the distinct cellular organization of the LLP correlated with a change in material properties of the cells, a general important question that has not yet been addressed in vivo. We found a pronounced gradient in several viscoelastic parameters along the axis of the LLP. Furthermore, we could link this graded change in material properties to a key cell signaling molecule, FGF. Our finding is likely to have an impact on the coordination of collective cell migration by mechanical signals.

Contents

1. Motivation **11**

I. Construction of a magnetic tweezer set-up for use in a zebrafish embryo **13**

2. Introduction **15**
2.1. Use of Magnetic Tweezers to probe biological systems 15
2.2. Magnetic tweezer construction 16
2.2.1. General Considerations 16
2.2.2. Physics of Magnetic Tweezers 16

3. Results **23**
3.1. General considerations 23
3.2. Magnetic beads 24
3.2.1. Choice of Magnetic beads 24
3.2.2. Fluorescent Labeling of magnetic beads 25
3.2.3. Delivery of magnetic beads 27
3.3. Magnetic Tweezer Set-up 32
3.3.1. The Mu-metal core 32
3.3.2. Cooling unit 32
3.3.3. Coils of the solenoid 33
3.4. Experimental set-up 35
3.4.1. Force calibration 35
3.4.2. Accessing migrating tissue with magnetic tweezer 37
3.5. Effect of magnetic beads and magnetic fields on the migration and differentiation of cells 38
3.5.1. The presence of magnetic beads has no impact on the migration and organisation of cells in early embryos 38

3.5.2. Primordia containing beads migrate at the same speed as wildtype primordia . . . 39
3.5.3. Beads do not influence primordial cell organisation . . . 39
3.5.4. Primordia migrate and differentiate normally in a magnetic field . 41

4. Summary and Discussion **43**

II. Forces and material properties in collective cell migration **49**

5. Introduction **51**
5.1. Cell migration . . . 51
5.1.1. Single cell migration . . . 51
5.1.2. Collective cell migration . . . 51
5.2. Forces in collective cell migration . . . 53
5.3. The actin cortex and its regulation . . . 55
5.4. Viscoelasticity . . . 57
5.4.1. Elasticity . . . 57
5.4.2. Viscoelasticity . . . 57
5.4.3. Constitutive models for linear viscoelastic behavior . . . 60
5.4.4. Viscoelastic measurements as a read-out for the state of the actin cell cortex . . . 64
5.5. The zebrafish lateral line primordium as a model to investigate collective cell migration . . . 65
5.5.1. Regulation of collective cell migration via cell-cell signaling . . . 65
5.5.2. Regulation of collective cell migration via mechanical signals . . . 67

6. Results - Force application on migrating tissues **71**
6.1. Forces between 400 pN and 1 nN are high enough to displace magnetic beads inside cells and to visibly deform cells . . . 71
6.2. Forces between 800 pN and 1.5 nN can pull beads out of the primordium 72
6.3. Application of forces on the lateral line primordium . . . 73
6.3.1. Application of force on cells in wildtype primordia . . . 73
6.3.2. Application of force on cells in wildtype primordia labeled with Lifeact-GFP . . . 74
6.4. Application of forces on cells in sdf-/- primordia . . . 74

7. Results - Development of a method to measure viscoelastic properties in embryos **77**
7.1. Method development . . . 77
7.1.1. Data collection . . . 77
7.1.2. Segmentation and displacement curves . . . 79
7.1.3. Comparison of different track shapes . . . 80
7.1.4. Fitting of the model and parameter extraction . . . 81
7.2. Experimental limitations . . . 84
7.2.1. Migration of the tissue during measurement . . . 84
7.2.2. Errors due to movement of the bead in z-axis . . . 85
7.3. Control measurements . . . 85
7.3.1. Repeated force application of the same cell . . . 85
7.3.2. Linear Elastic Control . . . 88
7.3.3. Blebbistatin . . . 88

8. Results - Viscoelastic measurements on a migrating tissue **91**
8.1. Probing differences in material properties across the lateral line primordium 91
8.1.1. Measurement of spatial changes in the viscosity in the lateral line primordium . . . 92
8.1.2. Measurement of spatial changes in the relaxation times in the lateral line primordium . . . 93
8.1.3. Measurement of spatial changes in the elasticity in the lateral line primordium . . . 93
8.2. Effect of cell-type differentiation on material properties . . . 99
8.2.1. Binning . . . 99
8.2.2. Viscosity . . . 100
8.2.3. Relaxation time . . . 100
8.2.4. Elasticity . . . 101
8.2.5. Conclusion . . . 103

9. Summary and Discussion **105**
9.1. Applying force on a tissue migrating in vivo . . . 105
9.2. Viscoelastic Measurements on the lateral line primordium . . . 107
9.2.1. Comparison with other viscoelastic measurement methods . . . 107
9.2.2. Control measurements . . . 108
9.2.3. Measurement of spatial changes in the viscosity in the lateral line primordium . . . 110

9.2.4. Epithelial differentiation changes the viscoelastic properties of cells in vivo . . . 113
9.2.5. Conclusions . . . 114

10. Materials and Methods **119**
10.1. Fish handling and embryo preparation . . . 119
10.2. Bead preparation . . . 119
10.3. Force Calibration . . . 120
10.4. Bead delivery . . . 121
10.5. External force application on migrating lateral line primordium . . . 122
10.6. Speed measurements of primordia containing beads . . . 122
10.7. Tracking cells and beads in early embryos . . . 123
10.8. Viscoelastic Measurements . . . 124
10.9. Drug treatments . . . 125

11. Appendix **127**
11.1. Statistics Definitions . . . 127
11.1.1. Mean, Standard deviation and Standard error of the mean . . . 127
11.1.2. Student's t-test, two-tailed, unequal variances . . . 128
11.1.3. Mann-Whitney U-test . . . 128
11.1.4. Pearson's correlation . . . 129
11.2. Results of viscoelasticity measurements of the untreated lateral line primordium . . . 130
11.3. Results of viscoelasticity measurements of the lateral line primordium treated with Blebbistatin . . . 132
11.4. Results of viscoelasticity measurements of the lateral line primordium treated with SU5402 . . . 133

1. Motivation

The aim of this work was to measure mechanical properties of cells *in vivo* and investigate the role of mechanical forces during collective cell migration. For this, a magnetic tweezer set-up for use in developing zebrafish embryos had to be constructed. The lateral line primordium was used as a model for studying collective cell migration *in vivo*. It is a group of collectively migrating cells whose function is to deposit a series of mechanosensory hair cell organs that allow detection of pressure changes in the surrounding water. This migrating primordium has a characteristic polarized cell organization, with a mesenchyme-like leading region and epithelial cell clusters, the progenitors of the mechanosensory organs, at the rear. It migrates directly under a very thin layer of skin cells, which means that it can be easily penetrated with small molecules for drug treatment. This position of the primordium also allows accessibility for mechanical manipulation and for the penetration of magnetic fields.

The direct application of defined forces to the migrating primordium would allow experimental investigation of the role of mechanics in two key aspects of this important biological process. Previous experiments had suggested that intercellular forces might be relevant for the cell- cell coordination of collectively migrating cells, however there was no direct evidence (See also Ch. 5.5 and 5.2). For this reason, we were interested in applying mechanical forces to the lateral line primordium to observe the reaction of the collectively migrating cells. Furthermore, the internal organization of the tissue into different cell types appears to be necessary for collective cell migration (This is further discussed in Ch. 5.5.2). Therefore, we wanted to measure if the distinct cellular organization of the primordium correlated with a change in material properties of the cells. It has been shown *in vitro* that different cell types can differ dramatically in their physical properties, such as surface tension or viscoelastic behavior of the cell cortex. These measurements are typically done *ex vivo* in a petri dish. Our goal was to measure physical properties directly in the embryo to learn whether the *in vitro* experiments reflect the *in vivo* scenario.

Magnetic tweezer set-ups consist of a magnetic probe (magnetic bead) on which forces can be applied via a magnetic field produced by an electromagnet or a permanent magnet. This kind of set-up was selected as the most appropriate method to apply forces to the primordium. However, several technical challenges had to be overcome, and several factors had to be accounted for before the set-up could be used. Among the questions that had to be answered before the first experiments could be performed were the choice of beads, which had to be carefully selected to prevent toxicity to the developing embryo. One major challenge was to develop methods to specifically apply beads to the migrating primordium, a group of a hundred cells within an embryo comprising of many thousands, without labeling surrounding tissues. Additionally, the influence of strong magnetic fields on the developing embryo had to be assessed. The magnitude of the forces required to deform cells in an embryo was not known previously and had to be empirically determined.

These challenges are addressed in part I of this thesis, which describes the construction of a magnetic tweezer set-up for use in a zebrafish embryo. Part II describes the application of forces onto the migrating lateral line primordium and the development of a method to measure its viscoelastic properties. Finally, I will discuss the results of these experiments.

Part I.

Construction of a magnetic tweezer set-up for use in a zebrafish embryo

2. Introduction

2.1. Use of Magnetic Tweezers to probe biological systems

Since magnetic tweezers are very versatile, they have been adapted to be used for many different applications in biology. They have been used to apply forces to single molecules, cell organelles, tissues and even whole embryos [1]. These force application experiments have not only been used to investigate the reaction of biological materials to an external force qualitatively, but also to measure mechanical properties to obtain a quantitative description of the material.

Magnetic tweezers were first used by Crick [2] in 1950 to drag and twist small magnetic particles around the cytoplasm of a cell with the aim of physically describing the cytoplasm. In 1992, magnetic tweezers were used for experiments on individual DNA molecules, which were tethered to a magnetic particle on one end and a surface on another end. The application of very defined small forces in the piconewton (pN) range allowed measurement of the mechanical properties of the DNA molecules during twisting and stretching [3]. Subsequently, magnetic tweezers were used to study local viscoelastic properties of actin networks *in vitro* [4]. In recent times most of the experiments conducted with magnetic tweezers have been on single molecules, and only a few conducted on measuring viscoelastic parameters on cells.

In 2008 Desprat et al. first applied magnetic tweezer experiments to Drosophila embryos [5]. They showed that intercellular forces can regulate gene expression, by using magnetic tweezers to apply forces on cells during blastoderm stage in a developing Drosophila embryo. The applied forces resulted in a redistribution of non muscle myosin II in the germband layer and altered gene expression patterns later during the development. Until today, this remains the only published use of magnetic tweezers in embryos.

2.2. Magnetic tweezer construction

2.2.1. General Considerations

A set-up that applies forces on magnetic particles using an external magnetic field is generally known as magnetic tweezer. Magnetic fields can penetrate many materials, including biological materials. Applying a force via magnetic tweezers is non-invasive, however, the presence of the magnetic particle inside the cell or embryo might perturb the natural environment. A variety of magnetic tweezer set-ups have been constructed. They are generally composed of various electromagnets or permanent magnets mounted on an optical microscope. When considering the construction of a magnetic tweezer set-up, three performance parameters need to be considered [6]:

- Amplitude and direction of the force: Force amplitudes can vary from a few piconewtons [7] [8] to tens of nanonewtons [9] [10] . The first few magnetic tweezer set-ups constructed could only apply forces in a unidirectional way. In recent years, more and more systems with force feedback loops, which allow force application in multiple directions have been published [11] [12] [13].[14]

- Timescale over which the force needs to be maintained or modulated.

- The spatial range of the force profile: Forces can be applied in a spatial range from micrometers [14] to centimeters [15].

2.2.2. Physics of Magnetic Tweezers

A magnetic particle in a magnetic field will be attracted towards the source of the field. When constructing the tweezers, there are two main components to regulate the applied force: the profile of the external magnetic field and the magnetic properties of the particle [6].

Magnetic Field

Both permanent magnets [16] [17] and electromagnets [15] [13] have been used as sources of external magnetic fields. Permanent magnets can generate strong, static magnetic fields, which can only be modulated by physical displacement of the magnet. In contrast, electromagnets generate fields that are typically considerably weaker, but allow control of the field through an applied electric current. The simplest electromagnet consists of a conductive wire wound into several coils (solenoid). When electrons flow through the coil, they generate a magnetic field along the axis of the solenoid. The strength of the magnetic field at the edge of a cylindrical solenoid can be approximated by the following equation in the case of $l >> r$:

$$B = \frac{1}{2}\mu_0\mu_r\frac{N}{l}I, \tag{2.1}$$

where B is the magnetic flux density,
μ_r is the relative magnetic permeability (a material constant),
μ_0 is the universal magnetic constant,
N is the number of coils in the solenoid,
l the length of the cylindrical solenoid,
r the radius of the solenoid and
I the applied electric current.

If the central space inside the solenoid is empty, the relative magnetic permeability μ_r is approximately 1 (Vacuum: 1, Air: 1.00000037). A magnetic core made from a material with a higher μ_r can be added to the solenoid to amplify the magnetic field. Cores are typically ferromagnetic materials with high saturations. A large number of coils or high currents are needed to produce large fields. High electric currents will produce heat, which could potentially damage the sample. Typically, cooling systems are used to transport the heat away from the sample.

Magnetic Material Properties

Materials can be classified by their response to an external magnetic field. The response is quantified by the magnetic moment $\vec{m}$ of the material and the magnetic permeability μ_r, which is a measure of the penetrability of a material for magnetic fields. Materials

used in the construction of magnetic tweezers are generally ferromagnetic, paramagnetic or superparamagnetic.

- Paramagnetic materials are non-magnetic in the absence of an external magnetic field. In the presence of an external magnetic field a magnetic moment $\vec{m}$ is induced in the material and it exhibits magnetic behavior. The magnetic moment $\vec{m}$ is generally rather small and linear proportional to the field strength. In this case the magnetic permeability μ_r is greater than 1.

- Ferromagnetic materials magnetize in an external magnetic field and exhibit magnetic behavior even after the external field has been removed. The atoms of a ferromagnetic material have magnetic moments $\vec{m}$ which interact strongly with their neighbours (Fig. 2.1a). As a result of this interaction, an external magnetic field will produce a much larger field in a ferromagnetic material compared to paramagnetic material. The magnetic permeability μ_r is very high (much greater than 1, $\mu_r >> 1$).

- Ferrimagentic materials are very similar to ferromagnets. The magnetic moments of a ferrimagnetic material are also interacting with their adjacent moments. But, contrary to ferromagnets, these moments are oriented in an antiparallel manner, which reduces the net-magnetization (Fig. 2.1b).

- Superparamagnetism is a size-based phenomenon. Ferro- and ferrimagnetic material have a magnetization in absence of a magnetic field on the macro-scale, as described above. When these materials are broken into nanoparticles, the energy required to disturb the alignment of the atomic magnetic moments decreases. At this stage, ambient thermal energy is sufficient to randomize the direction of the magnetic moment. As a result, powders containing these particles appear non-magnetic in the absence of an external magnetic field.

  Just like paramagnetic materials, in the presence of an external magnetic field, superparamagnetic material exhibits magnetic behavior. Most magnetic beads used in magnetic tweezer applications are superparamagnetic, since they are made of ferrite nanoparticles embedded in a spherical latex matrix.

Ferromagnetic materials exhibit an additional property, called hysteresis. The magnetic moment of a ferromagnetic material does not only depend on the currently applied field,

(a) Ferromagnet (b) Ferrimagnet

Figure 2.1.: Exchange coupling for ferromagnets and ferrimagnets. Image modified from [18]

but also on the history of magnetization of the material. After the application of the external magnetic field, the magnetic moments align themselves with the field. After the field is removed, part of this alignment is retained. The retained magnetization is called remanence. To eliminate the remanence it is possible to apply heat or a magnetic field in the opposite direction of the retained magnetization. For this, a defined magnetic field (a coercive field) is necessary to demagnetize the material completely without inducing a remanence in the opposite direction. In practice, de-magnetization is often achieved by oscillating the external field between the positive and negative values necessary for saturation, and gradually dampening the amplitude of oscillations down to zero.

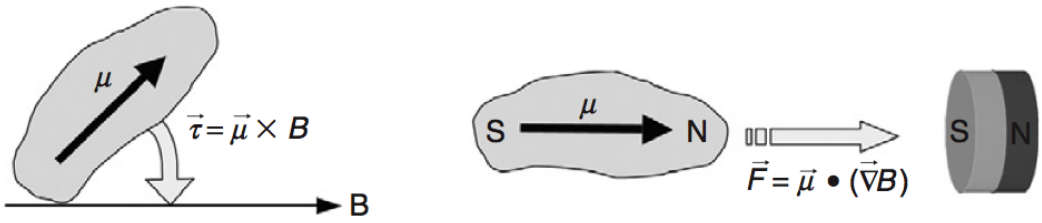

Figure 2.2.: behavior of nano particle in an external magnetic field [6]

An external magnetic field $\vec{B}$ has several effects on a magnetic particle with the magnetic moment $\vec{m}$ in that field [6]: A torque

$$\vec{\tau} = \vec{\mu_r} \times \vec{B}$$

rotates the particle to align the magnetic moment $\vec{m}$ to the external field (Fig. 2.2). Additionally, the particle experiences an force along the local field gradient

$$\vec{F} = (\vec{\mu_r} * \nabla)\vec{B}. \tag{2.2}$$

In other words, the particle is attracted towards regions of higher magnetic field (Fig. 2.2). It is important to note that the force exerted on the particle is proportional to the gradient of the field. Fields with steep gradients will result in high forces and smaller gradients result in lower forces.

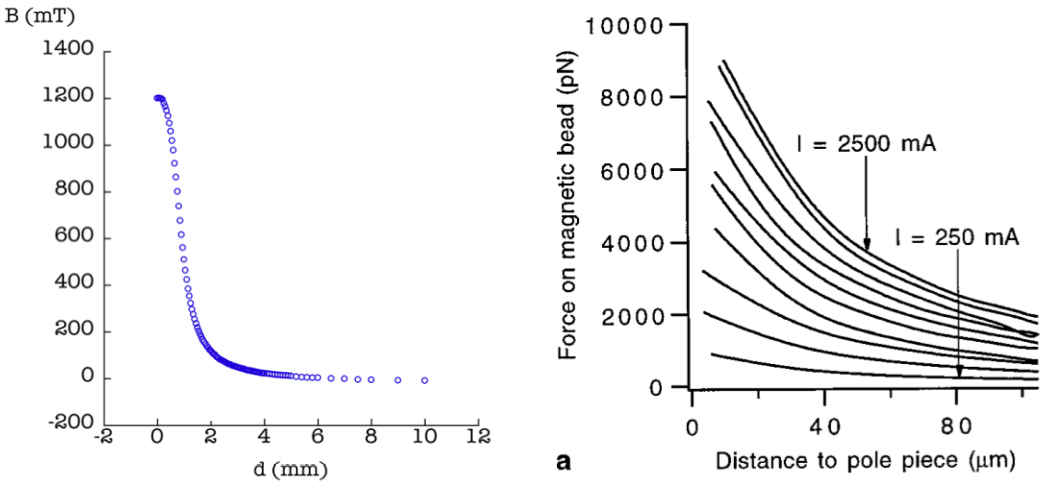

Figure 2.3.: Examples of force curves from the literature; left: Magnetic field as a function of the distance from the magnet for a set-up consisting of a permanent magnet [19]. The force applied by the magnetic field depends on the gradient of the field. ; right: Force applied on a magnetic bead (4.5 μm diameter) as a function of the distance from the electromagnet [9]. The force increases with increasing electric current.

The gradient profile of the field depends on the shape of the permanent magnet or the core of the electromagnet. A very sharp magnet will produce a field with a very steep gradient. This field would have a short range, because it would decline abruptly.

Beads for magnetic tweezer set-ups

The magnetic moment $\vec{m}$ of a superparamagnetic bead depends on the external magnetic field. For small external fields it is typically proportional to the field strength of the field. For high strength magnetic fields the magnetic moment saturates and reaches a

constant value. This value is independent from small variations in field strength. This value is called saturation magnetization M_{sat}. In that high range of magnetic fields, the magnetic moment of the bead can only be increased by adding more magnetic material thus increasing the volume V_{bead} of the bead.

For strong magnetic fields, equation (2.2) can be modified into

$$F = M_{sat} V_{bead} * \frac{dB}{dx}. \tag{2.3}$$

To achieve high forces, it is therefore beneficial to choose beads with a high saturation magnetization and with a large volume.
In summary, magnetic tweezer set-ups are very adaptable to a wide range of biological systems. When constructing magnetic tweezers the specific requirements in terms of the force applied, timescale of the biological process being investigated, and its spatial range has to be considered.

3. Results

3.1. General considerations

Magnetic tweezer set-ups are an appropriate method to apply forces to the primordium. However, several technical challenges had to be solved before the set-up could be used.

- Two major classes of magnetic tweezer set-ups have been used in the past; electromagnetic tweezers and magnetic tweezers constructed from permanent magnets. Permanent magnets made from rare earth metals generally produce stronger magnetic fields, but have the distinct disadvantage of being static. Therefore, after initial tests using permanent magnets, we chose to construct electromagnetic tweezers to be able to modulate the magnetic field.

- Since the magnitude of the force necessary to deform biological structures in embryos was unknown, we concentrated on developing a magnetic tweezer set-up that could apply as strong forces as possible, to ensure that sufficient force was applied on the tissue.

- The type of magnetic beads used had to be carefully chosen. On one hand, the material and bead size had to be chosen in a way that provided large enough forces. On the other hand, the beads had to be non-toxic for the cells of the embryo.

- Magnetic beads used in cell culture are typically not fluorescently labelled, since they can be easily observed using a simple brightfield microscope. However, embryos are more optically dense than single cells, which makes the tracking of beads inside embryos very difficult. Therefore, fluorescent magnetic beads had to be produced and tested for use in an embryo.

- In cell culture experiments, magnetic beads are usually coupled to the surface of cells biochemically, e. g. via transmembrane proteins and cell adhesion receptors. Due to spatial constraints, this was not possible in embryos. Therefore, a method to deliver magnetic beads to the interior of embryonic cells had to be developed.

- The presence of beads in cells should not have an influence on the function of cells in the tissue. In our case the focus is on the influence of forces on collective cell migration and the cellular organization of the lateral primordium. It therefore was essential that neither should not be disturbed by the magnetic beads in the absence of applied magnetic fields.

- As few studies have been reported on the influence of magnetic fields on biological tissues. Before applying forces on the lateral line primordium, we had to ensure that the applied magnetic fields alone did not change the collective migration behavior and cellular organization of the primordium.

- The shape and gradient of the electromagnetic field is determined by the shape of the magnet tip. To achieve high forces, the ideal magnetic field has a very steep field gradient over a very long distance. In reality, these fields tend to have either very steep field gradients that diminish fast or flat field gradients that last over a long distance. An optimum had to be found taking the local shape of the embryo into consideration.

- Electromagnets can produce considerable heat, which can damage the specimen and can lead to heat expansion of the electromagnet tip itself. Therefore, a cooling system had to be devised to avoid these effects.

The methods used to address these challenges are reported in the following chapters.

3.2. Magnetic beads

3.2.1. Choice of Magnetic beads

The appropriate choice of magnetic beads is an important factor for applying large enough forces during magnetic tweezer applications. The force depends critically on the volume

of the bead and the saturation magnetization of the material of which the bead is made of. Different types of magnetic beads are available commercially. We tested beads from three different suppliers: Chemicell, Bangs Laboratories and Invitrogen. The material commonly used in commercially available beads is magnetite (Fe_3O_4), a ferrimagnetic mineral. It is the most magnetic natural occurring mineral on earth. Beads from different sources contained different amounts of magnetic material. The beads produced by Bangs Laboratories, for example, only contain 10 % magnetite. The amount of magnetite in these beads was not high enough for generating the appropriate forces. For this reason beads with a higher amount of magnetic material and a high saturation susceptibility were needed. We chose to use Dynabeads, which showed the highest saturation susceptibility and the highest volume ($M_{sat} * V$) (Tab. 3.1). Dynabeads had the additional advantage of being very uniform in size (Fig. 3.1a). Since the applied force is proportional to the volume of the spherical bead, the following proportionality holds true:

$$F(x) = M_{sat} * V_{bead} * \frac{dB}{dx} \tag{3.1}$$

$$F \sim M_{sat} * V_{bead} * \frac{dB}{dx} \tag{3.2}$$

$$F \sim V_{bead} \sim r_{bead}^3 \tag{3.3}$$

Since the force is proportional to the cube of the radius of the bead, small variations in bead radius lead to large variations in force. We chose the largest bead diameter (2.8 μm) that would still be tolerated by embryonic cells. The magnetization of the bead is a measure for the response of the magnetic material to an external magnetic field. For high field intensities the magnetization reaches a saturated value, called the saturation magnetization (Fig. 3.1b).

3.2.2. Fluorescent Labeling of magnetic beads

To visualize the beads *in vivo*, it was necessary to label the beads fluorescently. Brightfield or differential interference contrast (DIC) imaging is not sufficient to reliably track the beads in the embryo. Bangs Laboratories produces polysterene beads, which are filled with a fluorescent dye and a magnetite core. While these beads are very bright, the small amount of magnetic material is a disadvantage for the production of high forces. We therefore coupled Dynabeads to a fluorophore via streptavidin- biotin binding.

Producer	**Diameter in μm**	**Material**	**Saturation Magnetization Msat**	**Msat*V in Am^2**	**Suszeptibility χ**
Chemicell Beads	1	Maghemite	3.7mT =2.9kA/m	1.5E-15	1.3
Bangs Lab - green	2.9	Magnetite 10%	45 kA/m	5.7E-14	2.5
Bangs Lab - far red	2.6	Magnetite 10%	45 kA/m	4.1E-14	2.5
Dynabeads	2.8	Magnetite	15 kA/m	5.6E-13	

Table 3.1.: Comparison of different beads from different manufacturers, source: Manufacturers

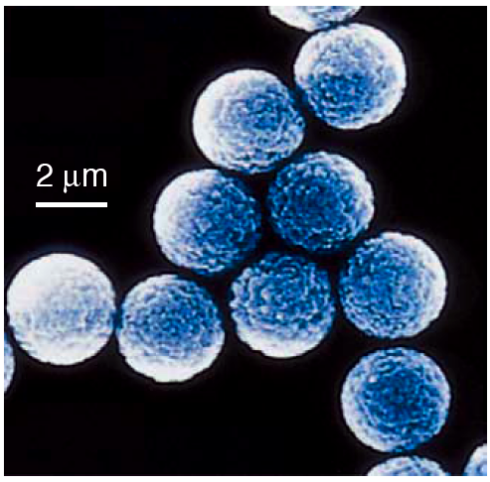

(a) scanning electron microscope (SEM) images of magnetic microspheres showing uniform size and shape: 2.8 μm M280 Dynabeads [20]

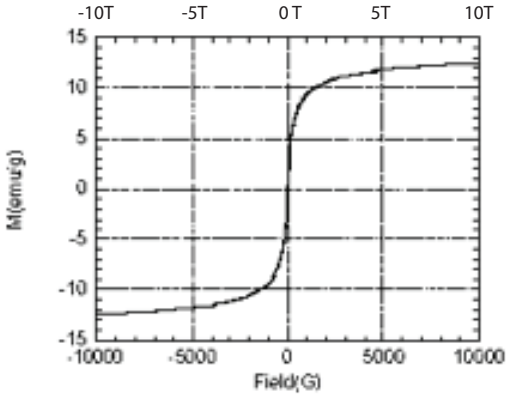

(b) Magnetization curve for Dynabeads M270. source: Invitrogen

Figure 3.1.

Fluorophores with a wide range of colors are available. We used "Atto 565" and "Atto 610" (purchased from atto-tec), which emit in the red and far-red region of the visible spectrum, respectively (Fig. 3.2). We chose not to use fluorophores in the lower range of the spectrum, to avoid exposing embryonic cells to large quantities of ultraviolet (UV) light. As a result of this labeling each magnetic bead is very bright and easily detectible under the fluorescence microscope.

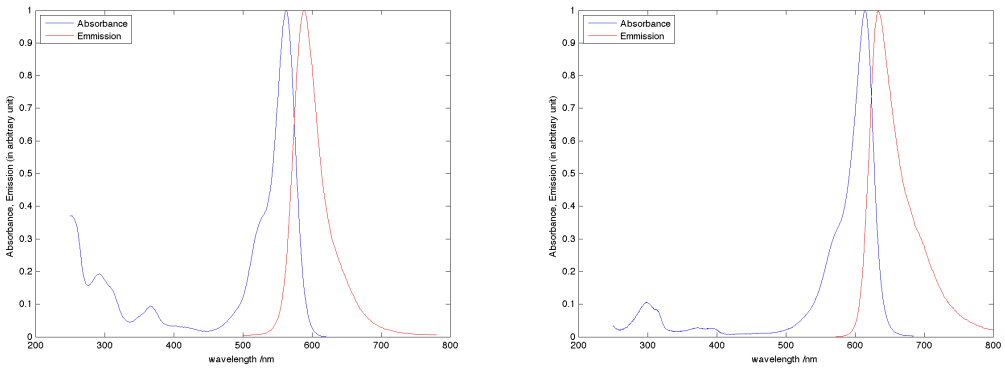

(a) Atto 565 (b) Atto 610

Figure 3.2.: Emission/absorption spectra for the fluorophores Atto 565 and Atto 610 (data from atto-tec).

3.2.3. Delivery of magnetic beads

At 24 hours post fertilization (hpf), the zebrafish embryo consists of approximately 10 000 cells. About 1% of these, approximately 100 cells, are part of the lateral line primordium, raising the challenge of how to specifically label our target tissue. Generally, specific genetic expression is used to deliver proteins and other biological molecules to specific cells in an embryo. Obviously, in our case the synthetic nature of magnetic beads excludes the possibility of expressing these in specific target cells under genetic control.

Besides the challenge of tissue-specific labeling, another issue is how the magnetic beads are coupled to the cells. In experiments performed in cell culture magnetic beads are usually coupled extracellularly to surface receptors of the cells. Due to limited access to the surfaces of cells in three-dimensional coherent tissues, like the primordium, this approach is generally not a viable option for studies in embryos. Therefore, in order to apply a force on the lateral line primordium, we investigated an approach that would allow delivery of beads into the primordial cells. Ideally, this approach would label the primordial cells with magnetic beads without labeling the surrounding tissues, in order to allow the application of forces specifically to the migrating tissue. To this aim, we tried three different methods of bead delivery.

Method I: Injection

A commonly used method for delivering substances and small objects into zebrafish embryos is injection during the one cell stage immediately post fertilization. At this stage the embryo consists of a single, large cell that is attached to the yolk. This single cell embryo can be easily penetrated by a microneedle to deliver the probe into the cell. 2.8 μm Dynabeads were injected using this method. Afterwards the embryo was left to develop for 24 hrs. This method resulted in embryos with evenly distributed beads (Tbl. 3.2). It was very efficient in delivering beads to the primordium, but surrounding tissues like muscle and skin cells were equally well labeled. Therefore it was not an appropriate method for bead delivery specifically to the primordium.

Method II: Cell transplantation

An established method for delivering cells with different properties to specific embryonic regions is cell transplantation. We therefore applied this method to transplant cells from 'donor' embryos that were injected with magnetic beads immediately post fertilization, as described above. At 8 hours post fertilization (hpf) cells from the donor embryo were transplanted into host embryos using a microneedle. At this stage, cells in the embryo are not tightly coupled together, which makes it very easy to remove or introduce cells. As the aim of this experiment was to target bead containing cells to the future lateral line primordium, we took advantage of a prexisiting 'fate maps' that allow reasonably accurate prediction of which regions will give rise to which tissues in the later embryo developing embryo. We therefore transplanted bead-containing donor cells to the top of the animal pole (Tbl. 3.2), as this contains the cells that later become the cranial region of the zebrafish, the birthplace of the migrating primordium. However, as the primordium then migrates away from this cranial region into the trunk, which is derived from another part of the fate map, transplantation provides a means to specifically label the primordium.

Indeed, this resulted in a number of nicely labeled primordia and only little labeling in the underlying somites. Unfortunately, cell transplantation labeling of the primordium proved to be rather low efficiency, most likely the result of patchy labeling of the donor cells with magnetic beads due to reduced dispersal of beads within the injected one cell stage embryo.

Method III: Late Injection

Cell transplantation experiments demonstrated high specificity labeling of the primordium. It was possible to place the beads in a specific embryonic region. However, its low efficiency encouraged us to look for alternative methods. We next tried to directly inject magnetic beads, again into the animal pole region that contains the cells that will later make up the cranial region of the fish.

Fig. 3.3a depicts an embryo 6 hpf, into which a mixture of fluorescent magnetic beads (red) and rhodamine-dextran (a membrane impermeable dye in white) have been injected. An injection needle with a diameter bigger than the typical cell diameter was used to ensure that the beads were not injected directly into a particular cell but rather into the extracellular space in this region. The co-injection tracer rhodamine dextran confirms the localization of the injection solution in the intercellular space. Injected embryos were then left to develop to 30 hpf, a stage when the lateral line primordium has commenced migration.

Fig 3.3b and Fig. 3.3c depict the same embryo at 30 hpf. Cell boundaries are marked with a membrane bound green fluorescent protein (GFP) expressed under the control of the ClaudinB promotor (ClaudinbGFP in green). The confocal slices in Fig. 3.3b and Fig. 3.3c show that the beads are located inside cells. Rhodamine-dextran was detected in spots, suggesting the dye was concentrated in vesicles. It appears that both the beads and the rhodamine-dextran were internalized into the embryonic cells, an unexpected but fortuitous finding.

Fig. 3.3d shows the survival rate of injected embryos over time. Embryos were injected at 5 hpf and dead embryos were counted at periodic time intervals. The survival rate after injection drops quickly to approx. 60% within the first 24 hpf and stays constant afterwards for several days. An embryo that has survived the first 24 hours is generally healthy and not adversely affected. The first 24 hours of development correlate with the crucial processes of gastrulation and segmentation. Experiments were typically started around 30 hpf, which meant that embryos selected for experiments were the ones that had survived the first 24 hpf. These were likely to have not been negatively affected by the injection and the presence of beads. Additionally, we actively selected healthy looking embryos. Approximately 1:30 to 1:60 embryos would had primordia labeled with beads, with the number of beads in surrounding tissues significantly lowever.

Method	Typical result	Advantages	Disadvantages
Early injection 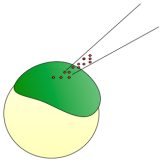	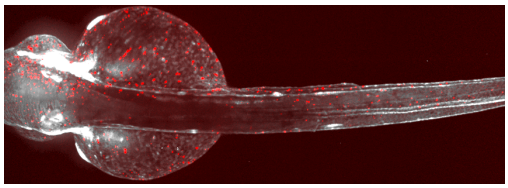 gray: ClaudinBGFP; red: beads	high efficiency	beads not localized
Late Injection 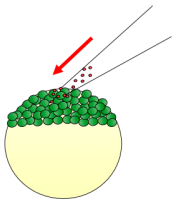	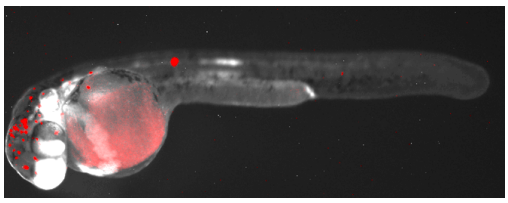 gray: ClaudinBGFP; red: beads	high efficiency beads are localized	-
Transplantation 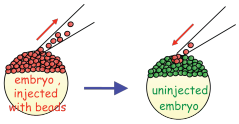	 Brightfield image. Transplanted cells are labeled with rhodamine dextran (red). Small inset: cluster of transplanted cells, which cluster in the cranial region. Only very view transplanted cells are visible. No beads are visible, due to the low efficiency of the method.	-	labor intensive low efficiency

Table 3.2.: Comparison of different bead delivery methods. The column "typical result" shows embryos at 24 hpf. The method late injection was chosen for the experiment, since it has a high efficiency and delivers the beads in a localized region of the embryo.

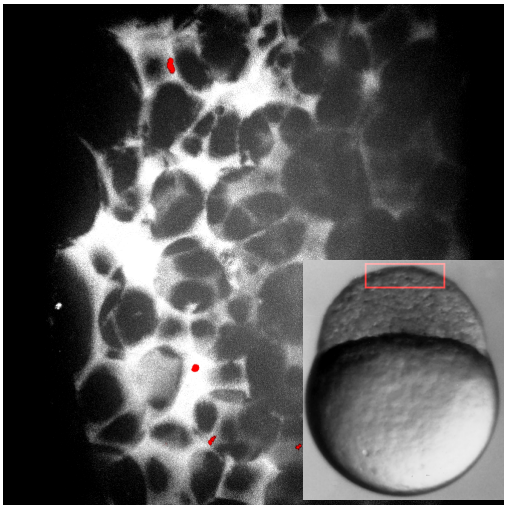

(a) Injected embryo 6hpf, projection of z-stack, rhodamine-dextran (white) and the magnetic beads (red) are located in the extracellular space. Cells are not labeled and appear dark. The inset shows a zebrafish embryo 6 hpf. The red square denotes the region imaged.

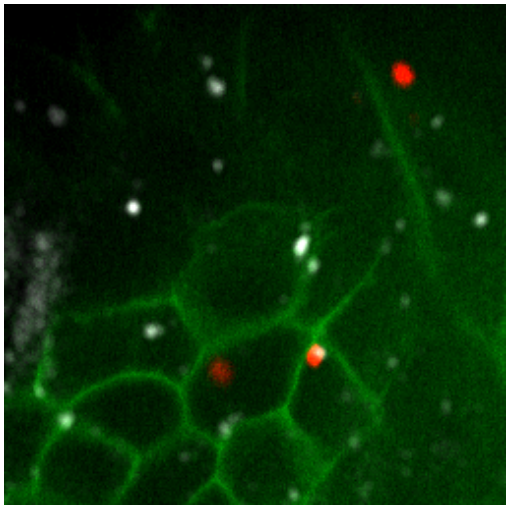

(b) Eye region of embryo 30hpf, confocal slice; claudinbGFP (green) marks cell boundaries; Magnetic beads (red) and rhodamine dextran (white) is located intracellularly.

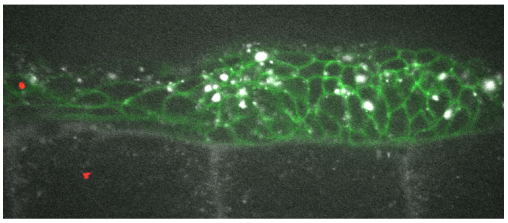

(c) primordium of the same embryo 30 hpf, one confocal slice, additionally to the rhodamine dextran (white) in the primordium the borders of the somite cells are visible. Only a small fraction of embryos (about 1 in 50) contain beads in the primodium. In this particular primordium, only two beads are visible in the field of view.

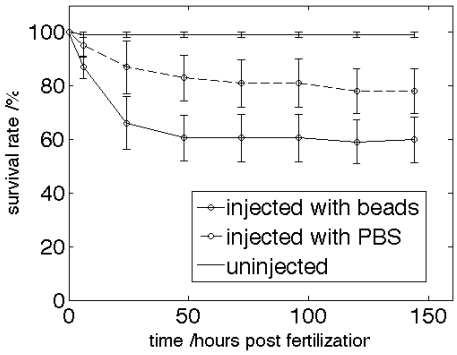

(d) Survival rate of embryos injected with beads, injected with PBS (balanced salt solution) and uninjected over time. Injections were done at 6 hpf. Errorbars are standard error of the mean. N=4 each.

Figure 3.3.: Images of embryo (late injection) immediately after injection (a) and at 30 hpf (b,c). The beads are injected into the extracellular space and are taken up by the cells during development.

3.3. Magnetic Tweezer Set-up

The magnetic tweezer set-up consists of three major parts: an electromagnet, a mu-metal (alloy) core and a cooling unit. The construction of these is discussed in the following section.

3.3.1. The Mu-metal core

The core of the electromagnet is made from mu-metal, a nickel alloy that is characterized by a high magnetic permeability (20 000 to 1000 000). This leads to a concentration of the magnetic flux in the material. When mu-metal is shaped or bent the magnetic permeability is reduced drastically, which is why mu-metal has to be annealed at high temperatures (1000 degrees Celsius or higher under vacuum) after every mechanical manipulation. The shape of the magnetic tip is a crucial factor in shaping the magnetic field. In order to achieve a high field gradient it is necessary to create an electromagnet tip that is as sharp as possible. We created electromagnetic tips which had diameters as low as 20 μm, allowing for high field gradients.

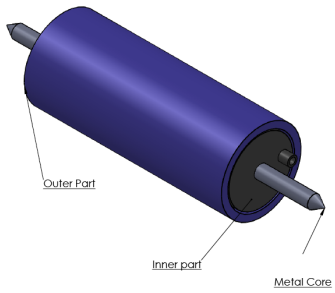

(a) Drawing of Set-up

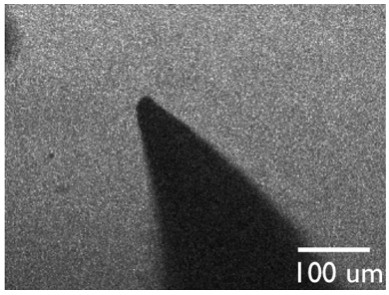

(b) Tip of the magnet, 20μm in diameter

Figure 3.4.

3.3.2. Cooling unit

Due to the use of high electric currents, there is a substantial heat generation during the use of the magnetic tweezer set-up, which makes it necessary to use a cooling system. Without the use of a cooling system the temperature of the tip can easily reach 100

degrees celcius or more, which damages the biological specimen.We created a cooling system by fitting a water tight covering over the solenoid. This allowed us to pump water from a reservoir through the solenoid. The reservoir acted as a heat sink, transporting the heat away from the solenoid.

In practice, no significant temperature increase at the tip could be measured even for currents higher than 4 amperes (A) (Fig. 3.5d). However, we observed an expansion of the mu-metal core for currents 5 A or higher. Presumably, heat was produced directly at the coil that was transduced onto the metal core. The heat was enough to expand the metal core by a few micrometers. We used fairly small distances between the magnetic beads and the electromagnet tip. Furthermore, the tip partially touches the sample and this could have lead to movement of the sample and inconsistencies in force measurements. To counteract this effect we did not use currents higher than 4A. Additionally, we constructed a holder that holds the set-up close to the sharpened end of the tip. (See Fig. 3.5c). In this set-up there would be no expansion occuring at the tip, any expansion would occur away from the sample.

3.3.3. Coils of the solenoid

To reduce the production of heat during the magnetic tweezers experiment, it was beneficial to add more coils to the solenoid rather than increasing the current.

$$P = U * I = R * I^2 \tag{3.4}$$

$$R \sim l \sim N \tag{3.5}$$

$$P \sim N * I^2 \tag{3.6}$$

The heat energy generated is proportional to the number of coils and proportional to the square of the electric current flowing through them. Our electromagnet contains approximately 1000 copper wire coils wound over 5 cm length. We used currents in the range of 1 to 4A.

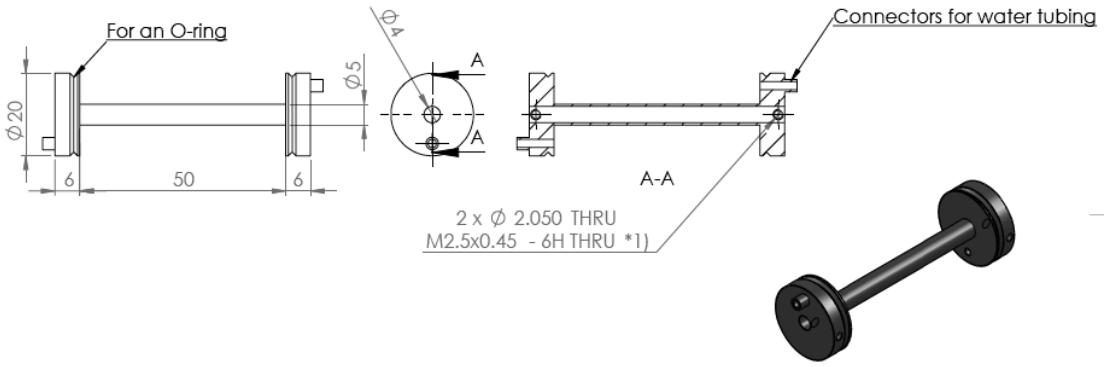

(a) Construction of the inner part of the cooling shell (with U. Krzic).

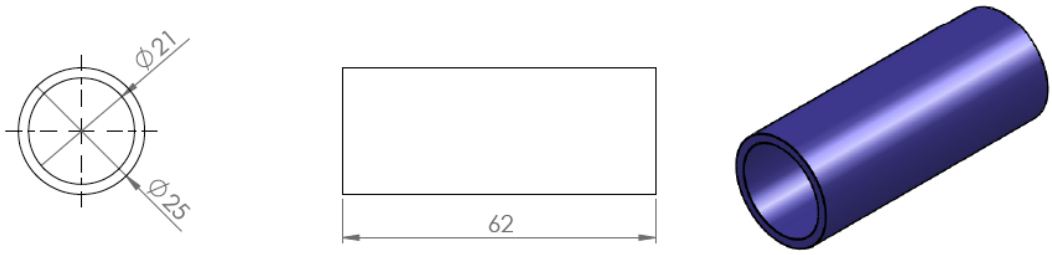

(b) Construction of the outer part of the cooling shell (with U. Krzic).

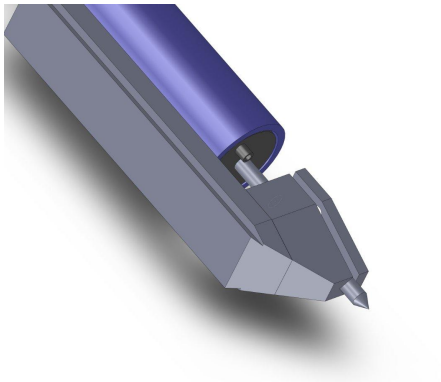

(c) Holder for the electromagnet. Holding the set-up close to the tip reduces heat induced elongation effects. (with U. Krzic).

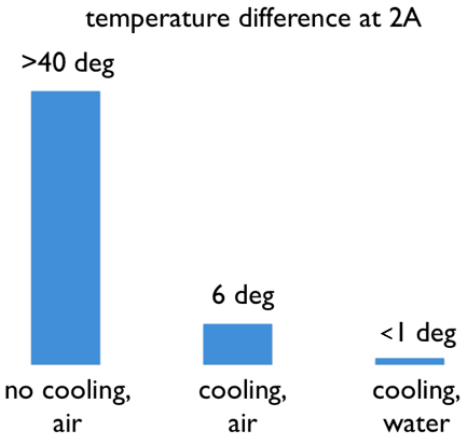

(d) Temperature change before and after cooling with the electromagnet tip immersed in water or air.

Figure 3.5.

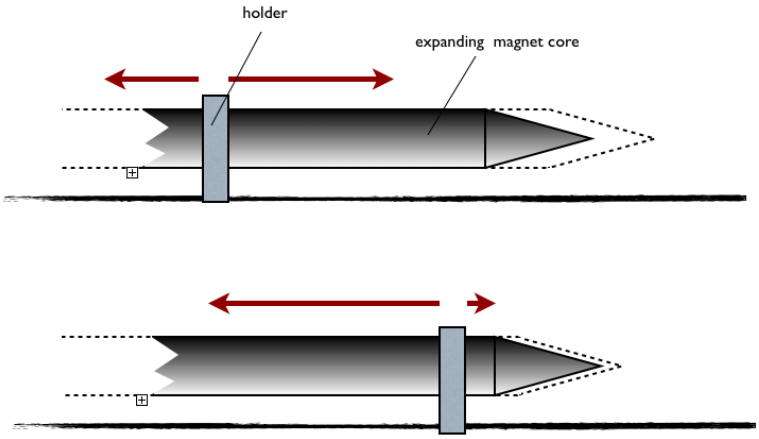

Figure 3.6.: Diagram of the influence of the position of the holder on the amount of heat expansion in each direction. Red arrows show the heat expansion in each direction. Top: The holder is further away from the tip. Bottom: The holder is placed closer to the tip. The metal expands the same length in both cases. In the bottom case most of the expansion is towards the back, away from the tip.

3.4. Experimental set-up

3.4.1. Force calibration

The force depends on the gradient of the field, which in turn is highly dependent on the shape of the magnet. We shaped the tip down to 20 μm in diameter to increase the force as much as possible. Since the magnet tips are very sensitive to mechanical deformation, the force curves had to be re-measured regularly.

Forces were measured by immersing fluorescent magnetic beads in a fluid of known viscosity [1] (see Ch. 10.3, page 120 for a description of dissolving the beads in DMPS) and measuring their speed. The electromagnet tip was placed close to the bead and the movement of the bead towards the tip was recorded using a microscope. The bead movement was tracked in digitized images using ImageJ. The speed in function of the

[1] DMPS purchased from Sigma

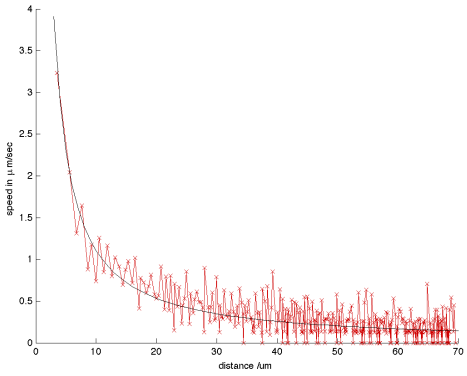

(a) Speed of a 2.8 μm bead moving towards the tip at a current of 4A for distances up to 70 μm between bead and magnetic tip

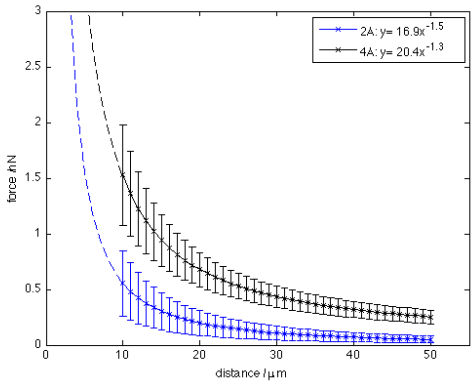

(b) Average force on 2.8 μm bead at a current of 2 A and 4A for distances up to 50 μm between bead and magnetic tip, error bars are standard error of the mean. N=5

Figure 3.7.

distance between bead an tip were determined. The force acting on the bead can be calculated using Stokes' law[2] :

$$F = 6\pi\eta Rv$$

Since the fluid is very viscous, the placement of the electromagnet tip in the fluid induces flows in the fluid. To monitor these flows, we added non-magnetic beads[3] to the fluid. Generally, after placement of the electromagnet tip we waited for approximately 60 minutes for the flows to stop.

Several force-distance curves were averaged to achieve higher precision. The resulting curve was then fit with a power law (see Fig 3.7 for an example). During the experiment, distances (from bead to electromagnet tip) greater than 10 μm were used.

Depending on the distance between bead and electromagnet, using a current of 4A we can exert a force of up to 1.5 pN onto the bead.

[2]where F is the frictional force acting on the interface between the fluid and the particle which is equal to the kinetic force,
η is the dynamic viscosity (in N s/m^2),
R is the radius of the spherical object (in m),
and v is the velocity of the particle (in m/s).

[3]Invitrogen, 1 μm, red fluorescent

3.4.2. Accessing migrating tissue with magnetic tweezer

The primordium migrates between the 5 micron thick embryonic skin layer, the periderm, on top of a sheet of muscle cells. Since the cells have a thickness of up to 15 μm, the migrating primordium lifts the skin from the muscles, causing it to bulge (Fig. 3.8c). It follows the horizontal myoseptum, a membrane that runs parallel to the main body axis and along the midline of the myotomes, or muscle blocks. The horizontal myoseptum is located about 100 μm below the dorsal surface from the back of the embryo (Fig. 3.8b, top panel). However, to apply the appropriate forces the distance between the bead and the magnet tip is required to be 50 μm or lower. Therefore, we placed the tip on top of the skin, in close proximity of the primordium (Fig. 3.8c, lower panel).

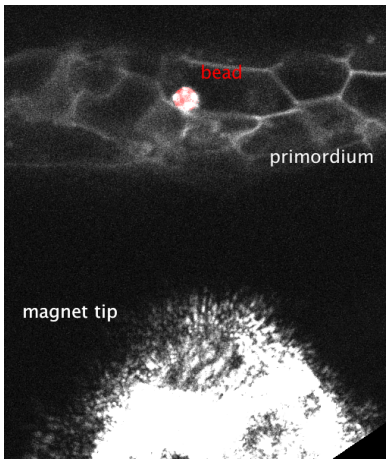

(a) View of primordium and tip. The laser light is reflected off the electromagnet tip.The bead is inside a primordial cell.

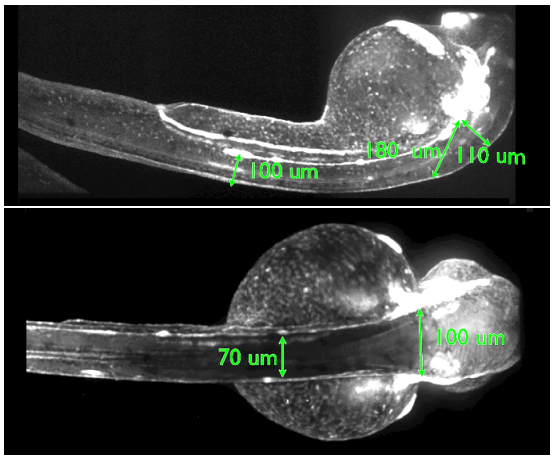

(b) Embryo at 30 hpf. Green: ClaudinbGFP labeling.

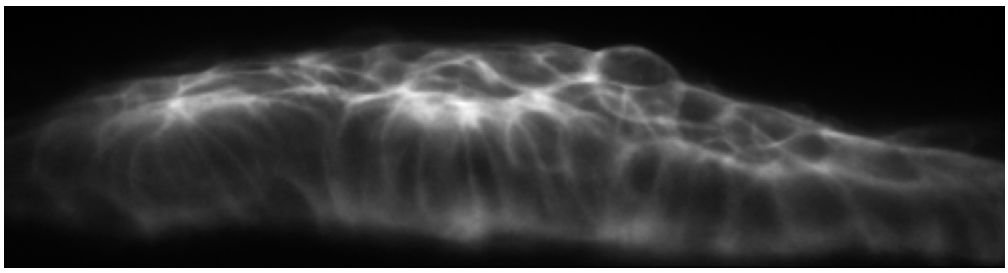

(c) Sideview of primordium. The primordium is raised against the muscle cells.

Figure 3.8.

To simultanesously image the primordium during the application of the magnetic tweezer it was necessary to use an upright microscope. The embryo was mounted on a drop

of 1.5% agarose (see Ch. 10.1, page 119) and immersed in E3 solution. The tip was placed in between the objective and the sample. This way the tip of the magnet and the primordium could be imaged in the same field of view (Fig. 3.8c).

3.5. Effect of magnetic beads and magnetic fields on the migration and differentiation of cells

Several control experiments were performed to investigate whether the presence of beads or magnetic fields alone have an impact on the migration and differentiation of cells in different stages of development or have an influence on collective cell migration and the cellular organization of the primordium.

3.5.1. The presence of magnetic beads has no impact on the migration and organisation of cells in early embryos

To investigate the migratory behavior of cells containing beads in early embryos, we traced and analyzed the movement of cells containing beads in early zebrafish embryos. We performed the following transplantation experiment: donor embryos were injected with a mixture of magnetic beads and rhodamine-dextran, a membrane impermeable dye, as a control. It is a standard dye for tracing cells in the zebrafish embryo [21]. Afterwards, claudinbGFP host embryos were transplanted with cells from the above donor embryos. After the transplantation, the host embryos contained not only cells filled with rhodamine dextran alone, but also cells filled with rhodamine dextran along with magnetic beads. The embryos were imaged from 3 to 11 hours after transplantation using a spinning disk microscope (Fig. 3.9). During that time, the embryos underwent gastrulation and somite development. A fraction of both rhodamine dextran containing and beads+rhodamine dextran containing cells where tracked (Fig. 3.10). To quantify the spatial motion of the cells, the mean square displacement (MSD) for all tracks were calculated. The MSD contains information about the speed of the cells and their directional persistence. The average MSDs are plotted in Fig. 3.10. The mean square displacement curve of cells filled with beads and cells filled with rhodamine are not significantly different. The presence of beads does not limit the cells in it's movement. The beads do not appear to have

an impact on the speed and directional persistence of migration. The embryos develop normally.

3.5.2. Primordia containing beads migrate at the same speed as wildtype primordia

The experiments described show that bead labeling does not have a strong effect on migration and behaviour in embryonic cells in general. However, it was then important to determine whether labeling with beads had an impact on the collective migration of the primordium, the model tissue that is the focus of our study. We therefore performed a higher resolution comparison of the migration speed of labeled and unlabeled primordia. Time- lapse images were taken of injected and uninjected embryos using spinning disk microscopy. 10 embryos were imaged for both conditions. The injected embryos contained on average (2.3 ± 1.4) [4] beads per primordium. We imaged for a long time span (4 hours) to reduce the influence of short-term variations in speed. During this time, the primordium migrates roughly 200 μm, which is about twice its own length, and deposits one or two rosettes. Since the migration speed of the primordium is dependent on the temperature under which the measurements are taken, all measurements were taken under the same microscope under the same conditions. The average speed of unlabeled primordia was $(47\pm14)\mu$m/h, while the average speed of labeled primordia was (42 ± 19.3) μm/h (Fig. 3.11). The speed of both groups is not significantly different ($p \gg 0.5$, two-tailed t-test with unequal variances). The presence of a small number of beads therefore did not impact collective cell migration.

3.5.3. Beads do not influence primordial cell organisation

To investigate the effect of the presence of magnetic beads in the primordial cells, we injected claudinbGFP embryos with fluorescent magnetic beads (2.8 μm diameter). We tracked the cells containing beads over a long time period. The behavior of these cells is not noticeable different from their unlabeled neighbors: They organized themselves into epithelial-like rosette cells and became part of the rosette cluster (Fig. 3.12). Thus, the presence of beads alone appeared not to have an effect on the behavior or on the characteristic cell organization of the primordium.

[4] all numbers given in (average $\pm$ standard deviation)

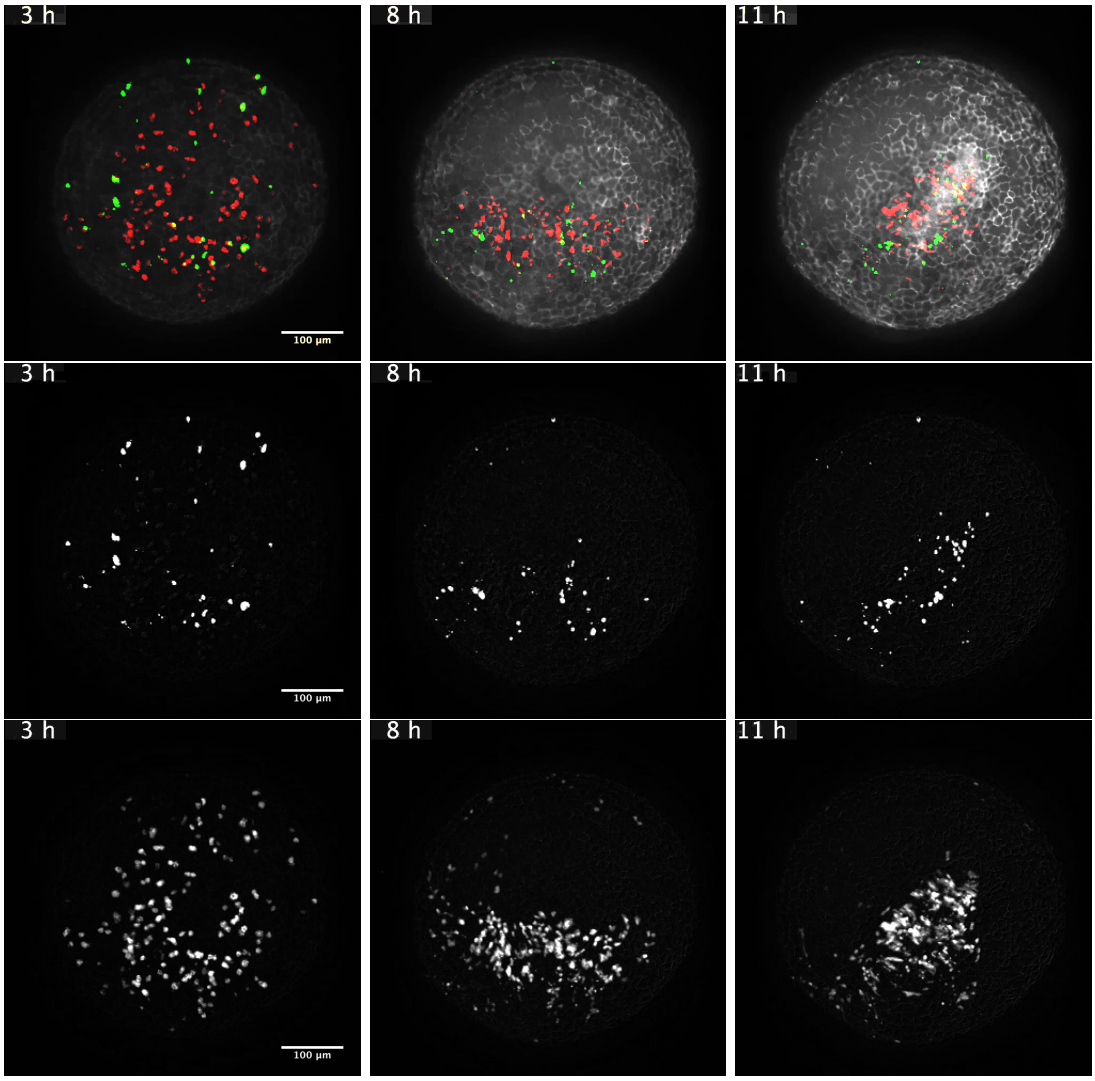

Figure 3.9.: **Example of a timelapse of Transplanted embryo:** Each column represents another time point in the timelapse. The time after transplantation is given in the upper left corner of each panel. The top row is a merge of an embryo labelled with claudinbGFP (gray), rhodamine dextran injected cells (red) and magnetic beads (green). For better visibility the channel showing the beads (middle) and the channel showing the rhodamine dextran filled cells (bottom) are shown separately below.

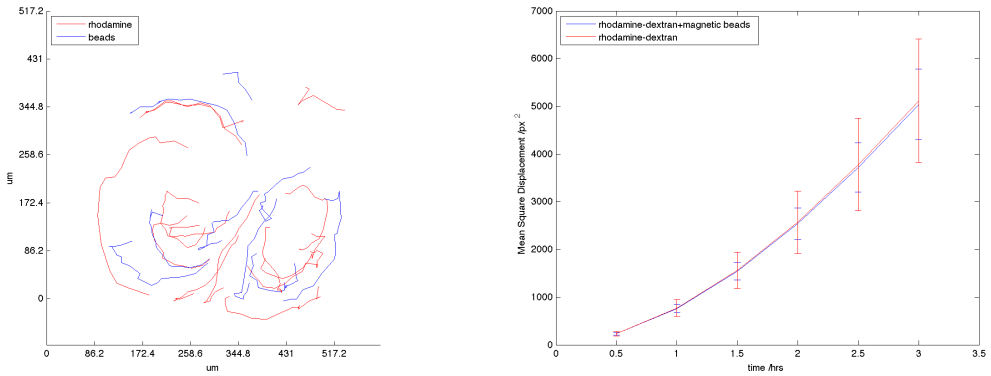

Figure 3.10.: **Tracks of rhodamine dextran filled cells and cells containing magnetic beads in an developing embryo (left) and average mean square displacement curves for both cell populations(right).** The tracks were obtained from the timelapse movie in Fig. 3.9. The mean square displacement curves were calculated from the tracks (N=15 for rhodamine dextran, N=10 for magnetic beads). Error bars are standard errors of the mean.

3.5.4. Primordia migrate and differentiate normally in a magnetic field

To investigate the effect of a magnetic field alone on the primordial cells, we applied an external magnetic field to unlabeled primordia. The electromagnet was placed at a distance of approx 30-50 μm. A magnetic field was produced by applying an electric current of 4A for one hour. Unlabeled primordia were not affected by the external magnetic field. Migration and differentiation proved to be normal. The characteristic front-back polarity and the dropping of rosettes appeared to be undisturbed. No apparent differences could be detected between primordia migrating in a magnetic field and wildtype primordia.

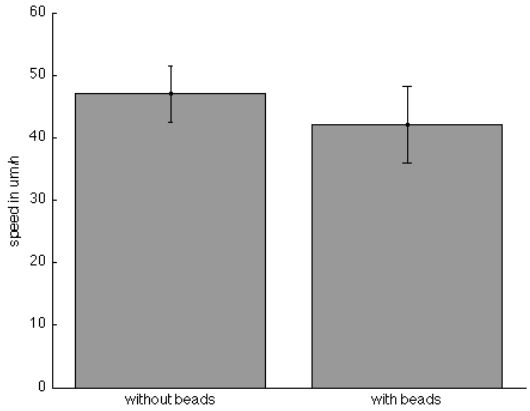

Figure 3.11.: Primordia labeled with beads migrate with the same speed as unlabeled primordia. (p≫0.5 two-tailed ttest with unequal variances), N=10 each

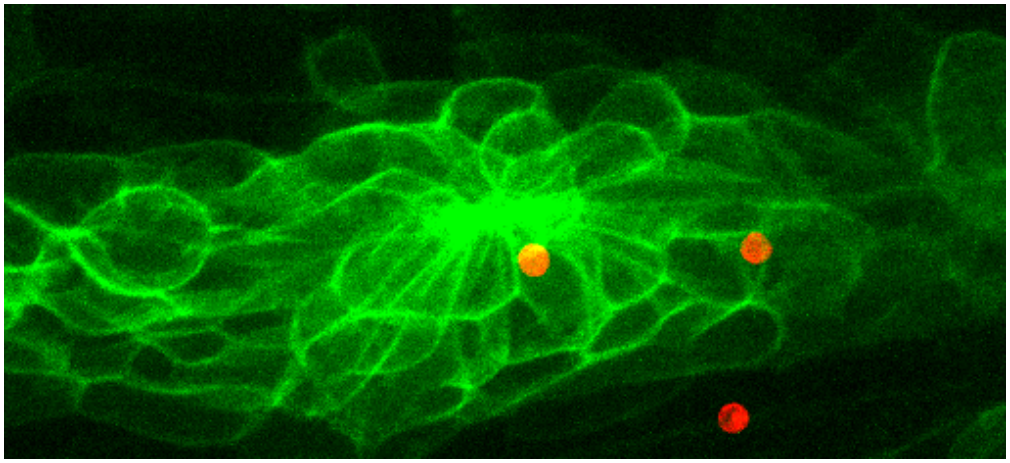

Figure 3.12.: Rosette of claudinbGFP (green) labeled embryo containing fluorescently labeled 2.8 μm dynabeads (red). Z-stack, projected.

4. Summary and Discussion

Set-up summary

The design of our magnetic tweezer set-up was based on the need to perform experiments in living embryos. Several challenges had to be addressed for its construction. We chose to construct electromagnetic tweezers so that the applied magnetic field could be fine-tuned for the experiments. To prevent heat damage to the embryo, we constructed a cooling unit that reduced the heat transferred from the magnet to the embryo dramatically.

Since the force required to deform cells in embryos was not known previously, we developed a magnetic tweezer set-up that could apply as large forces as possible. Forces up to 1.5 nN can be reached with our set-up. In Ch. 6 (page 71) we discuss that these forces are sufficient to break the cell boundaries in the primordium and pull magnetic beads out of cells.

The shape of the constructed magnetic field was designed to match the dimensions required for applying forces within the developing embryo. Therefore, we needed to produce a very narrow magnet tip, which allowed us to place the magnet tip very close to the cells in the primordium. At the same time, these narrow tips produced very steep field gradients allowing us to apply high forces on the magnetic beads.

We constructed electro magnetic tweezers with 1000 coils spanning over 5 cm length. As a core we used mu-metal sharpened to a tip with 20 μm diameter. Depending on the distance between bead and electromagnet, using a current of 4A we can exert a force of up to 1.5 nN onto the bead with 2.8 μm diameter. When using these high electric currents, a cooling system is necessary to deal with the substantial heat generation. The cooling system consists of water being pumped through the solenoid into a water reservoir, which acts as a heat sink.

Comparison with previously reported magnetic tweezer set-ups

Our set-up is most similar to the magnetic tweezer of Alenghat et al. [7] and Bausch et al. [9]. Both set-ups used larger (4.5 μm) dynabeads, but smaller currents. Bausch et al. [9] reached forces up to 10 nN at 2A electric current and 10 μm distance from the pole piece, while Alenghat et al. [7] reached a force of 220 pN at 1A and a distance of 200 μm.

Our set-up is unidirectional, it can only exert force in one direction. Multidirectional set-ups have been constructed among others by several groups [15], [12], [13] and [11]. These set-ups require automatic tracking of the magnetic probe and a force feedback loop to adjust the force according to the position of the magnetic probe. However, for our purposes a uni-directional set-up was sufficient.

Magnetic fields have no effect on cells in the lateral line primordium

Before applying forces on the lateral line primordium, we had to ensure that the applied magnetic fields did not change the collective migration behavior and cellular organization of the primordium. The presence of a magnetic field did not appear to alter the migration of the lateral line primordium. This result is in agreement with several *in vitro* experiments, which have found only minor effects on cell growth even after prolonged exposure to high magnetic fields [22] [23] [24] [25]. However, high magnetic fields have shown some mutagenic effects and oxidative damage of DNA, but only when combined with drugs (oxidants) or x-ray radiation [26] .

Introducing magnetic beads into embryonic cells proves to be unexpectedly simple

We chose to use 2.8 μm Dynabeads (Invitrogen) as magnetic probes. These beads have the advantage of being very uniform in size. Additionally they reach a high $(M_{sat} * V)$-value, which allowed us to apply high forces. Another advantage of Dynabeads is that they can be labeled with streptavidin, which allowed us to couple bright fluorophores to them. This allowed us to visualize and track the beads inside a developing embryo.

Delivering magnetic beads into embryos proved to be unexpectedly simple. Our goal was to achieve labeling of a specific tissue (the lateral line primordium), while minimizing the labeling of cells in the surrounding tissues. We developed a technique to label the primordium with magnetic dynabeads, which have been coupled to a fluorophore for better tracking in the embryo. An injection of magnetic beads into the animal pole of the embryo at 6 hpf resulted into embryos whose cranial region and lateral line primordium is preferentially labeled with magnetic beads, while labeling of somites and skin is less likely. Directly after injection the beads appeared to be located in the intercellular space in the embryo. At 24 hpf the beads could be detected inside the cell boundaries. It appears, that cells internalize beads and other extracellular material sometime between 6 hpf and 24 hpf. This is supported by the observation that the non-membrane permeable dye rhodamine-dextran,which was injected in a similar manner, could be detected intracellularly. Rhodamine-dextran was concentrated in dots, presumably small vesicles, at 24 hpf inside embryonic cells. Internalization of nano- and micro particles into cells in cell culture has been reported previously by several groups [27], [28] and [29], among others. Dos Santos et al. [29] showed that even cells not specialized for phagocytosis are able to internalize particles up to 2 μm in diameter. Fig. 4.1 shows electron micrographs of endothelial cells during phagocytosis of micrometer sized silicon particles ([30]).

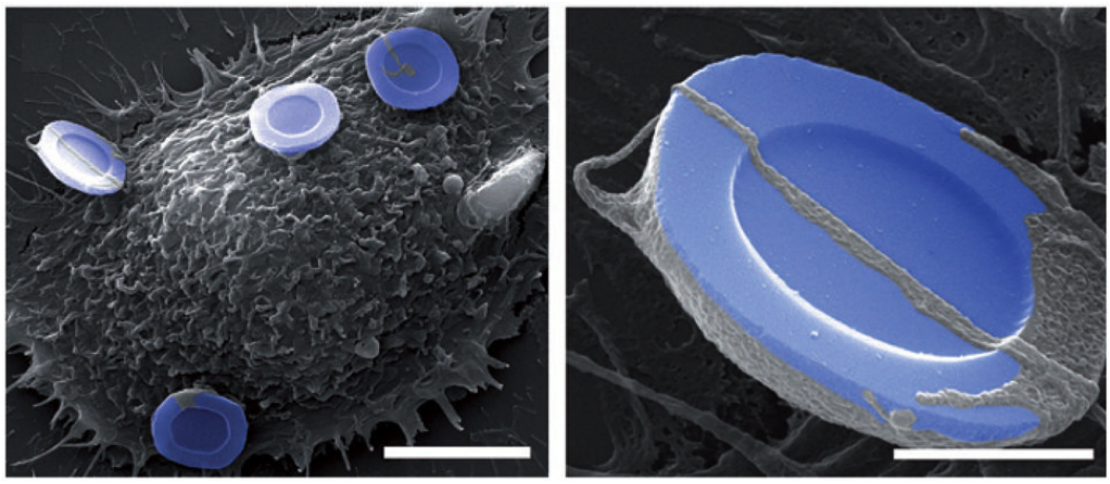

Figure 4.1.: Phagocytosis of silicon microparticles by endothelial cells. Pseudo-colored scanning electron micrographs show the formation of lamellopodia looping over the microparticles, initiating internalization. Bars 5 μm (left) and 1 μm (right) [30]

Other methods of bead delivery include injection at 0 hpf and the transplantation of cells labeled with magnetic beads. The first method resulted in embryos with an even distribution of beads throughout the embryos, while the second method achieved specific labeling of the lateral line primordium, albeit more laborious.

Microparticles have no effect on cells in the lateral line primordium

Ideally, the presence of beads in cells in a tissue should not have an influence on the function of those cells. Therefore we tested whether the presence of the beads affected collective cell migration and the cellular organization of the primordium.

We investigated the perturbation caused in the embryo due to the presence of magnetic micrometer sized beads. We showed with transplantation experiments that cells containing beads migrate in the same way as their neighbors which do not contain beads in early embryos. We also showed that the speed of migration of the lateral line primordium does not change significantly due to the presence of magnetic beads.

There are a number of publications reporting cytotoxicity of small particles, but the majority of these studies focus on nanoparticles (particles smaller than 100 nm), and only a few use magnetic particles. A number of studies [31] [32] [30] found no adverse effects on cells that internalized nano- and microparticles. Serda et al. [30] observed that vascuar endothelial cells maintain cell morphology, viability and mitotic trafficking even after the uptake of silicon microparticles. Hamasaki et al. [31] found no significant change in axon growth potential of neural progenitor cells labeled with magnetic beads. Zhang et al. [32] found no cytotoxicity due to oligosaccharide nanoparticles in mouse embryo fibroblasts. However, both Hamasaki et al. [31] and Zhang et al. [32] used particles in the nanometer range. Serda et al. [30] used microparticles with an approximate diameter of 2 μm, but these particles were not magnetic.

In contrast to these results, other reports have documented ([33], [34], [35] and [36]) toxic effects of nano- and microparticles on cells and embryos. Tan et al. [36] found a disorganized cytoskeleton in human umbilical vein endothelial cells after the uptake of superparamagnetic iron oxide nanoparticles. Tiwari et al. [34] observed the behavior of the same cells coated with 4.5 μm Dynabeads and found a a reduction in the rate of cell proliferation and cell metabolism. Asharani et al. [33] showed that the toxicity of nanoparticles in zebrafish embryos depends on its material. No toxicity was recorded for

embryos that had internalized gold nanoparticles, but the internalization of silver and platinum nanoparticles resulted in an increase of mortality and hatching delays of the larvae. In conclusion, small particles can have no effect on embryonic cells or effect them adversely depending on the material they are made of. We did not observe any negative effects of 2.8 μm Dynabeads on cell migration and cellular differentiation of the lateral line primordium.

Part II.

Forces and material properties in collective cell migration

5. Introduction

5.1. Cell migration

Cell migration is an important process during embryonic development, when single or collectively migrating cells change their position in the embryo to form new organs or shape the embryo. It is also an important process during cancer metastasis and responsible for the spread of cancer cells in the body.

5.1.1. Single cell migration

Single cell migration is a well characterized process. Single cells generally migrate through several cyclical steps. First, the cell polarizes and forms a protrusion at one end, the leading edge. This leading edge attaches to the substrate in the immediate surrounding medium. Upon attachment, focal adhesions in the cell are broken and the cell body contracts, resulting in a net displacement of the cell in the direction of the protrusion [37]. This process is mediated by the contractile actomyosin network, which forms the cell cortex. It consists of actin filaments, which are connected by cross-linking proteins. The contractile property is conferred by myosin motor proteins, which attach to neighboring actin filaments and help in the contraction of the network. However, most studies on single cell migration have been carried out *in vitro*.

5.1.2. Collective cell migration

In reality however, migrating cells are not found in isolation, but rather co-occur with other cells. In such cases, co-occurring cells can move together in a process known as collective cell migration, where cells are held together via cell-cell junctions. Since

these cells are spatially restricted by their neighbors, collective cell migration requires coordination between neighboring cells to achieve effective migration. This collective mode of migration is known to be important in many biological processes. For example, during wound healing epithelial cell sheets migrate collectively to close wounds [38] and cancer growth and metastasis takes place via collective cell migration [39]. Additionally, most dynamic processes during embryonic development use collective cell migration such as gastrulation [40] [41], blood vessel development and the migration of the lateral line primordium [37] .

Despite its importance, mechanisms of collective cell migration are not as well studied as the mechanisms of single cell migration. One reason for this is the convenience of studying single cell migration processes *in vitro*. The study of collective cell migration in developmental processes often requires more elaborate *in vivo* experiments. Additionally, the high diversity of cell types and processes which require collective cell migration makes it likely that the diversity of molecules and mechanisms required to achieve this process is also high, in comparison with single cell migration. Nevertheless, certain characteristics have been identified previously for collective cell migration processes by several studies [37] :

A leading edge: The first group of cells in the collectively migrating tissue is known as the leading edge (as seen in the direction of migration). Migrating cells in tissues usually have cells positioned at the edge of the tissue making up the leading region of the cell sheet. These cells tend to be morphologically distinct from the trailing cells.

Apico-basal polarity: Collectively migrating cells very often have a very distinct apico-basal [1] polarity, with defined actin filled protrusions extending from the basal part of the cells.

Cell-cell communication: Communication between cells is necessary to coordinate collective movement. This communication can either be mechanical or via receptor molecules (chemical).

Principal mechanisms governing collective cell migration have not yet been fully revealed. This is likely due to the diversity in cell types and due to the biological scenario in which collective cell migration occurs.

[1] apical: The top-most part of the cell. basal: The bottom part of the cell.

5.2. Forces in collective cell migration

It has been shown that cells are able to sense, integrate and react to external applications of force. Stem cells differentiate into differing cell types depending on the stiffness of their extracellular environment [42]. Cells in culture react to an external stretching force with a universal physical response of fluidizing their cytoskeleton [43]. It has also been shown that nanoscale forces are able to activate signaling pathways such as Ca^{2+} signaling and Rho GTPase[2] pathways [44]. Furthermore, it has been shown that shear forces in the order of 200 nN in magnitude are able to induce nerve fibre growth [45].

Forces have also been shown to be important for several developmental processes. They have been shown to regulate cell sorting and molecular dynamics. Tensile forces regulate germ-layer organization in zebrafish embryos [46]. The dynamics of myosin II is regulated by tension during drosophila axis elongation [47]. Gene expression during drosophila development has been shown to be regulated by intercellular forces [5].

Mechanical forces seem to be critically important during collective cell migration. However, only a few attempts have been made to quantify intercellular forces during collective cell migration, all previous studies have being performed on in vitro cultured monolayers. Petitjean et al. [48] compared velocity fields of collectively migrating and single migrating cells and found significantly longer correlation lengths in collectively migrating cells. These collectively migrating cells were able to coordinate their migrational behavior over long distances. Trepat et al. [49] quantified traction forces of an advancing cell sheet and found that intercellular forces were highest many cell rows behind the leading edge, and not at the leading edge as one would expect. Angelini et al. [50] found that confluent cell layers behaved analogous to classical glass forming systems, which could undergo a rapid transition from solid-like states to viscoelastic states.

An important mechanism in collective cell migration has been discovered in 2011. Plithotaxis describes the tendency of collectively migrating cell to migrate along the axis of their largest tension.

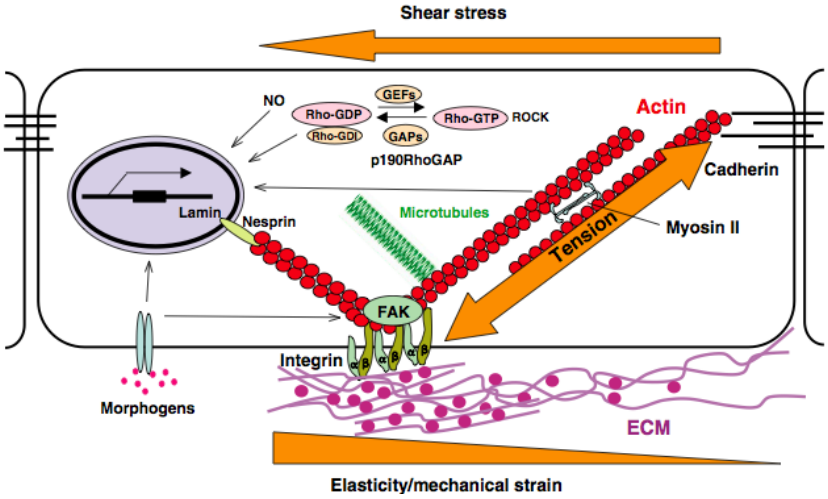

Figure 5.1.: An overview over mechanosensing mechanisms. Figure modified from [51].

The molecular mechanisms that underly mechanosensation and mechanotransduction

Several underlying molecular mechanisms of force sensing have been discovered. The most important identified class of molecules are:

Stretch-activated ion channels The best studied group of cellular force sensors are stretch-activated ion channels. Stretch-activated ion channels are transmembrane ion channels that open their pores in response to stretch of the plasma membrane or actin cortex [52]. These channels allow cells to respond to a wide range of physical stimuli [53]. However, they are only found in certain cell types and bacteria and are probably not responsible for many mechanosensory phenomena during development.

By contrast, two classes of cell adhesion proteins which are widely expressed in embryos have been recently identified to be important for mechanosensory processes:

Cadherin Cadherins are a class of transmembrane proteins which are involved in cell adhesion. Specifically E-cadherin has been characterized to be widely abundant in epithelial cells. It consists of an extracellular region, a transmembrane region and a

[2]The Rho GTPase family of proteins are known to regulate actin dynamics

highly conserved cytoplasmic tail [54]. The cell-cell adhesion mediated by cadherin is calcium dependent. It is connected to the cell cortex by cytoplasmic proteins called catenin [53]. It has been shown that the presence of E-cadherin regulates lamellipodia activity [55]. It has also been shown that E-cadherin participates in mechanosensory pathways [56] [57].

Integrin Integrins are proteins that are responsible for the attachment of the cell to neighboring cells or the extracellular environment. Many types of integrins are known and cells typically express several different types of integrins simultaneously. Depending on their structure, they bind to several extracellular matrix proteins such as fibronectin, laminin and collagen [58].

The sites of integrin extension to the cytoskeleton are called focal adhesions. Focal adhesions are large macromolecular assemblies that connect the cytoskeleton of the cell to the extracellular matrix (ECM). It consists of several proteins, such as vinculin, α-actinin, paxillin, and talin. Integrins generally help connect the focal adhesions to the ECM. It has been shown that focal adhesion transmit mechanical stresses across cells [59]. At the same time, the maturation of focal adhesion requires tension [60].

The protein that transmits these forces to the cytoskeleton in focal adhesions is called vinculin. It is part of the focal adhesion complex. Its structure is 20%-30% similar to α-catenin, which has a similar function as vinculin. Several cell functions are impacted when vinculin is lost: focal adhesion complexes can not form anymore and cell-adhesion and cell spreading is inhibited [61].

5.3. The actin cortex and its regulation

The actin cortex is a meshwork of proteins, that mechanically supports the plasma membrane of eukaryotic cells. This meshwork forms a stabilizing structure that gives cells shape. It regulates cell morphology during the important processes of cell division, cell growth and cell migration. It also stabilizes the cells and protects them against external mechanical influences. The actin cortex is a critical component of the cell cytoskeleton.

The actin cortex consists of long, flexible actin filaments (Fig. 5.2), which are cross linked by various proteins, forming a dynamic mesh of polymers. Actin filaments self-assemble via polymerization of G-actin (globular - actin, the monomeric form of actin). This process is initiated by ATP hydrolysis, a chemical reaction which delivers energy for many cellular processes. Actin filaments are polarized, which means that both ends are structurally different from each other. The growth of the filament takes place at the so-called barbed end. At the so-called pointed end there can be slow growth or even shrinkage. This constant growth and shrinkage of the filament is called treadmilling.

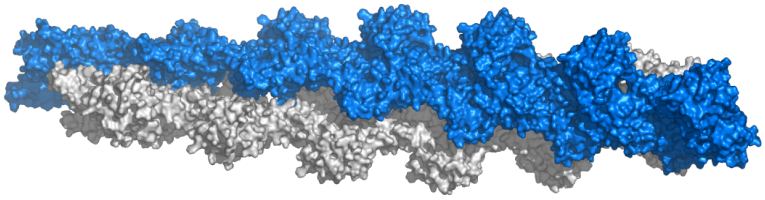

Figure 5.2.: atomic structure of an actin filament with 13 subunits; surface representation [62]

Multiple families of actin binding proteins are known to regulate the length and treadmilling properties of actin filaments:

Several proteins initialize the nucleation of actin polymerization. The ARP2/3 complex, for example, is well known to bind to the side of an actin filament and initialize the nucleation of a new filament branch. Gelsolin, on the other hand, binds to the barbed end of the actin filament and prevents binding of other capping proteins

Capping proteins can bind to both ends of the filament. Depending on the particular protein, they either stabilize the filament or promote its disassembly. Therefore, they play a crucial role in determining filament length. Examples of capping proteins are Tropomodulin, which caps the pointed end, preventing filament shrinkage and CapZ proteins, which prevent growth at the barbed end [63].

Cross linking proteins join actin filaments into bundles or networks by binding to several actin filaments at once. Examples of these are α-actinin and villin, which organize actin into parallel bundles, while proteins like filamin organize actin filaments into loose networks [64].

Actin depolymerizing factors (ADFs) bind along the side of actin filaments and disrupt the helical twist of the filament. This leads to breaks in the filament, which promotes depolymerization.

These few examples, which have been selected from a very large set, show that the regulation of the actin cytoskeleton is a highly complex process. Different regulatory proteins can bind to actin filaments in different combinations, this explains the vast variety of cell cortex behavior observed in cells.

5.4. Viscoelasticity

5.4.1. Elasticity

Elasticity is the tendency of solid materials to return to their original shape after being deformed. An elastic material stores, but does not dissipate energy under an applied load. After the load is removed the material returns to its original shape [65] .

Many elastic materials can be described by Hooke's law of linear elasticity for small strains:

$$\sigma = E * \epsilon \tag{5.1}$$

with σ denoting the applied stress (stress definition), ϵ denoting the strain (a geometrical measure of deformation as a response to stress) and E denoting the Young's modulus.

If a sinusoidal force is applied on an ideal elastic material, the resulting strain is sinusoidal in shape and in phase with the applied force [65] (Fig. 5.3).

5.4.2. Viscoelasticity

In reality all materials deviate from Hooke's law [65]. Many biological materials are not purely elastic, but viscoelastic. They exhibit elastic, as well as viscous-like behavior in response to an applied force. The exact nature of the response depends on the timescale over which the force is applied: For short timescales the material behaves like an elastic

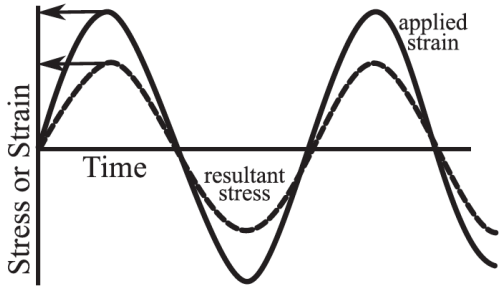

Figure 5.3.: Sinusoidal strain and resulting stress induced in an elastic material. Figure modified from [65]

solid, while it behaves like a viscous fluid for longer timescales. If a sinusoidal stress is applied to a viscoelastic material, the resulting strain will have a sinusoidal shape, similar to the elastic case. However the strain will be phase-delayed and energy dissipation occurs [65] (Fig. 5.4).

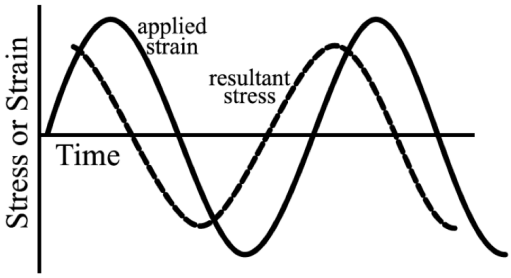

Figure 5.4.: Sinusoidal strain and resulting stress induced in an viscoelastic material. Figure modified from [65]

Experimental characterization of viscoelastic materials

There are many different ways to characterize the reaction of a viscoelastic material to an applied force, but most commonly used are two: creep and stress relaxation [66].

- Creep. A creep test measures the time dependent strain ϵ of a material during an applied stress σ (Fig. 5.5). The applied stress is uniaxial and constant over time.

If the material is linear viscoelastic, the initial length of deformation is proportional to the applied force and the strain curves scale linearly with the stress (expressed mathematically, $\epsilon(a * \sigma) = a * \epsilon(\sigma)$, where a is a constant). A stress-strain curve for each material can be obtained from measuring the strain for different stresses by plotting the strain at a given time point against the applied stress. For a linear material, the stress-strain curve will be a straight line [66]. The ratio of strain to stress is called compliance $C(t) = \frac{\epsilon(t)}{\sigma}$ [66].

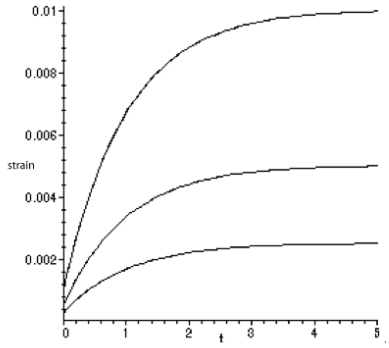

Figure 5.5.: Example curve for creep strain at various constant stresses. The x-axis denotes time. The y-axis shows strains in random units. The three curves are the strains measured at three different stress levels, each one twice the magnitude of the previous one. Images modified from [66].

- Stress Relaxation. The stress relaxation behavior of the viscoelastic material can be determined by measuring the time dependent relaxation after applying a defined strain. In a linear viscoelastic material, the relaxation curves scale with the strain. Analogous with creep compliance a "relaxation modulus", defined as $E(t) = \frac{\sigma(t)}{\epsilon}$ can be introduced.[66]

The creep and stress response both stem from the same molecular mechanisms. However, both responses are generally not related. For most materials the relaxation response equilizes faster than the creep response [67] [66]. It has been shown in shear experiments on fibroblast cell monolayers that creep response and stress relaxation are linear proportional for long timescales even for large deformations (in this case 100 sec or longer) [68].

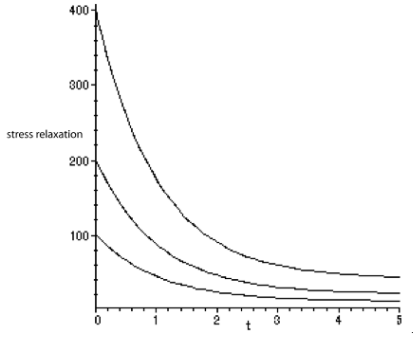

Figure 5.6.: Example curve for relaxation response. The y-axis shows strains in random units. The three curves are the strains measured at three different stress levels, each one twice the magnitude of the previous one. Images modified from [66].

5.4.3. Constitutive models for linear viscoelastic behavior

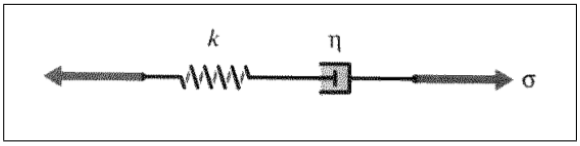

Figure 5.7.: Maxwell spring dashpot model. Figure modified from [66].

The Maxwell spring dashpot model The Maxwell spring dashpot model is the simplest model to describes the behavior of viscoelastic materials under force influence. A convenient way for visualizing this model is using the mechanical analogy of a "Hookean" spring and a "Newtonian" dashpot connected in series. The behavior of the spring is described by Hooks law, with σ denoting the stress and ϵ the strain:

$$\sigma = k * \epsilon \tag{5.2}$$

The spring describes the immediate bond deformation of the material. The deformation is proportional to the applied force. The behavior of the dashpot is described by

$$\sigma = \eta * \frac{d\epsilon}{dt} \tag{5.3}$$

The dashpot describes the slower uncoiling of the filaments. Very often the ratio

$$\tau = \eta/k \tag{5.4}$$

is used. τ has the unit of sec and is called relaxation time. Since these elements are connected in series, the stress on the spring and on the dashpot is the same, while the total strain is a sum of the strain of both elements:

$$\sigma = \sigma_{spring} = \sigma_{dashpot} \tag{5.5}$$

$$\epsilon = \epsilon_{spring} + \epsilon_{dashpot} \tag{5.6}$$

The combined description of the Maxwel spring dashpot model is the following differential equation:

$$k * \frac{d\epsilon}{dt} = \frac{d\sigma}{dt} + \frac{1}{\tau} * \sigma \tag{5.7}$$

This constitutive description of the time response to an applied force describes a material where the flow of the material is practically unrestricted.

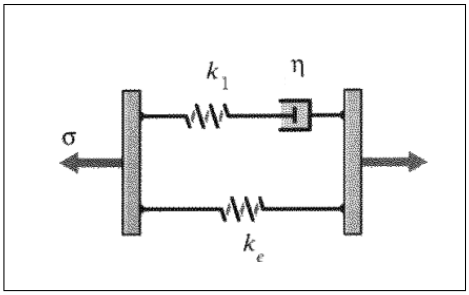

Figure 5.8.: Standard linear solid model. Figure modified from [66].

The standard linear solid model The standard linear solid model is an extension of the Maxwell spring dahpot model. It is the simplest model that predicts creep and relaxation behavior at the same time. It places a second spring in parallel to the Maxwell spring dashpot model. The behavior of this new spring can be described by Hooks law, as well:

$$\sigma = k_e * \epsilon, \tag{5.8}$$

with

$$\sigma = k_1 * \epsilon, \tag{5.9}$$

$$\sigma = \eta * \frac{d\epsilon}{dt}. \tag{5.10}$$

The following constraints describe the relation between the stresses and strains in the modell:

$$\sigma_{tot} = \sigma_{maxwell} + \sigma_{k_e} \tag{5.11}$$

$$\epsilon_{tot} = \epsilon_{maxwell} = \epsilon_{k_e} \tag{5.12}$$

$$\sigma_{maxwell} = \sigma_{\eta} = \sigma_{k_1} \tag{5.13}$$

$$\epsilon_{maxwell} = \epsilon_{\eta} + \epsilon_{k_1} \tag{5.14}$$

The mathematical description of the model can be written as:

$$\frac{d\epsilon(t)}{dt} = \frac{1}{(k_1 + k_e)} * \left(\frac{d\sigma(t)}{dt} + \frac{k_1}{\eta}\sigma(t) - \frac{k_e k_1}{\eta}\epsilon(t)\right) \tag{5.15}$$

The solution for eq. 5.15 for a deflection as a result of an application of a unit-step function force can be written as [69]:

$$\frac{x(t)}{F} = \frac{1}{k_e} * \left(1 - \frac{k_1}{k_e + k_1} * e^{-\frac{t}{\tau_\sigma}}\right) \tag{5.16}$$

with

$$\tau_\sigma = \frac{\eta(k_e + k_1)}{k_e k_1}. \tag{5.17}$$

The Standard linear solid model predicts the general shape of time dependent strain curve using three parameters (k_e, k_1, η). It accurately describes the behavior of a viscoelastic material under loading conditions, but gives less accurate results describing this behavior numerically. If a load is applied quickly to a material, it shows an instantaneous elastic response. If it is applied for much longer, the spring k_e (Fig. 5.8) will extend to its limit and impede any further extension of the material [70] (Fig. 5.9b).

Standard linear solid model superimposed with a serial dashpot Adding a serial dashpot in series to the standard linear solid model improves the description of the stress-strain behavior of biological viscoelastic materials. The additional dashpot introduces the ability of the material to "melt" after long application of force (see Fig. 5.9b for a comparison with the standard linear solid model).

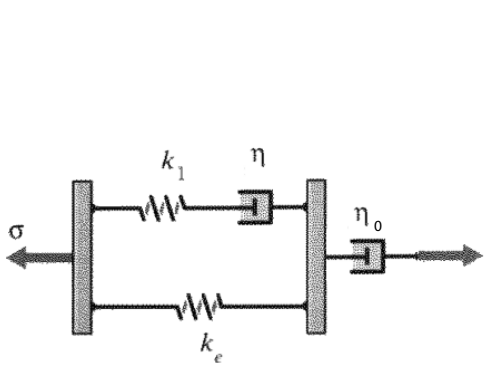

(a) Standard linear solid model with a serial dashpot. Figure modified from [9].

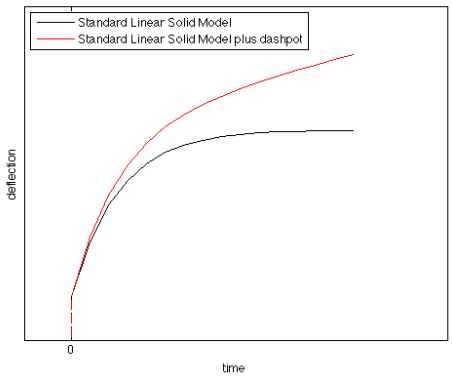

(b) Comparison of the response curves to a step function force for the standard linear solid model (in black) and the standard linear solid model with an added dashpot (in red). The difference between both curves becomes apparent at later timepoints. The extra dashpot allows continued deformation of the material at later timepoints.

Figure 5.9.

According to Fung [69], the response curve to a step function force profile can be expressed as a superposition of the response curve of the standard linear solid model (eq. 5.17) and of a dashpot:

$$\frac{x(t)}{F} = \frac{1}{k_e}\left(1 - \frac{k_1}{k_e + k_1} * e^{\frac{-t}{\tau}}\right) + \frac{t}{\gamma_0}, \tag{5.18}$$

$$\tau = \frac{\eta(k_e + k_1)}{k_e k_1}, \tag{5.19}$$

$$k = k_e + k_1, \tag{5.20}$$

$$\gamma_0 = \eta_0. \tag{5.21}$$

This model increases the accuracy of a numerical description of a biologic viscoelastic material [69]. It has previously been applied to the measurement of the viscoelasticity of cell cytoplasm [71] and of the actomyosin cortex [9].

5.4.4. Viscoelastic measurements as a read-out for the state of the actin cell cortex

The active behavior of the actin cortex

It has been shown by various *in vitro* and *in vivo* experiments that the actin cortex behaves like a viscoelastic material. However, the actin cortex is not a passive network of polymers, but actively generates forces. Additionally, active polymerization and depolimerization of actin fibers, as well as the presence of actin crosslinkers have been shown to influence the mechanical behavior of the actomyosin cortex.

One source of force generation is family of proteins known as myosins. Myosins are actin binding proteins [72] that are able to transform chemical energy into force and movement. They are mainly responsible for the contractility of the actomyosin cortex. One protein of this family, myosin II, is frequently found in mammalian cells. It consists of a myosin dimer that is attached to two antiparallel actin filaments [73] [74]. Both of the dimers are able to move along the filament. As a result they cross link the filaments together while applying a contractile force.

Myosin II acts as a crosslinker of the actin cortex. The small molecule Blebbistatin is able to selectively block the contraction of myosin II in the unattached state [75] [76]. It has been shown that the contractility as well as the stiffness of the actin cortex decreases after treatment with drugs that disrupt myosin II function [77] [78] [79].

The viscosity of the actin cortex depends on the density of the meshwork and the binding strength of the cross-linking proteins [80]. A denser mesh and strongly bound cross-linking proteins increase the internal friction of the material, leading to an increase in force necessary to deform the material in a viscous manner [81].

The relaxation time has been shown in computer simulations to be dependent on the turnover rate of the actin cortex. A fast turnover rate will reduce the relaxation time, as a faster treadmilling of the filament will lead to an adaptation of the material to the applied force. The turnover rate is, in general, related with the lifetime of the cross-links [82].

5.5. The zebrafish lateral line primordium as a model to investigate collective cell migration

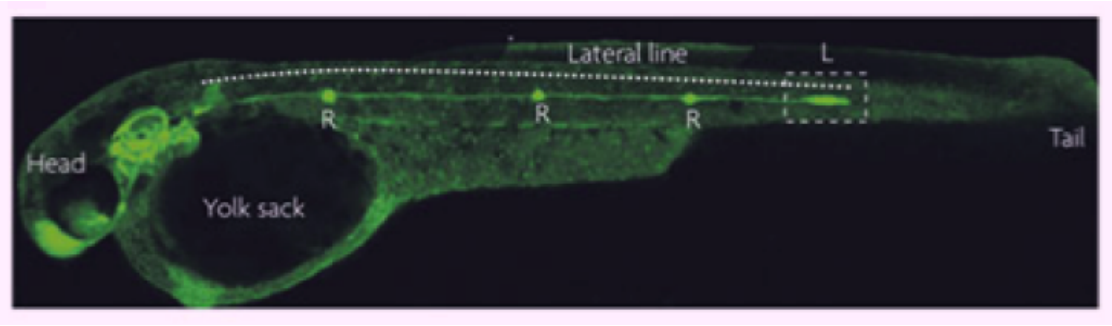

Figure 5.10.: Confocal micrograph of a zebrafish embryo. The lateral line primordium (L) migrates from the head to the tail of the embryo, while depositing clusters of cells, called rosettes (R). Image modified from [83].

To study collective cell migration, we decided to use the lateral line primordium as a model. The lateral line primordium consists of a group of about 100 cells migrating collectively from the cranial region of the embryo towards its tail. During the migration, the cells form organized clusters, called rosettes which are deposited along the axis of migration by collective reduction of the speed of the rosettes (Fig. 5.10). These clusters later develop into sensory hair cells, which form the lateral line system of the adult fish. Mechanical signaling has not yet been demonstrated conclusively in the lateral line primordium. There are, however, several experiments performed in the Gilmour lab that point to the existence of mechanical signaling in the lateral line primordium.

5.5.1. Regulation of collective cell migration via cell-cell signaling

Chemokine directed migration

Previous studies describe the chemokine SDF1a system as a guiding system for the lateral line primordium [85] [86]. The small chemokine SDF1a is expressed along the horizontal myoseptum, a layer of cells located underneath the migration path of the primordium. SDF1a activates the CXCR7 and CXCR4b receptors, which are expressed in different regions of the lateral line primordium. Both receptors are essential for the collective cell migration of the lateral line primordium.

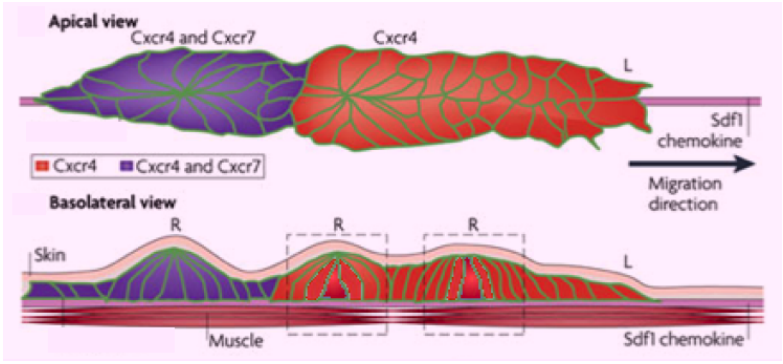

Figure 5.11.: Apical and basolateral depiction of the primordium during migration along a pre-patterned strip of Sdf1. The leading region of the primordium (L) detects the Sdf1 using the Cxcr4 receptor. The trailing region of the primoridium expresses the Cxcr7 receptor in addition to the Cxcr4 receptor. Rosettes are marked with 'R'. Figure modified from [84].

If either CXCR4b or CXCR7 is absent, collective cell migration in the lateral line primordium is arrested. The cells comprising the lateral line primordium are themselves motile and able to migrate individually over small distances. But since this migration is not coordinated, there is no measurable overall displacement of the lateral line primordium itself. Transplantation experiments show that a small number of wildtype cells are able to rescue the migration of CXCR4b-/- and CXCR7-/- mutants [86] (Fig. 5.12). A signaling event between the transplanted cells and the mutant cells that could explain the coordinated movement of the rescued primordium has yet not been unambiguously described.

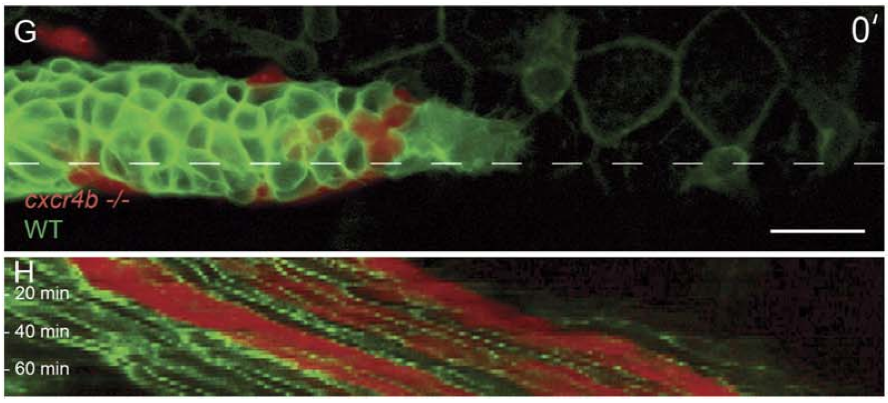

Figure 5.12.: Red: CXCR4b cells , Green: ClaudinbGFP, dotted line:the region used for the kymograph. Two-color time-lapse of a mosaic primordium. (H) Kymograph time-lapse movie from (G). [86]

5.5.2. Regulation of collective cell migration via mechanical signals

Laser Cutting experiments reveal that the primordium is under tension

Laser cutting experiments showed a difference in tension along cell boundaries between the axis of migration and perpendicular to the axis of migration. Cell boundaries were cut along the axis of migration and the speed of opening of the cut was measured. The speed of opening is proportional to the elastic tension the cell boundaries are under. These experiments reveal an increased tension along the axis of migration and a reduced tension perpendicular to the axis of migration (Fig. 5.13).

These findings are interesting under the aspect of a recently discovered mechanism in collective cell migration called plithotaxis. Plithotaxis describes the tendency of cells to migrate along the axis of maximal tension [87]. A similar mechanism might be responsible for the coordinated migration of the lateral line primordium. However, so far plithotaxis has only been described by experiments on cell monolayers consisting of the same cell type. It is currently not known how the presence of several cell types in a layer of collectively migrating cells influences tissue internal tension.

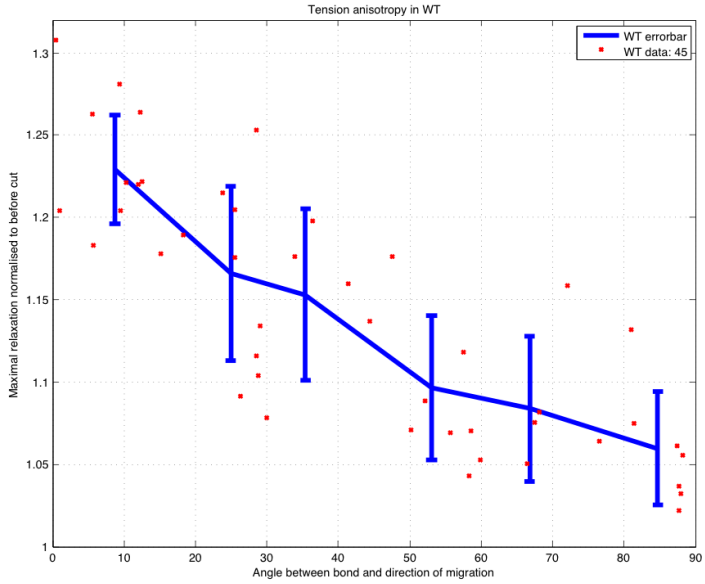

Figure 5.13.: Laser cuts reveal a stronger tension along cell boundaries oriented along the axis of migration (0°). [S.Streichan]

Occurrence of different cell types in the lateral line primordium are mediated by Fgf. Cell type differences seem to be necessary for migration.

Another important feature of the lateral line primordium is the morphological front-back polarity of the tissue. The tissue is organized from cells of several cell types. These cell types are morphological and functionally different. The leading region of the primordium consists of very flat, mesenchymal-like cells. Towards the back of the primordium the cells become increasingly taller. In the far back of the primordium, the cells organize themselves in rosettes. A rosette is a radially organized, discrete structure of approximately 25 cells that form the pre-neuromasts of the organs of the lateral line (Fig. 5.15). The rosette cells have typical markers of epithelial cells, like the apical protein aPKC and the tight junction protein ZO-1 [84]. The formation of the rosettes has been shown to be induced by the ligands Fgf3 and Fgf10, which are recognized by the Fgf receptor [84]. Interestingly, the front-back polarity of the primordium seems to be necessary for its migration. Blocking the Fgf receptor with the small molecule SU5402 or using Fgf mutants result in a loss of rosettes as well as a loss of migration (Fig. 5.15 and 5.16). In this case, collective cell migration is less effective and appears uncoordinated. After a washout of the small molecule, migration resumes only after the rosettes are reassembled. This migration defect is surprising, since a priori Fgf signaling is known to regulate cell fate, but not implicated in cell migration.

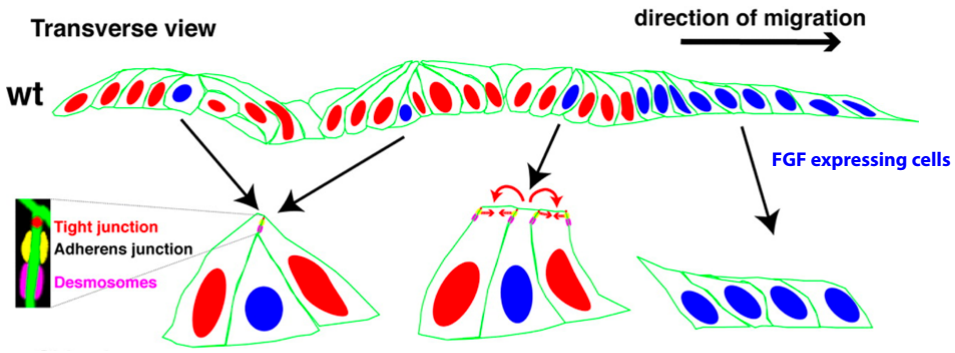

Figure 5.14.: Model of the FGF-driven radial epithelialization leading to rosette assembly. Blue nuclei denote cells expressing Fgf ligands. In the leading region, cells have a mesenchymal-like characteristic. In the trailing region, Fgf-expressing cells induce the epithelialization of their neighbors. In absence of FGF activity, all cells are equally mesenchymal-like and no rosette can form. Figure modified from [84].

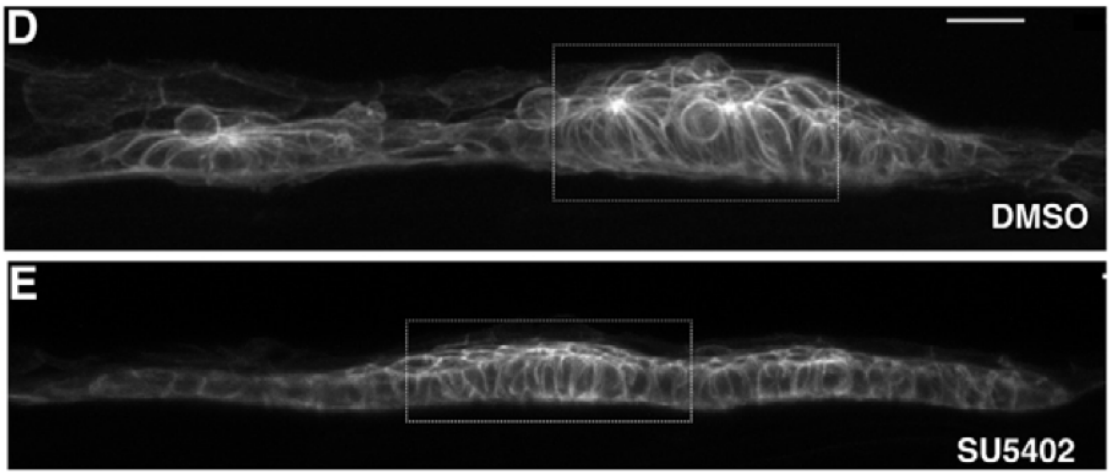

Figure 5.15.: Cells lacking FGF signaling are flatter and wider than control primordial cells. Confocal images show the primordium from the side in DMSO , and in SU5402, maximal projections. [84].

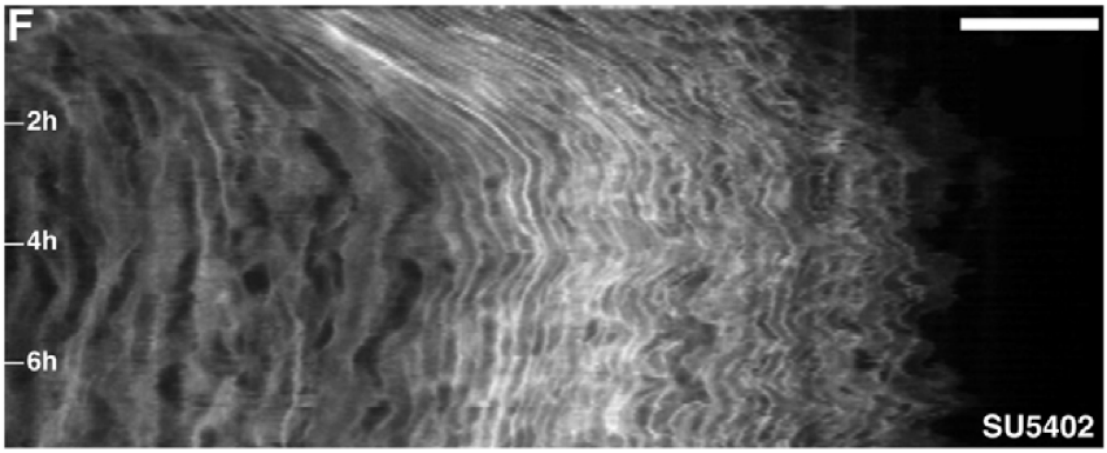

Figure 5.16.: Kymograph of a primordium treated with SU5402. The migration is uncoordinated and ineffective [84].

Laser cutting experiments reveal that cell type differences are necessary for migration.

Laser cut experiments revealed that both the leading regions as well as the rosettes were necessary for a coordinated migration of the lateral line primordium. Using a pulsed UV laser, it was possible to separate the leading region of the lateral line primordium from the trailing region:

- Ablating the leading region of the lateral line primordium yielded a primordium consisting only of rosettes. If the laser cut was made towards the younger rosette, the rosette cells are able to change their morphology from epithelial to mesenchymal cells. The primodium was then able to migrate normally.

- Ablating the rosette cells left a fragment of mesenchymal leader cells. Despite consisting of highly motile cells, this fragment did not migrate for more than a few microns.

- Ablating the primordium after the fist rosette leads to a fragment consisting of mesenchymal leader cells and epithelial rosette cells. In some cases these fragments are able to migrate normally.

These experiments show, that only primordial fragments containing both cell types are able to migrate in a coordinated fashion.

Summary

It appears that the coordination of collective migration of the lateral line primordium has several mechanical components. On one hand, transplantation experiments show that leading cells might be able to direct the cells following using mechanical signaling. On the other had, cell type differences seem essential for collective cell migration. However, it is difficult to de-couple biological/chemical signaling from the above described results, because in each of the experiments mechanical perturbation of the embryo also resulted in a change in its biological composition. Therefore, a method to apply force directly to the primordium was necessary. With the magnetic tweezer setup we were able to test the reaction of collectively migrating cells in the lateral line primordium.

6. Results - Force application on migrating tissues

After developing the magnetic tweezer, we first needed to test whether the force produced with our magnetic tweezer set-up was sufficient to move magnetic beads in embryonic cells and to deform the cells. Additionally, we were interested in the behavior of primordial cells under a force load.

6.1. Forces between 400 pN and 1 nN are high enough to displace magnetic beads inside cells and to visibly deform cells

We applied forces between 400 pN and 1 nN on lateral line primordia loaded with beads and observed the behavior of these magnetic beads inside cells. The applied forces were sufficient to move the beads. The reaction of the beads to the force was instantaneous. After the force application ended, the magnetic beads remained in their new position and did not move back into their previous position in the cell. In addition, these forces were sufficient to visibly deform cell boundaries in the lateral line primordium.

Fig. 6.1 shows an example for this behavior. It shows the same primordium before and after force application.The beads moved towards the gradient of the magnetic field and were visibly displaced.

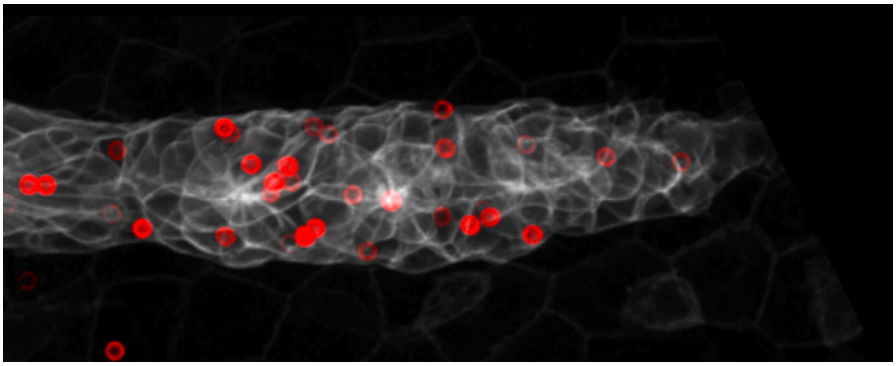

(a) before force application

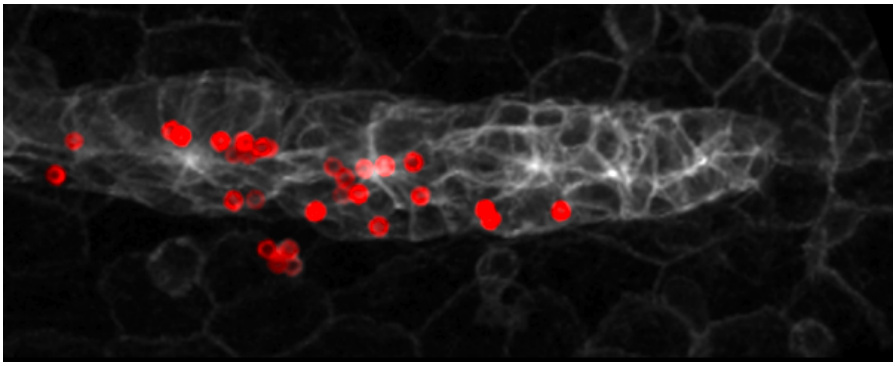

(b) after force application

Figure 6.1.: white: claudinbGFP, red: Dynabeads 2.8 μm; This figure shows the distribution of beads in the same lateral line primodium before and after force application perpendicular to the axis of migration.

6.2. Forces between 800 pN and 1.5 nN can pull beads out of the primordium

We applied forces between 800 pN and 1.5 nN on lateral line primordial cells loaded with beads and observed the behavior of magnetic beads. In addition to the displacement of beads and the deformation of cell boundaries described above, we also observed magnetic beads leaving the cell boundaries. The magnetic beads were being pulled out of the cells of the primordium, but remained under the skin of the embryo as a pool of beads (Fig. 6.2). Curiously, such primordia and the affected cells continued to migrate collectively.

These results show, that the forces we were able to apply with our magnetic tweezer set-up were sufficient to displace magnetic beads inside embryos and deform cells. In

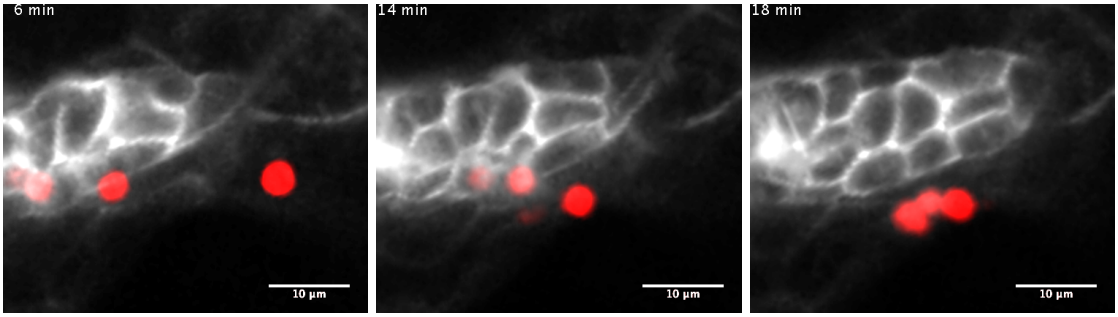

Figure 6.2.: Beads are being pulled out of cells of the lateral line primordium. These beads cannot be detected inside cell boundaries anymore and they do not move with the migrating primordium.

some cases, these forces were strong enough to pull beads out of living cells. We therefore concluded, that our magnetic tweezer set-up did not need to be adapted for producing even higher forces.

6.3. Application of forces on the lateral line primordium

Next, we explored the influence of an applied force on the behavior of collectively migrating cells of the lateral line primordium.

6.3.1. Application of force on cells in wildtype primordia

To test, whether we could observe a reaction in collectively migrating cells to an applied force, we applied a continuous magnetic field to lateral line primordia labeled with magnetic beads. Forces applied ranged from 800 pN to 1.5 nN over time spans of 30 min or more. Their behaviour under this continuous force was monitored using a confocal microscope. While the beads were clearly attracted to the magnetic tip, the tissue itself migrated past the force field and was not influenced by it (Fig. 6.4).

Using the claudinbGFP marker, we were not able to detect any effects of force application on the primordium, such as redirection of the tissue migration or migration arrest. We therefore tried another marker to be able to detect a possible re-orientation of cell protrusions.

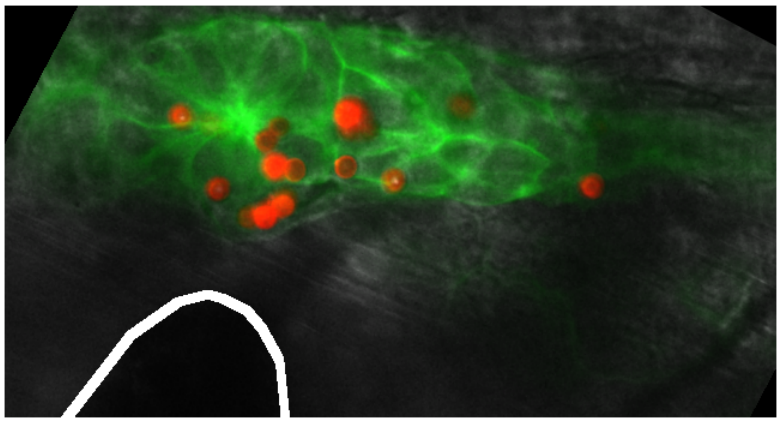

Figure 6.3.: Overview of a pulling experiment. Beads are marked in red, the lateral line primomordium is marked in green, the dark shadow in the bottom of the image is the tip of the magnetic tweezer that has been placed on the skin outside the zebrafish embryo.

6.3.2. Application of force on cells in wildtype primordia labeled with Lifeact-GFP

To monitor the direction of cell protrusions during force application we repeated the above experiments on embryos labeled with Lifeact-GFP, an actin marker that labels filamentous actin specifically [88]. Forces between 700 pN and 1.2 nN were applied for up to 90 min. The cell behavior under this continuous force was monitored using a confocal microscope. Similar to the experiment described above, the beads were attracted to the magnetic tip, but the tissue itself migrated past the force field (Fig. 6.5). On visual inspection of the recorded movies we could not detect a redirection of lamellopodia or filopodia during the application of the force (Fig. 6.5).

6.4. Application of forces on cells in sdf-/- primordia

Since there was no observed effect on the lateral line primordia in the above described pulling experiments, we wanted to test whether the migrating cells of the primordium were compensating for the applied force in some way. For example, cells in normal tissues may not react to increased force from their neighbours as they are all able to be guided by the extrinsic guidance cue, SDF1a. We reasoned that cells would be more

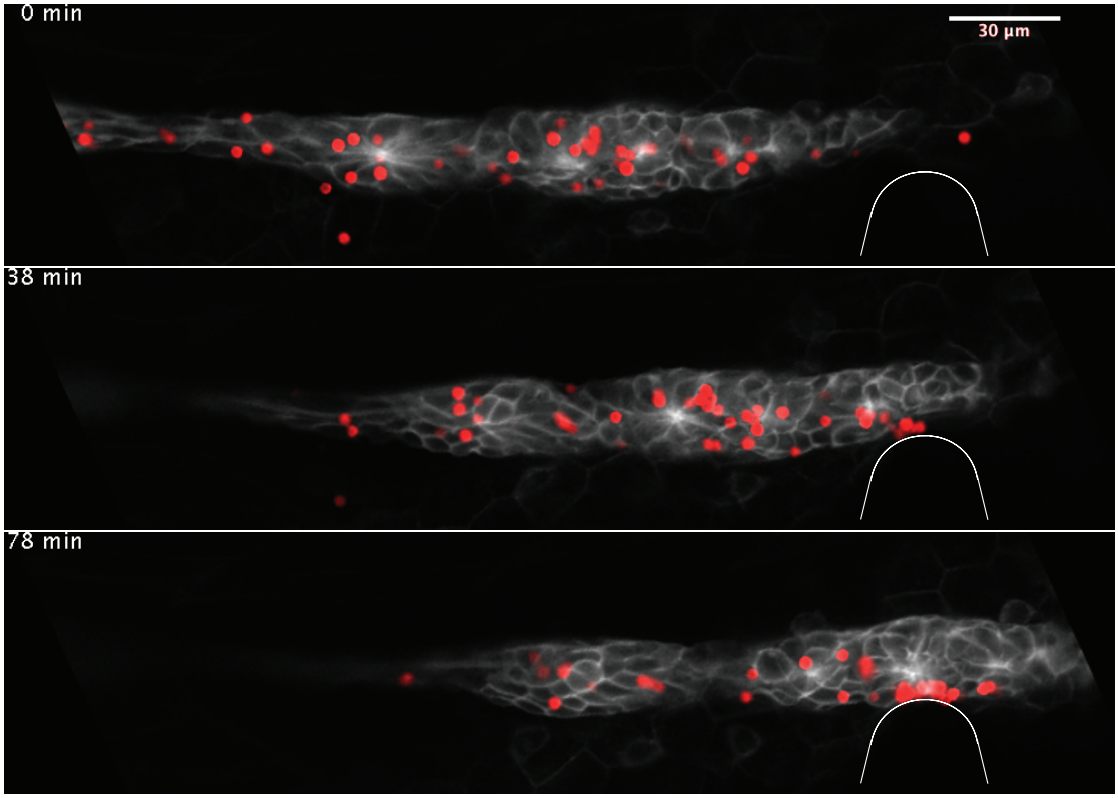

Figure 6.4.: Timelapse of force application on a primordium labeled with beads. The position of the magnet tip is marked with a white line. The migration speed of the primordium is not affected.

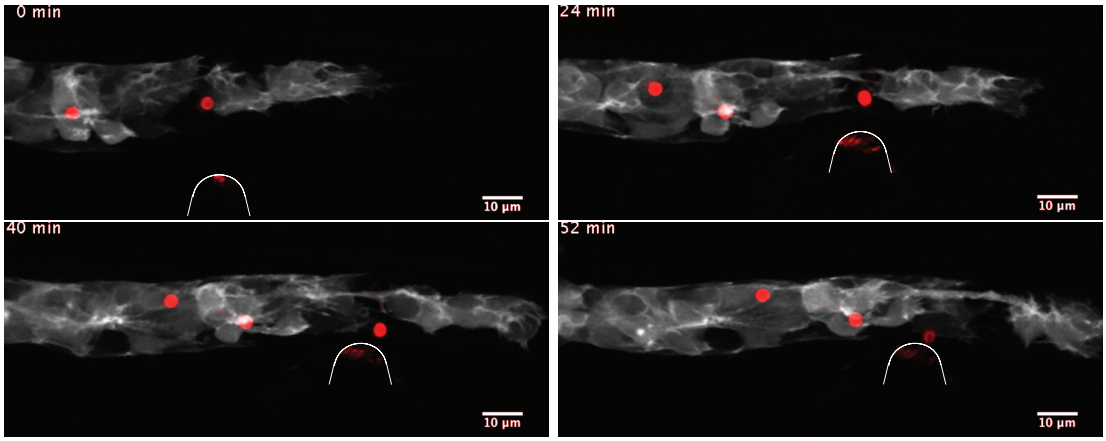

Figure 6.5.: Lifeact-GFP labeled primordium (white) with fluorescent magnetic beads (blue). The position of the magnetic tip is sketched in white. Transgenic embryos made by C. Revenu.

depdendent on the guiding influence of their neighbours in the absence of this extrinsic cue. For this reason, we took advantage of sdf -/- mutant embryos which have a genetic deletion of this signaling protein. The lateral line primordia in these mutants are motile, but do not migrate very far from the cranial region of the embryo, due to a lack of cell coordination. The defect in tissue migration made it more difficult to label the primordium without labeling of the background tissue, reducing the number of samples we could analyse. However, in those case where we could apply the magnetic tweezer approach, the application of a force of 800 pN or more for a minimum of 60 minutes did not lead to migration of the primordia or polarization of the cells.

7. Results - Development of a method to measure viscoelastic properties in embryos

As described in the previous section, the mechanical properties of a cell, like stiffness or softness, are critically affected by the composition of its actomyosin cortex. We wanted to investigate the mechanical properties of the cells in the lateral line primordium, as it is known that cell type differences are very important for its collective migration. For this we developed a method to measure these properties in cells in migrating tissues in a living embryo using magnetic tweezers.

7.1. Method development

To measure mechanical properties of cells in the lateral line primordium using magnetic tweezers, it was necessary to label primordia with magnetic beads. After applying a defined force to such beads, the deflection of each bead would deform the actin cortex of the cell. From the magnitude and speed of this deflection, viscoelastic properties could be calculated. These properties describe the elasticity, viscosity and viscoelastic relaxation time of the cell under investigation.The method used to determine these properties is described in detail in the following chapters.

7.1.1. Data collection

Embryos were labeled with magnetic beads using late-stage injections as discussed in Ch. 3.2.3. Experiments were conducted under an upright confocal microscope with a

0.8 numerical aperture 40x water dipping objective. The objective was chosen due to its long working distance, which allowed us to fit the magnet tip between the embryo and the objective.

Embryos were mounted on top of an agarose drop, with the primordium exposed. The magnet tip was placed at a distance of 10 - 40 μm from the primordium at a 90° angle from the direction of migration. Images were recorded at maximum speed, typically 0.066 s/frame to achieve a high time resolution. The movies were taken with a very high magnification, up to a resolution of 0.020 μm/px. The recording was started approximately 5 sec before the force was applied. The force was applied for 10 sec. A current of 4A was used, but since the distance between the magnet tip and the bead varied in each experiment, the applied force varied as well. The bead deviated from its original position under the action of the force.

After the force application was stopped, the bead relaxed back but did not reach its original position (see also Fig. 7.1). This was because the deviation was not only elastic. The viscous drag component of the deviation did not allow the bead to relax back elastically. The above measurements were repeated 3-5 times for the same bead, to achieve higher accuracy. After these measurements, a lower magnification overview image was acquired to determine the relative position of the magnet tip and the bead.

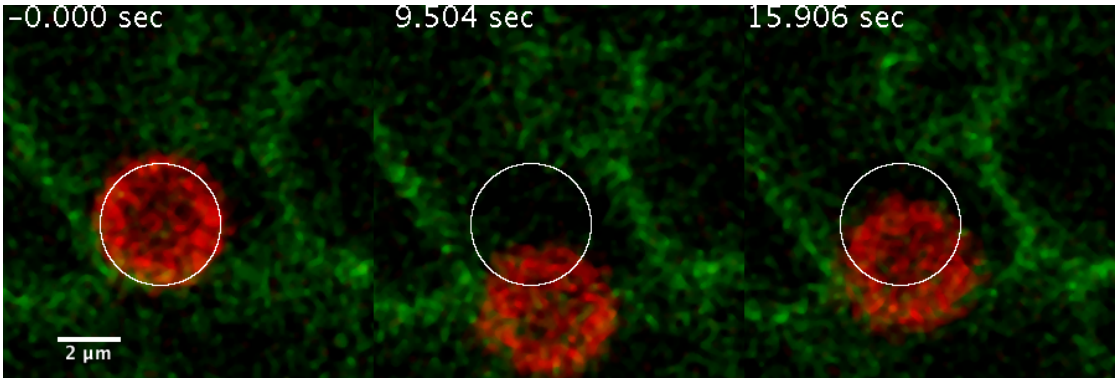

Figure 7.1.: Red: Dynabead 2.8 μm coupled to the fluorophore Atto 565, Green: Claudinb-GFP labeled cell. The panels show, from left to right, the position of the bead before, during and after force application. The white circle shows the original position of the bead. Due to the viscoelastic behavior of the cell, the bead does not relax back to its original position.

7.1.2. Segmentation and displacement curves

To quantify the deflection of the bead during the force application, an accurate method for determining the position of the bead prior and during the experiment needed to be developed. We used edge detection methods implemented in Matlab to segment the bead in the frames of the recorded movies.

Each frame was median filtered to remove speckles and re-sized to 3 times its original size (Fig. 7.2). Each bead was detected as a distinct object using thresholding. Any holes in the detected object were closed. In some of the movies the beads were not exactly spherical, since the image quality was sacrificed to achieve a higher sampling rate. To deal with this, we did not fit a circle around the bead, but decided to define the centroid position of the selected bead as the position of the bead.

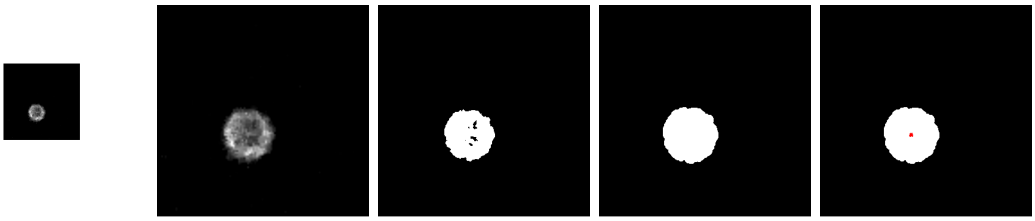

Figure 7.2.: Segmentation steps. From left to right: median-filtered image of Dynabeads, increased in size using bicubic interpolation, thresholded, holes filles, center of mass of the object was detected

In Fig. 7.3 the same track was first calculated using this algorithm and then the bead was tracked by hand. The automatic track was smoother and more precise since the automatic tracking reaches sub pixel resolution. Hand tracking was less precise, since the center of the bead had to be estimated and the precision of the bead position is limited to one pixel.

The relative position of bead and magnet tip was determined manually in the overview image. To calculate the displacement curve, only the component of the movement in direction of the tip was considered. Extracting these displacements lead to the characteristic displacement curve shown in Fig. 7.4.

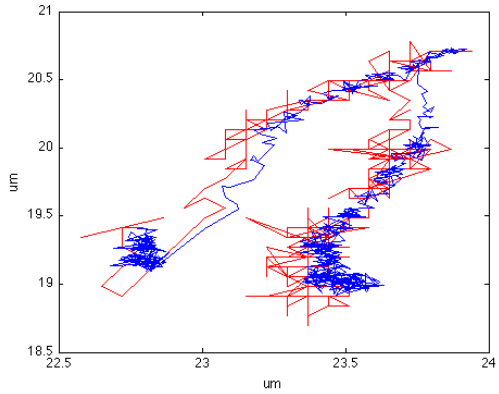

Figure 7.3.: Comparison of computer tracked bead (blue) position with hand tracked bead position (red) .

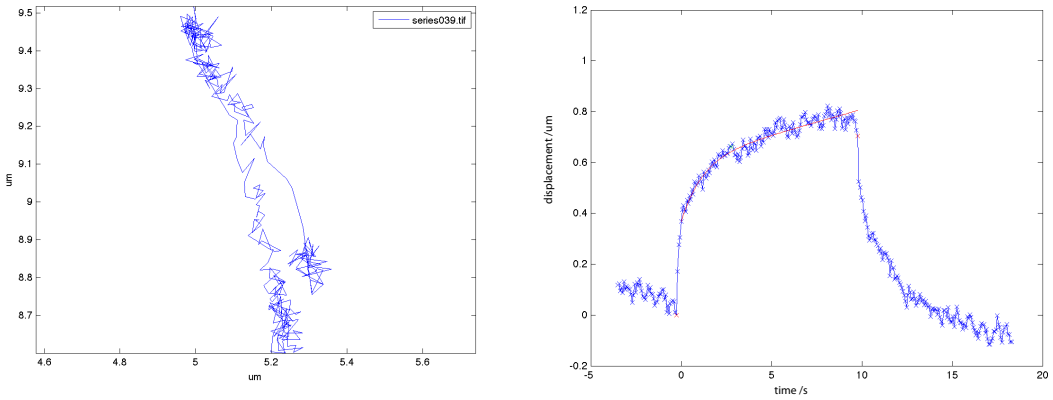

Figure 7.4.: Left: bead track; Right: component of movement of the bead in direction of the magnet tip

7.1.3. Comparison of different track shapes

The displacement curves of measurements performed on different cells are visually different. Fig. 7.5 (left) shows two deflection curves for beads located in two different cells (18 and 137 μm from the tip of the primordium). The deflection curves were normalized by the applied force for easy comparison. The bead located close to the tip of the primordium shows a higher deflection per force unit, than the bead located in the back of the primordium.

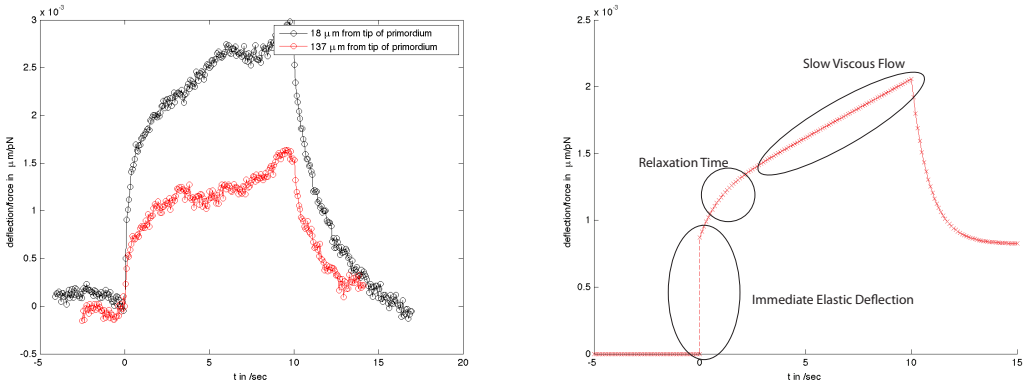

Figure 7.5.: Left: Deflection curves (normalized by the applied force) of two cells. One cell is located in the tip region of the primordium (black), one is located in the rosette region of the primordium (red). :

In some cases the second half of the curve is not completely smooth. These variations could be due to the migration of the primordium (see also discussion in Ch. 7.2.1). An alternative explanation could be an active retraction of the cell in response to the applied force.

7.1.4. Fitting of the model and parameter extraction

The reaction of a viscoelastic material to an exerted force can be described by the following equation (also discussed in Ch. 5.4.3).

$$\frac{x(t)}{F} = \frac{1}{k_e}\left(1 - \frac{k_1}{k_e + k_1} * e^{\frac{-t}{\tau}}\right) + \frac{t}{\gamma_0}, \tag{7.1}$$

$$\tau = \frac{\eta(k_e + k_1)}{k_e k_1}, \tag{7.2}$$

$$k = k_e + k_1 \tag{7.3}$$

The displacement curve $\frac{x(t)}{F}$ is described by three parameters. $k = k_e + k_1$ is a measure for the elasticity, γ_0 is a measure for viscosity and τ describes the relaxation time required by the system to switch from the elastic regime to the viscous regime.

The least square method was used to fit the theoretical curve to the acquired data in the following manner:
First, the factor $\frac{t}{\gamma_0}$ was fit to the viscous part of the curve. This was possible, because the $\frac{1}{\gamma_0}$ corresponds to the slope of the curve (see Fig 7.6 for illustration). The start of the viscous part was defined as starting three seconds after force application.
Second, the parameter $\frac{1}{k}$ was was fitted by manually defining the initial fast elastic reaction of the bead according to Fig. 7.6.
Finally, the rest of the of the curve was fitted within the parameter contraints defined in the previous steps and the viscoelastic parameters were extracted.

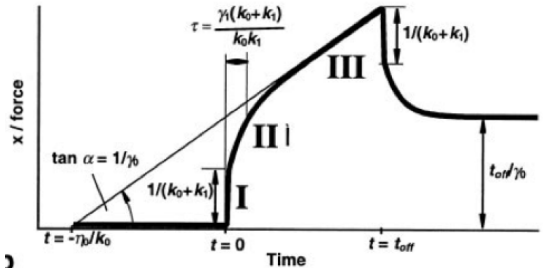

Figure 7.6.: Theoretical deflection curve of a viscoelastic material [9]. The parameter k_0 corresponds to k_e in equation 7.3

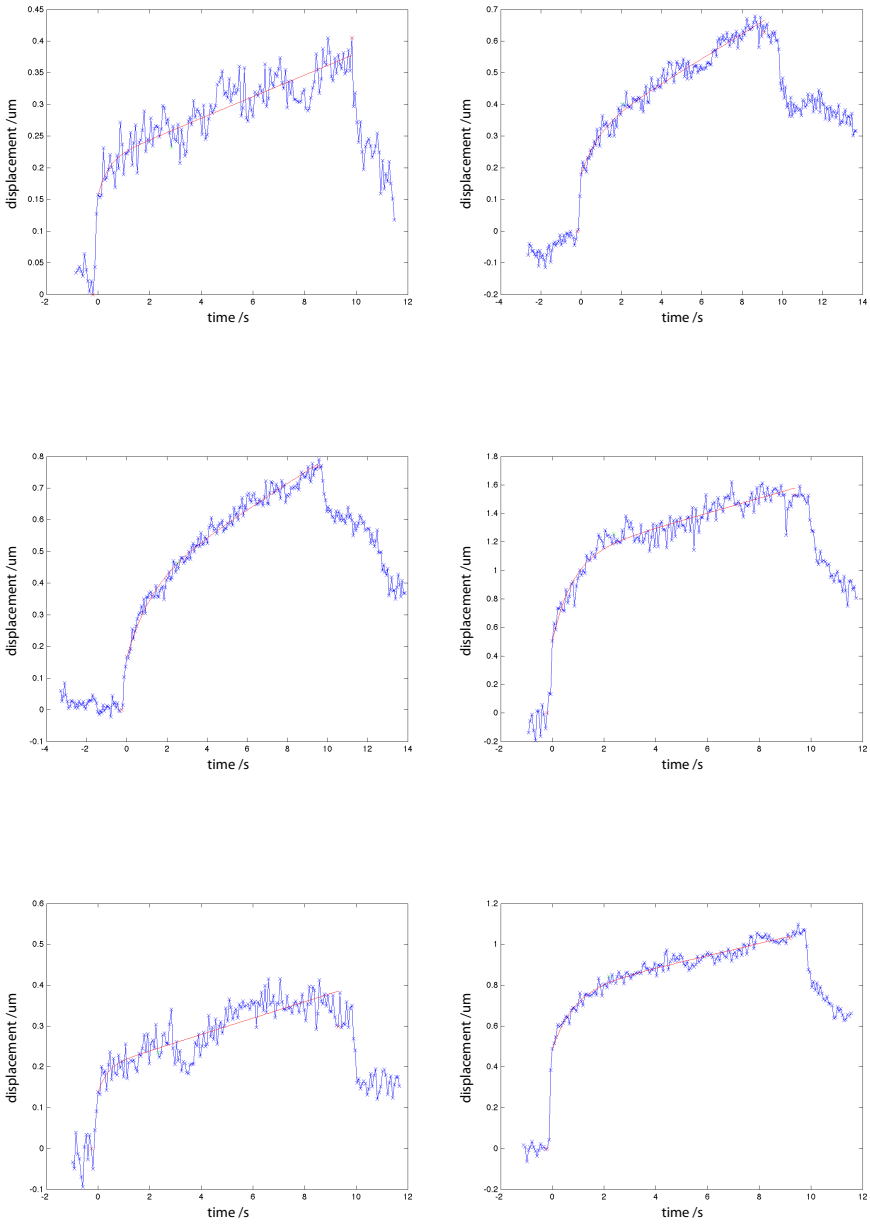

Figure 7.7.: Fitting example curves. Blue: Displacement curves as extracted from the timelapse images. Red: Fitted curves.

7.2. Experimental limitations

7.2.1. Migration of the tissue during measurement

The primordium migrated with an average speed of about 50 μm/h or 0.8 μm/min. This means, in a time span of 10 sec, the primordium migrated about 100 nm. It was difficult to uncouple the movement of the bead due to primordial migration and due to the magnetic field. This was because the bead movement was not smooth and uniform. If a force were applied for a long time, the bead movement due to primordial migration would be reflected in the displacement curves and make the fitting of the data less precise. However, the time of force application needed to be long enough, to collect a sufficient number of data points to ensure a good fit. Therefore it was necessary to find a good compromise between these two requirements. We decided on a force application of 10 sec, since we typically did not see a substantial migratory movement during that time.

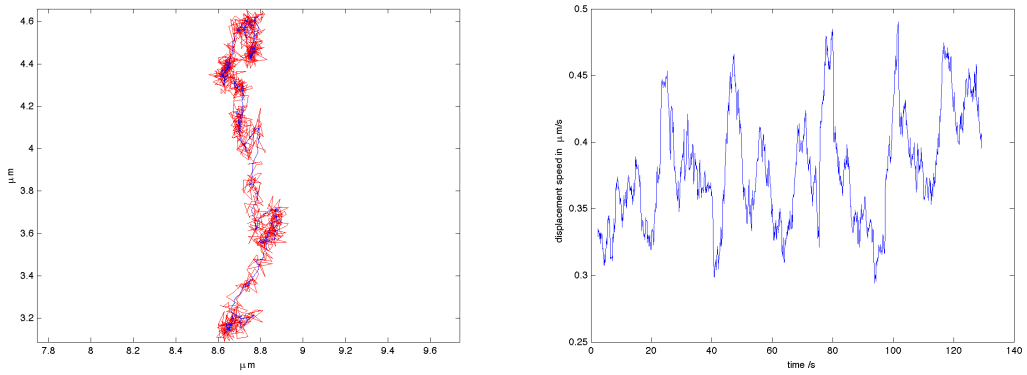

Figure 7.8.: Left: Track of a magnetic bead in a cell over 2 minutes. The displacements observed are due to the migration of the primordium. The original track is given in red. The blue line depicts the smoothed track of the bead. The moving average filter was used. Right: Displacement speed of the bead. The displacement for each timepoint was measured and the speed at each timepoint was calculated. A moving average filter was applied to emphasize the changes in speed. The displacement speed of the bead is not uniform, but varies considerably over the course of time. This displacement contributes to the deflection curve recorded during the experiment.

7.2.2. Errors due to movement of the bead in z-axis

For the reasons described above, image acquisition had to be as rapid as possible. This prevented us from tracking bead movement in 3D, due to the time required for z-stack imaging. However, it was possible to detect by visual inspection of the data whether the bead stayed in the same plane during the experiments (Fig. 7.9). Beads in the focus plane display a clearly visible fluorescent ring, while beads not in the focus plane are less well defined (Fig. 7.9, right). Experiments where the bead moved out of focus were excluded from the analysis.

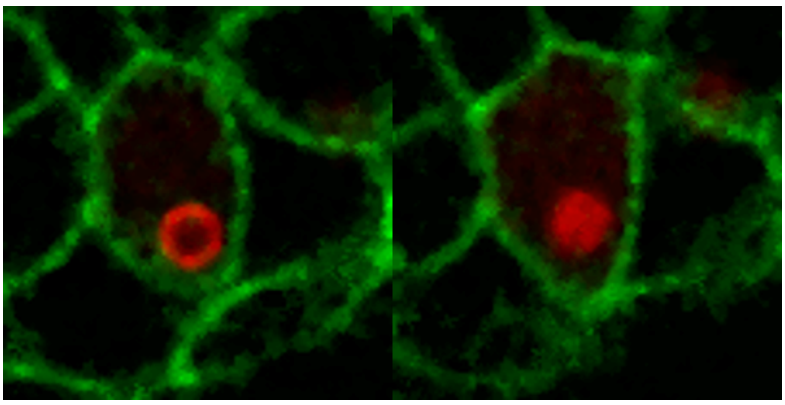

Figure 7.9.: Red: Dynabead, Green: cells marked with claudinbGFP. Image of the same bead in focus(left) and out of focus (right)

7.3. Control measurements

7.3.1. Repeated force application of the same cell

To check whether an active reaction of the cell to the applied force can be detected, experiments were performed where a force was repeatedly applied to the same cell. Fig. 7.10 shows the deflection curves for a cell on which a force of 366 pN was applied for 10 seconds each, with a 10 second break in between. This oscillation was repeated over 11 cycles (over 220 seconds). For each cycle the displacement curve was extracted (Fig. 7.10). The basic shape was the same for each curve. Variations were especially visible in the later parts of the force application, which is the part describing the viscous drag

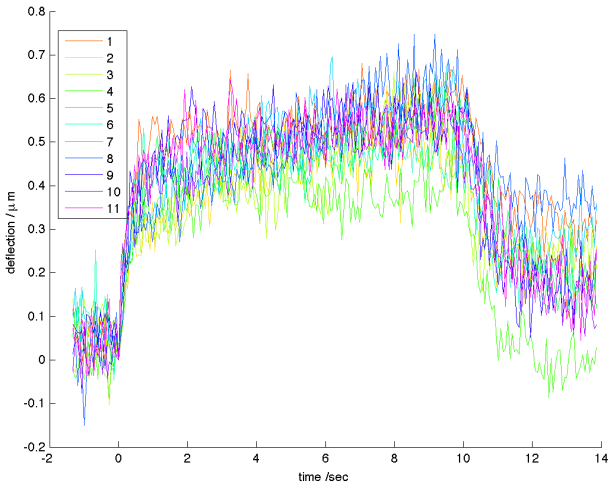

Figure 7.10.: displacement curve of same cell, measured 11 times with a force of 400 pN

of the bead (Fig. 7.10). The viscosity parameter γ_0, the elasticity parameter k and the relaxation time τ were extracted from each curve.

To verify that parameters do not change over the course of the measurements, we compared the averages of the first five measurements, with the averages of the last five measurements for all three viscoelastic parameters. The averages for each parameter are displayed in 7.11, left column. We found no significant difference for all three parameters. Each extracted parameter does not depend on the number of previous measurements. The cell does not react to a repeated force application with a stiffening or loosening of the actin cell cortex.

To measure the random error in our experiment, the relative standard deviations for each parameter were calculated. The relative standard deviation is smallest for k (9% standard deviation/mean) and larger for τ and γ_0 (68% and 40%, respectively) .

Due to these variations, we decided to do repeated measurements for each cell. Averaging the results of these measurements allowed us to increase their accuracy. In Fig. 7.11, right column, the averages of the first three, the first five and all measurements are compared. This was done to test how many measurements are necessary to calculate an average that does not deviate significantly from the average of all measurements anymore. After three cumulative averages none of the parameters change significantly any further, allowing us to limit measurement to 5 per cell.

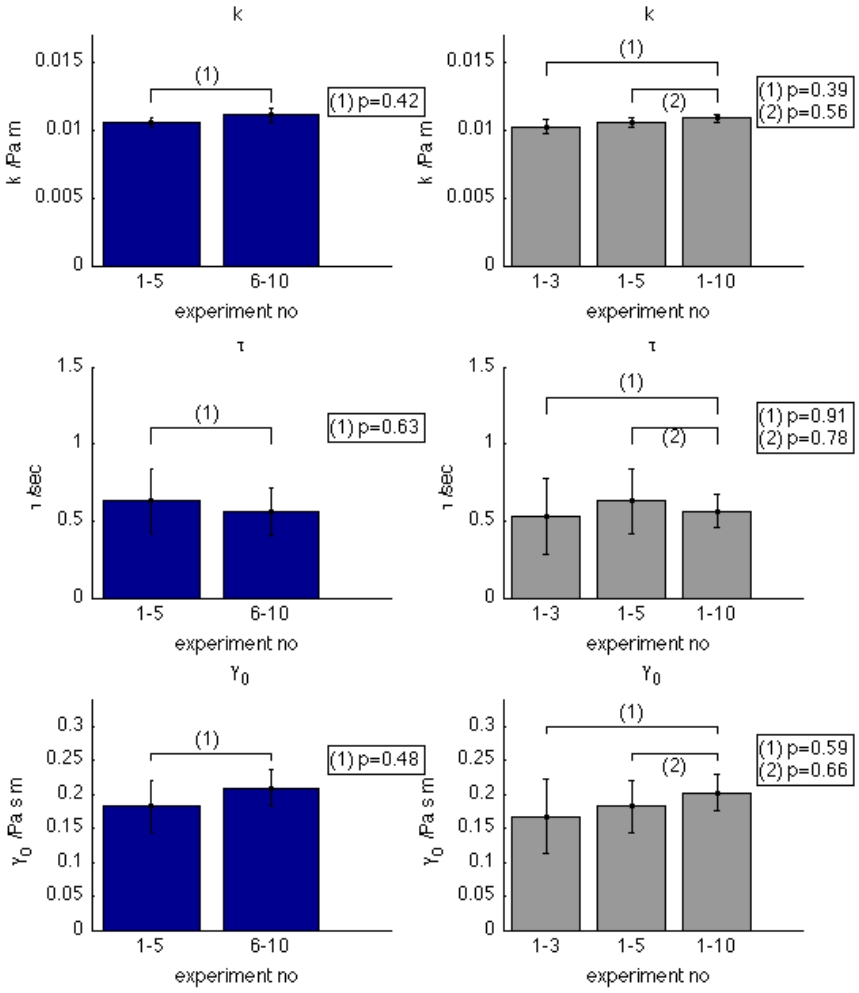

Figure 7.11.: Left column: Comparison of the averages of the first five measurements (1- 5), with the averages of the last five measurements (6-10) for all three viscoelastic parameters. Error bars are standard error of the mean (See footnote page 127 for definition). The p-values (as calculated by a two tailed t-test) are given in each panel. We find no significant difference in any of the parameters.
Right column: The averages of the first three, the first five and all measurements are compared. All error bars are standard error of the mean. The p-values (as calculated by a two tailed t-test) are given in each panel. After three cumulative averages none of the parameters change significantly any further.

7.3.2. Linear Elastic Control

Any elastic expansion of a linear viscoelastic material has to be linearly proportional to the applied force. To test this assumption three beads were measured repeatedly after applying a range of forces on them. The initial deflection of the bead in each case was measured. Each measurement was repeated five to eight times and the results were averaged (Fig. 7.12).

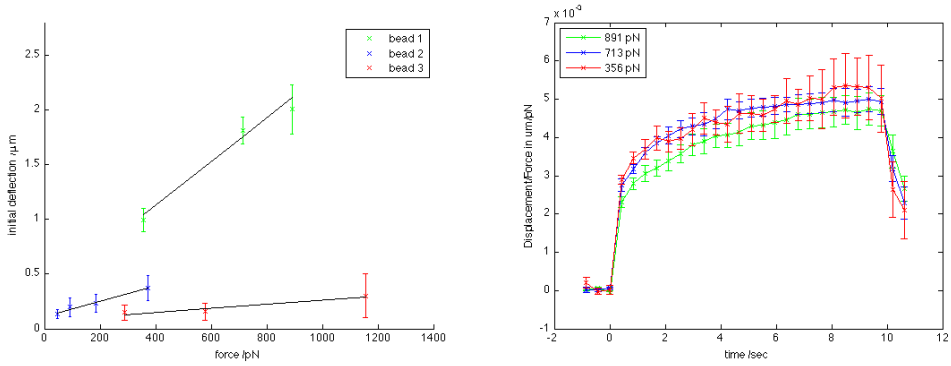

(a) Initial deflection measured for three beads. Error bars are standard deviations of the measurements.

(b) Example for deflection curves normalized by the applied force with different colors denoting different applied forces. The force was applied several times and the deflection curves were averaged. Error bars are standard errors of the mean.

Figure 7.12.

7.3.3. Blebbistatin

To show that the measurements of viscoelastic parameters are indeed a reflection of the structure of the cortex, we treated embryos with 20 μM Blebbistatin (Bb), a myosin II inhibitor, for 30 min and measured the change in viscoelasticity. After 30 min treatment with Blebbistatin the primordium stops migrating and loses cohesion. The viscosity γ_0 of cells treated with Bb does not change significantly. The elasticity parameter k and the relaxation time τ decreases (Fig. 7.13).

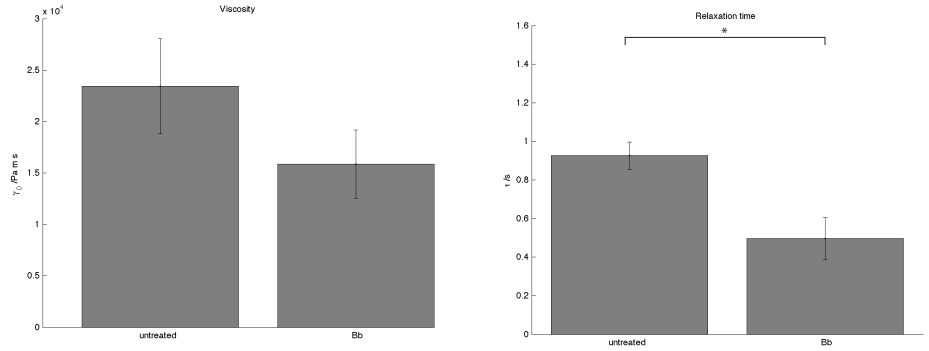

(a) Viscosity before and after treatment with 20 μM Blebbistatin. The difference is not significant (p=0.28, paired t-test)

(b) Relaxation time before and after treatment with 20 μM Blebbistatin. The difference is significant (p<0.01, paired t-test)

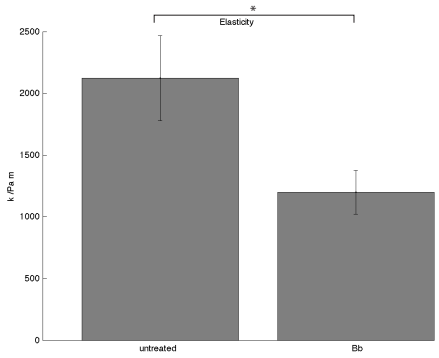

(c) Elasticity before and after treatment with 20 μM Blebbistatin. The difference is significant (p=0.03, paired t-test)

Figure 7.13.: All error bars standard error of the mean, N=11

8. Results - Viscoelastic measurements on a migrating tissue

8.1. Probing differences in material properties across the lateral line primordium

Having established a method to probe material properties of cells of the primordium, we turned our attention to the influence of cell position on these key parameters. To investigate the viscoelasticity of the wild-type migrating primordium, 49 cells from 18 embryos were measured. The measurements were repeated up to ten times for each cell. The three viscoelastic parameters were extracted and averaged for each cell. All together, I performed 315 measurements.

parameter 1	**parameter 2**	**Pearson's r**	**p**
k	γ_0	0.135	$p<0.05$
τ	k	-0.072	$p>0.1$
γ_0	τ	0.007	$p>0.1$

Table 8.1.: Pearsons correlation coefficient and p values for 300 measurements

We calculated the Pearson's correlation coefficient (see 11.1 for definition) between the three parameters, to test if they correlate with each other(see 11.1 for definition of Pearson's correlation coefficient). A positive correlation between the elasticity and viscosity was found (Tab. 8.1, $p<0.05$). The other parameters did not correlate with each other. This means, that cells with a higher elasticity parameter tend to be more viscous as well. However, while being significant, this correlation is not very strong.

Since the primordium shows a clear front to back polarity, we plotted the measurements as a function of distance from the primordium front tip. To reduce the noise, we binned

the data into 30 μm or 50μm size bins. Fig. 8.1 shows the number of cells and the number of different embryos in each bin.

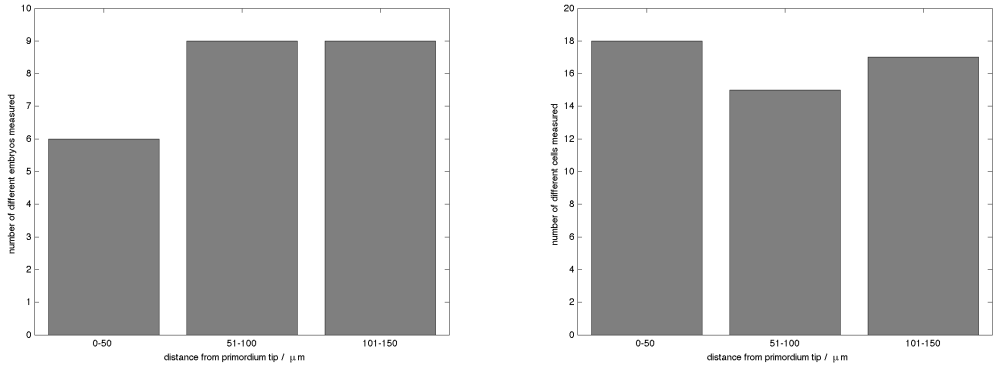

Figure 8.1.: Number of different cells and different embryos measured in each 50 μm bin

8.1.1. Measurement of spatial changes in the viscosity in the lateral line primordium

The viscosity is a measure for the viscous flow of the bead in the second half of the viscoelastic regime. An increase in the viscosity parameter γ_0 denotes an increase in the viscosity of the material. Boxplots were used to visualize the viscosity as a function of the position of the cell (distance from the front primordium tip)[1].

The viscosity of 49 cells was measured. The average viscosity of all 49 cells was 0.0163 Pa s m with a standard deviation of 0.0088 Pa s m. There was no significant difference between the viscosity of the front tip of the primordium and the back (Fig. 8.3).

Histogram. Fig. 8.4 shows a histogram of the viscosities of 49 measured cells. There is a strong peak at a viscosity of 0.013 Pa s m to 0.015 Pa s m, with the values of the measurements skewing slightly towards smaller numbers.

[1]Boxplots visualize several values at once:
The red line represents the median.
The bottom of the box represents the 75th percentile, while the top represents the 25th percentile.
The vertical length of the box represents the interquartile range (IQR). 50 % of the measurements lie within the IQR.
The whiskers represent all measurements that are within 1.5 times IQR. The rest of the measurements are defined as outliers.
Outliers are represented as dots.
The width of the boxplot does not signify anything.

8.1.2. Measurement of spatial changes in the relaxation times in the lateral line primordium

The relaxation time is a measure of the time it takes for the system to switch from the elastic regime to the viscous regime. The average relaxation time measured for 49 cells was 0.91 sec with a standard deviation of 0.35 sec.

When plotted over the length of the primordium, a distinct pattern is visible (Fig. 8.5). The average relaxation time is significantly lower in the first 50 μm of the primordium, measured from the front tip ($p<0.01$, Mann-Whitney U-test).

The average relaxation time increases from 0.79 sec $\pm$ 0.18 sec [2] in the first 50 μm from the front tip of the primordium to 1.05 sec $\pm$ 0.4 sec in the region between 51μm to 100 μm from the front tip. The average relaxation time decreases to 0.91 sec $\pm$ 0.38sec in the last third (101 μm to 150 μm from the front tip) of the primordium ($p=0.07$, Mann-Whitney U-test).

Histogram. The histogram in Fig. 8.5 shows a strong peak in relaxation time at 0.69 sec. 30 % of the measurements fell within that interval.

8.1.3. Measurement of spatial changes in the elasticity in the lateral line primordium

The elasticity is a measure for the immediate reaction of the cell material to an applied force. For the linear elastic case the deformation force F, the elasticity parameter k and the elastic deformation length x have the following relation:

$$F(x) = k * x$$

Therefore, a material with a high elasticity parameter is more resistant to an external deformation force.

The elastic parameter k was measured for 49 cells. The average elasticity was $1.6 * 10^{-3}$ Pa m with a standard deviation of $1.1 * 10^{-3}$ Pa m.

[2] all numbers are average $\pm$ standard deviation

Boxplots were used to visualize the elasticity as a function of the position of the cell (distance from the tip of the primordium). Two different bin sizes were chosen to depict trends in the change of the elasticity parameter k as a function of the position of the cells (Fig. 8.7 and Fig. 8.8).

Bins of the size of 50 μm divide the primordium into three parts (Fig. 8.7). There is a significant increase in the average elasticity parameter k between the first third (0 to 50 μm from the front tip of the primordium) and the latter two thirds (p=0.02, Mann-Whitney U-test). The elasticity increases from (0.96 $\pm$ 0.56) $*10^{-3}$ Pa m [3] to (1.7 $\pm$ 1.1) $*10^{-3}$ Pa m. This denotes a 70% increase of the elasticity parameter. The elasticity parameter continues to increase in the last third of the primordium (101-150 μ m from the front tip of the primordium) to (2.1 $\pm$ 1.2) $*10^{-3}$ Pa m (p$<$ 0.001, Mann-Whitney U-test). The average elasticity parameter k increases by 220 % between the first third of the primordium and the last third. The difference in average elasticity parameter between the second and last third is not significant (p=0.058, Mann-Whitney U-test).

To visualize the behavior of the elasticity parameter k more in detail, we plotted it against the position of the cells in 30 μm bins (Fig. 8.8), which divide the primordium in five parts of equal length. The average elasticity parameter is constant for the first 60 μm of the primordium: (1.1 $\pm$ 0.7) $*10^{-3}$ Pa m and (1.1 $\pm$ 0.37) $*10^{-3}$ Pa m. The average elasticity parameter increases slightly for cells in the range between 61 and 90 μm to (1.6 $\pm$ 1.2) $*10^{-3}$ Pa m. Cells situated between 91 and 120 μm reach the highest average elasticity parameter: (2.5 $\pm$ 0.9) $*10^{-3}$ Pa m. This is a 220% increase in relation to the previous bin. Cells in the range between 121 and 150 μm from the front tip of the primordium show a slightly decreased average: (2.2 $\pm$ 1.3) $*10^{-3}$ Pa m compared to the previous bin.

Histogram. Fig. 8.7 shows a histogram of the elasticities for all 49 measured cells. The histogram is strongly skewed towards smaller values of k. 34% of all values fall in the range of 0.3 $*10^{-3}$ Pa m and 0.85 $*10^{-3}$ Pa m.

[3] all numbers are average $\pm$ standard deviation

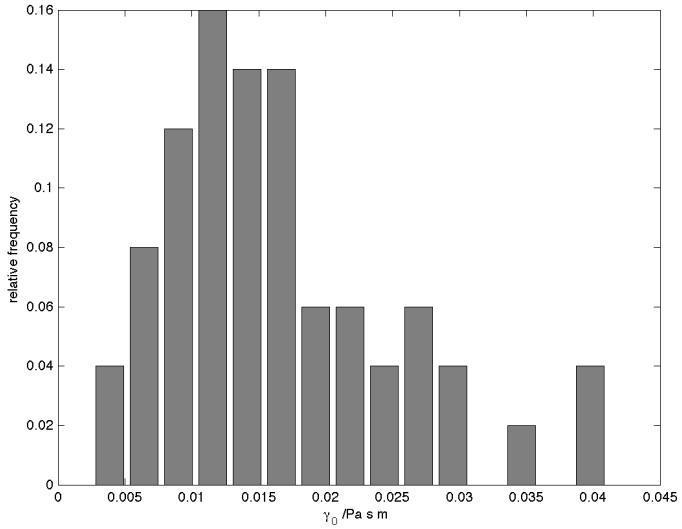

Figure 8.2.: Histogram of the measured viscosity for 49 cells in the primordium.

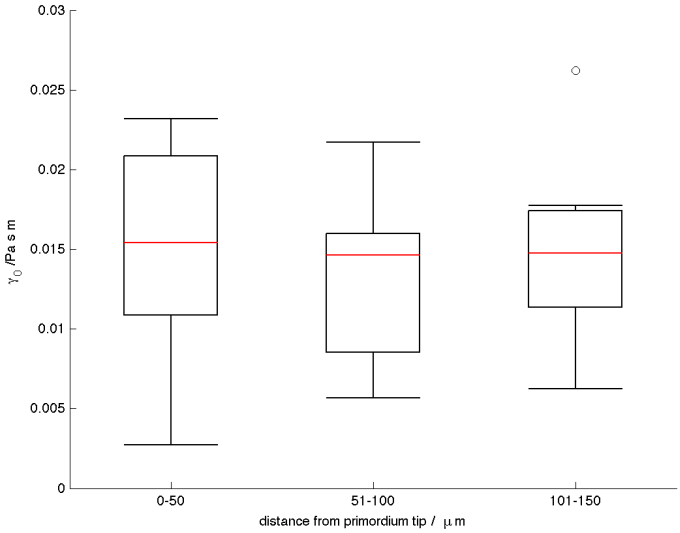

Figure 8.3.: Spatial changes of viscosity in the lateral line primordium. The x-axis describes the position of the measured cell as a distance from the primordium tip.

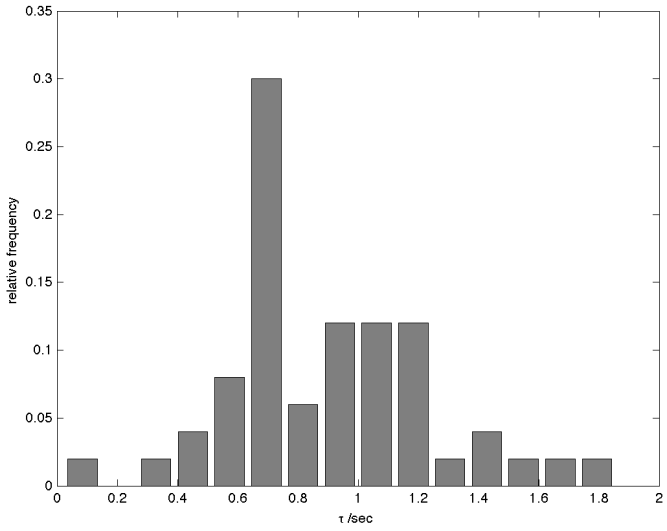

Figure 8.4.: Histogram of the measured relaxation time for 49 cells in the primordium.

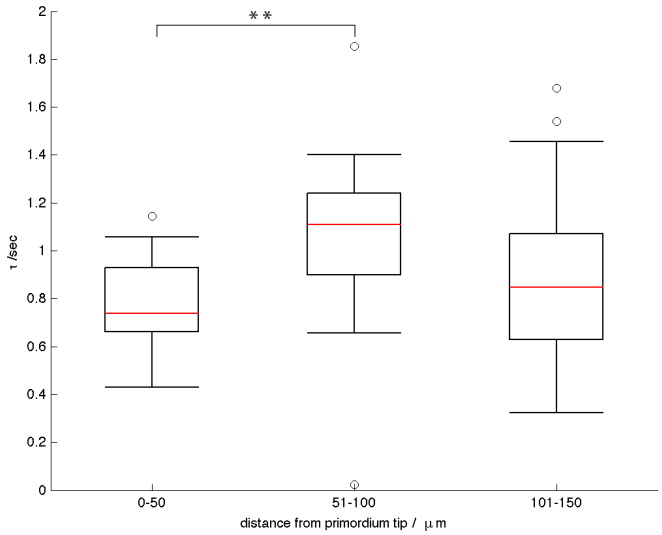

Figure 8.5.: Spatial changes of relaxation time τ in the lateral line primordium. The x-axis describes the position of the measured cell as a distance from the primordium tip.

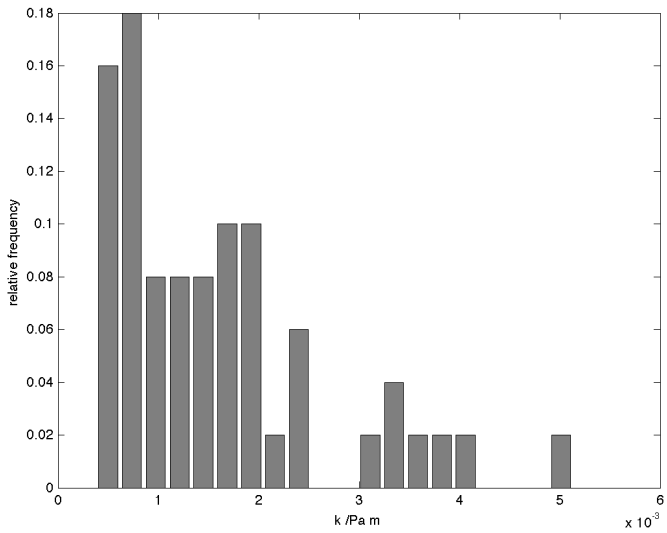

Figure 8.6.: Histogram of the measured elasticity parameter for 49 cells in the primordium.

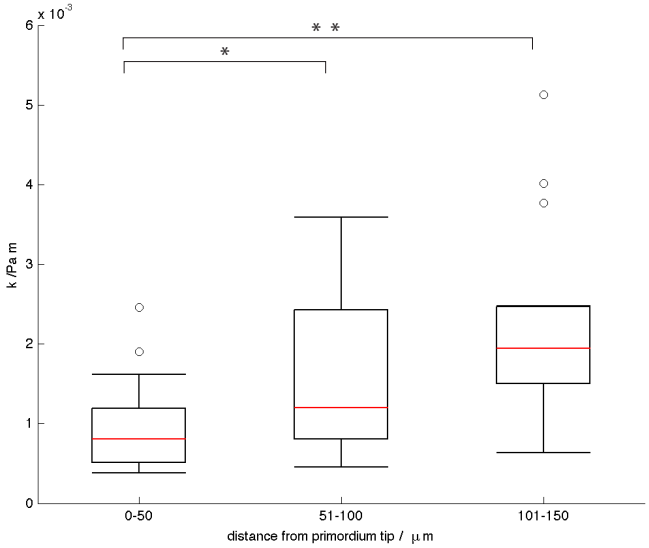

Figure 8.7.: Right: Spatial changes of the elasticity parameter in the lateral line primordium. The x-axis describes the position of the measured cell as a distance from the primordium tip.50 μm bins

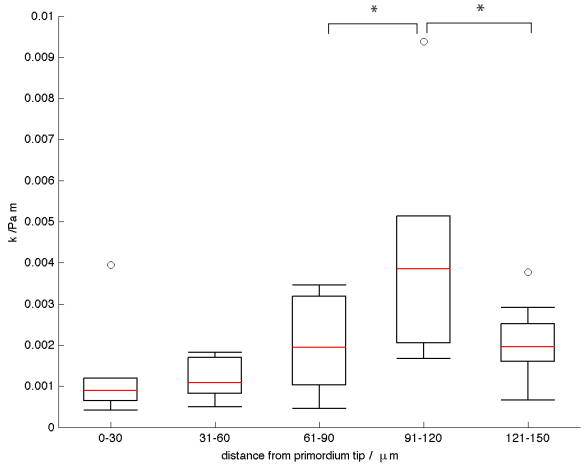

Figure 8.8.: Spatial changes of the elasticity parameter in the lateral line primordium. The x-axis describes the position of the measured cell as a distance from the primordium tip. 30 μm bins

8.2. Effect of cell-type differentiation on material properties

Previous work has shown that cells in the primordium undergo a mesenchymal epithelial transition as they go from the front of the primordium towards the back. These changes can be observed using cell shape and morphology. The cells in the tip of the primordium are flat, while the cells in the back form tall, immotile rosettes. These changes correlate with the migrational behavior of the cells. The leading region is very motile, while the trailing region is less active with the back slowing down in speed. It is not known however, if these changes also correlate with a change in material properties.

It has been shown, that the formation of rosettes is induced by the ligand FGF (fibroblast growth factor). The corresponding FGF-receptor can be inhibited by a small molecule called SU5402, treatment with which causes the primordium to lose rosettes and migrational ability. We therefore decided to use SU5402 to measure the effect epithelial differentiation has on material properties.

8.2.1. Binning

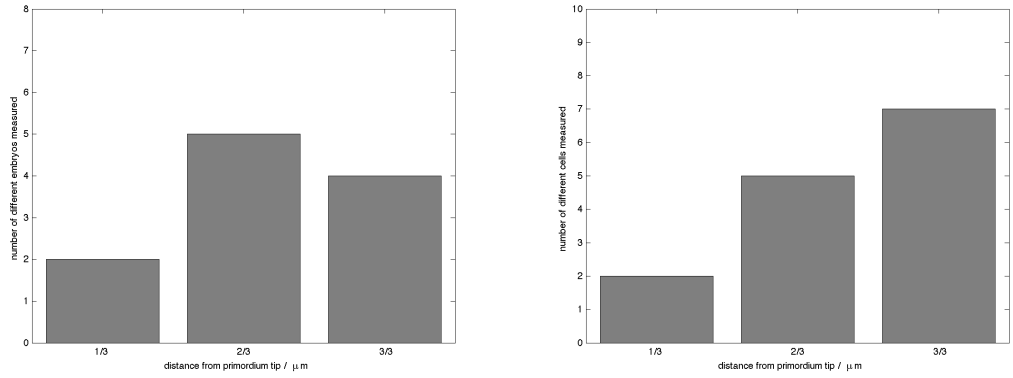

Figure 8.9.: Number of different Cells and different embryos measured in each 60 μm bin

We wished to compare the viscoelastic properties of the primordium in an untreated situation with a primordium treated with SU5402, a membrane permeable FGF receptor inhibitor. It has been shown that during SU5402 treatment the lateral line primordium stretches. It becomes longer and thinner. The average length of the primordium increases from 150 μm to approximately 180 μm. For a better comparison between the two

conditions, the size of the bins during data analysis was changed from 50 μm in the untreated case to 60μm in the SU5402 treated case. In other words the primordium was divided into thirds in both cases. For clarity we will call these three parts the tip region, center region and back region of the primordium.

So far, we were only able to measure two cells in the first third of the primordium. For this reason a statistically sound comparison of cells in the tip region of the primordium was not possible. For completeness we included these measurements in Fig. 8.10, 8.11 and 8.12.

8.2.2. Viscosity

The average viscosity for all measured cells was (0.01$\pm$ 0.008) [4] Pa s m. Compared to the average relaxation time from untreated measurements ((0.01 $\pm$ 0.009) Pa s m) we find no significant difference.

The viscosity in SU5402 treated cells was highest for cells in the center region of the primordium at (0.015$\pm$ 0.011) Pa s m. It was not significantly different from untreated cells in that region. The viscosity dropped by 210 % to (0.007 $\pm$ 0.004) Pa s m for cells positioned in the back region of the primordium. In this region, the viscous parameter in the SU5402 primordium is significantly different from untreated cells ($p < 0.01$, Mann-Whitney U-test) (Fig. 8.10).

8.2.3. Relaxation time

The average relaxation time for all cells was (0.85 $\pm$ 0.16) sec. Compared to the average relaxation time from untreated measurements (0.91 $\pm$ 0.35) sec) we find no significant difference. The average relaxation time decreased significantly in the center region of the primordium ($p < 0.05$, Mann- Whitney U-test).

Compared with untreated cells, the average relaxation time decreased significantly in the center region of the primordium, while the back region showed no significant difference (Fig. 8.11).

[4] all numbers are average $\pm$ standard deviation

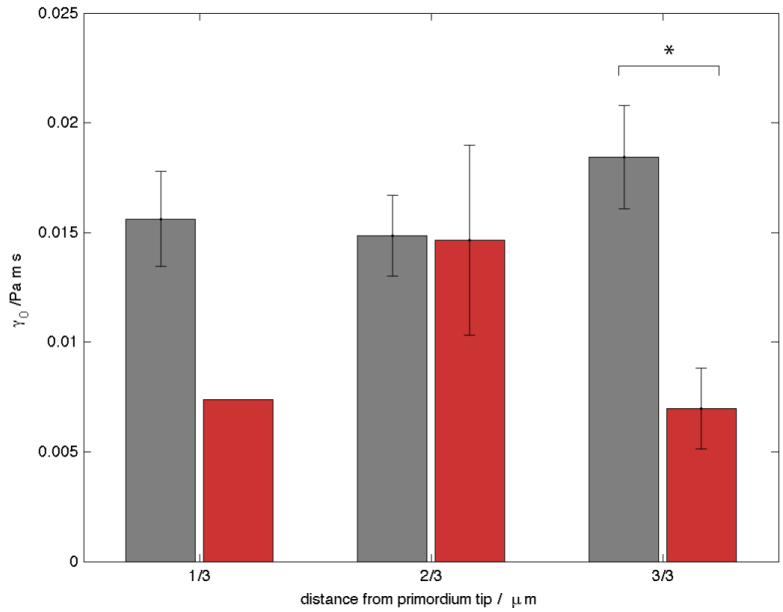

Figure 8.10.: Viscosity: Comparison of treated and untreated primordia; gray: untreated primordium, red: SU5402 treated primordium
($p < 0.01$ Mann- Whitney U-test)

8.2.4. Elasticity

The average elasticity for all cells was $(6 * 10^{-4} \pm 4 * 10^{-4})$ Pa m. This is significantly smaller than the average relaxation time from untreated measurements (0.002 $\pm$0.001) Pa m) .

The average elasticity in SU5402 treated embryos decreased from the tip region to the back region of the embryo. In comparison with untreated cells, less force needs to be applied to those cells to achieve the same deformation. Both, in the center and the back region of the primordium we measured a significantly decreased elasticity parameter k compared with untreated cells (Fig. 8.12).

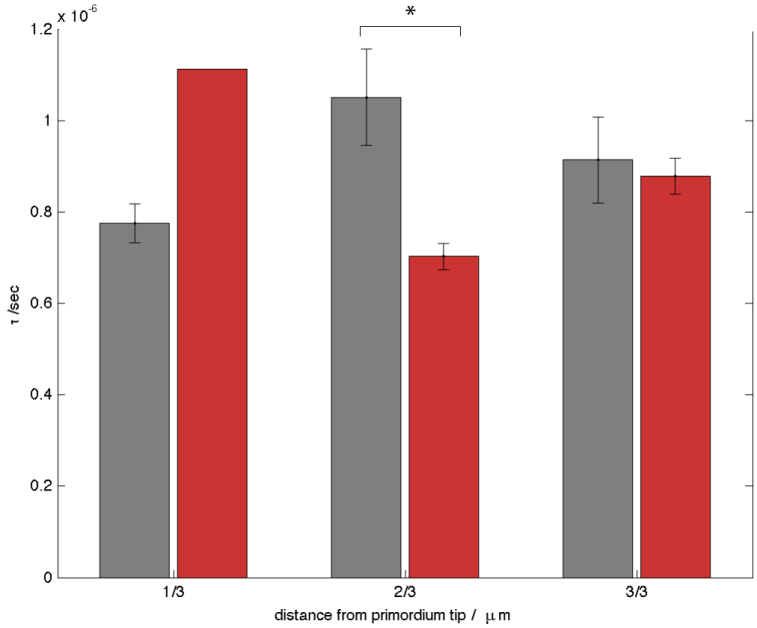

Figure 8.11.: Relaxation time: Comparison of treated and untreated primordia; gray: untreated primordium, red: SU5402 treated primordium ($p < 0.05$ Mann-Whitney U-test)

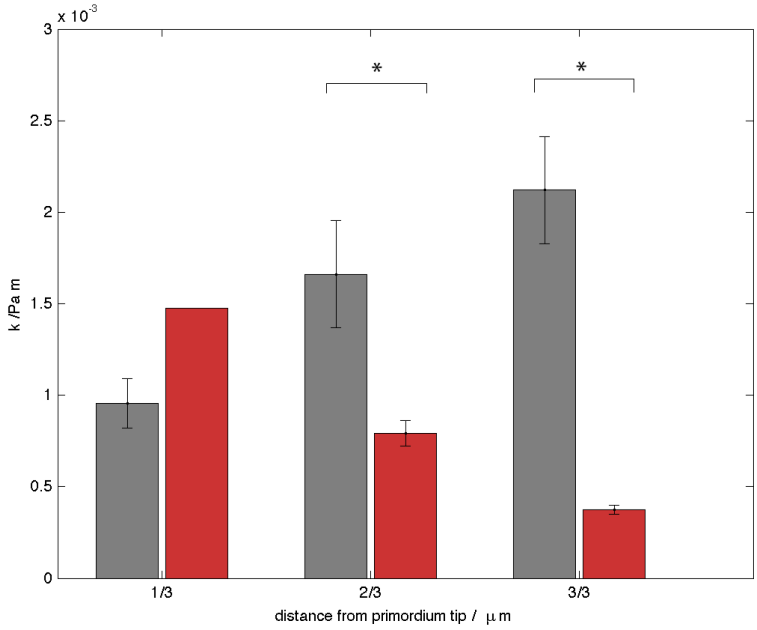

Figure 8.12.: Elasticity: Comparison of treated and untreated primordia; gray: untreated primordium, red: SU5402 treated primordium, ($p < 0.01$ for both cases)

8.2.5. Conclusion

The treatment with SU5402 not only leads to morphological changes in the primordium, it also has an effect on the mechanical properties of the constituent cells. The profiles of all three viscoelastic parameter differ significantly from their untreated counterparts. This change is most pronounced in the back region, but it is interesting to note, that the cells in the center region of the primordium behave in all three parameters exactly like untreated cells of the tip region. From a mechanical/ viscoelastic point of view, treatment with SU 5402 prolongs the tip region further into the primordium. The rosette cells become more like mesenchymal cells.

However for better statistical treatment, the number of measurements of SU5402 treated is still rather small and needs to be increased, particularly in the leading region of the primordium.

9. Summary and Discussion

9.1. Applying force on a tissue migrating in vivo

Constant forces were repeatedly applied to the lateral line primordium, while observing the migratory behavior of single cells. We could not detect any difference in migratory behavior of these cells in comparison with lateral line primordia in the control situation (i.e. when no force was applied). This experimental observation was further substantiated using actin markers to visualize changes in lamelopodia/filopodia behavior. In this case we also detected no visible differences between control experiments and force application experiments. It is possible that this indicates a complete lack of mechanosensation in the lateral line primordium. However as I will discuss in the following paragraphs, additional experiments are needed to define the impact of pulling forces on cell guidance.

We have been applying forces in the range between 800 and 1200 pN (or more). Since these forces are high enough to pull beads out of the primordium and since the observed cortex deformations are much more severe than usually observed, it is more then likely that we are already applying forces which are much stronger than those present in the natural environment. Therefore it is unlikely that stronger forces are needed for these experiments. There is a small possibility that mechanosensitive mechanisms operate on weaker forces. However, migratory reaction of single cells to an applied force has been described [10]. In these experiments a force of 1.5 nN had been applied directly to the mechanosensitive cadherin complex. These forces are in the same order of magnitude as the forces used in our experiments. This indicates that weaker forces will not have a different effect on the migratory behavior of the lateral line primordium.

We applied forces to the cytoskeleton that were constant over time. However, these viscoelastic measurements in our experiments suggest that the relaxation time of the cytoskeleton after application of an external force in the lateral line primordium is in the

order of magnitude of about one second [10]. For longer relaxation times, the actin cortex switches from an elastic behavior to a viscous behavior, which makes force propagation along the cell cortex less likely. This is because compared with an ideal elastic material, viscous material show viscous damping which is due to the internal resistance of viscous fluids and the energy dissipation that accompanies it.

It is possible that shorter cycles (less than 1 sec) of applied force might have a more noticeable effect on the migration of the primordium, as these forces would always be applied to materials in an elastic regime. Of course our experimental approach aims to define the nature of the forces that are normally transmitted between cells during this collective process. While the temporal features of cell-cell force transmission remain unclear, a number of recent studies have shown that related actomyosin driven processes are pulsatory in nature [89] [90] [91]. Future experiments could therefore investigate the role of pulsatory force application on reorientating cells.

Our expectation was that applying defined pulling forces would cause the redirection of juxtaposing cells and, ultimately, the entire migrating tissue. However a recent study by Weber et al. [10] showed that single explanted Xenopus mesendoderm cells react to an applied external force by migrating in the opposite direction of the applied force. It appears that resistance against the external force stimulates these cells to migrate in the opposite direction. If this behavior is applicable to our experiments, then it could explain the lack of change in filopodia direction in the measured cell, since the redirection of the filopodia would be towards the center of the primordium. In this case the redirection of the filopodia would be directly opposite to the applied force.

However, the experiments performed by Weber et al. [10] differ in several aspects from our experiments. While Weber et al. redirected the migration of single cells on culture dishes, we applied forces on a tissue consisting of one hundred collectively migrating cells inside the embryo. Another major difference is that Weber et al. applied forces via a magnetic bead directly coupled to a cadherin complex, while beads in our experiments were located inside cells. We applied forces to the cells directly. It is possible that any discrepancies between our results and the results described by Weber et al. can be explained by these differences.

Additional experiments should be conducted, in which the experimental factors discussed above are varied: Lower forces on shorter timescales should be applied. Another issue is the expected outcome of force application to the migrating collective. It would be

interesting to repeat the experiment while applying forces from different directions relative to the direction of migration.

It is however also possible, that additional experiments will not result in change of the migratory behavior of the lateral line primordium. Due to its biological importance for the schooling behavior and survival of the zebrafish, strong evolutionary pressure towards a very robust mechanism of development might have been present. This evolutionary selection might have resulted in several layers of redundant control mechanisms to reduce the error rate during the lateral line development. In this case, a variation of a single parameter, like force, might not be enough to significantly disturb the lateral line primordium.

9.2. Viscoelastic Measurements on the lateral line primordium

9.2.1. Comparison with other viscoelastic measurement methods

Previous work in this area has been confined to measurements on single, isolated cells *in vitro*. However, results presented in this thesis represent the first measurements on migrating embryonic cells in the context of the tissue *in vivo*. Several different approaches to measure viscoelastic parameters with magnetic tweezers have been used by different groups around the world, for example [92], [93], [94] [95] [1]. Our approach is most similar to the approach described in [71] and [9]. The main difference between the experimental setup presented in this thesis and previous work is that the magnetic bead is located inside the primordium pressing directly against the cell wall, while [71] and [9] coupled the bead via transmembrane protein to the actin cortex.

The nature of the measurement causes some inherent limitations. The migration of the lateral line primordium during measurements reduces the reliability of the viscous part of the measurements. We minimized this problem by applying forces for only 10 seconds. Similarly, the analysis was performed in two dimensions, since very fast imaging rates were necessary. Finally, any measurements during which the bead showed a movement in z direction were excluded.

9.2.2. Control measurements

Linear elastic control

Applying different forces to the same cell and measuring the elastic reaction of the cell shows that elasticity and the applied force are linearly proportional. The cells can therefore be considered a linear elastic material for the range of forces applied. Therefore, we apply the theory of linear viscoelasticity to our measurements.

Reproducibility and the influence of viscoelastic measurements on the cell cortex

Repeated viscoelastic measurements on the same cell in the lateral line primordium showed that these measurements are reproducible. The reproducibility was measured by calculating the standard deviation of eleven repeated measurements. Elasticity (k) was found to be the same in all measurements and there was essentially no deviation between measurements. The viscosity and relaxation time were were slightly more variable, but still had a relative standard deviation of 68% and 40% respectively.

It has been shown *in vitro* that an actomyosin meshwork reacts to an applied external force with a change in its molecular composition. This underlying molecular change is reflected in the bulk material as a change in viscoelastic parameters [96]. *In vivo*, our measurements show that this does not appear to be the case for the timescales and magnitudes of forces used in our experiments.

Change of viscoelastic parameters after treatment with Blebbistatin

Treatment of the lateral line primordium with Blebbistatin, a selective myosin II inhibitor, resulted in a significant change in the viscoelastic parameters of the migrating primordium. The elasticity parameter k decreased significantly. This result is in agreement with several *in vitro* studies performed on single cells. Several groups have shown that stiffness, elastic modulus and elastic tension decreases after treatment with Blebbistatin [97] and [98] [99].

Balland et al. [100] proposed the following explanation for the increase in elasticity and viscosity parameter:

The elasticity parameter of the material decreases, since Blebbistatin blocks myosin II in an unattached state and decreases the motor activity of the molecule, which leads to less resistance to elastic deformation per applied unit of force. Our results agree with this explanation.

Blebbistatin blocks myosin II in an unattached state, which also results in a reduction of the number of crosslinks in the actin mesh. The decrease in the number of crosslinks would decrease the viscosity of the actin meshwork. We therefore expect a reduction of the viscosity parameter γ_0. Our measurements show a decrease of the viscosity parameter γ_0 in 11 measured cells. However, this decrease is not statistically significant. Since the measurement of the apparent viscosity parameter γ_0 is very noisy, we likely need more experiments to confirm or reject this observation.

The third viscoelastic parameter, the relaxation time τ decreases significantly after treatment with Blebbistatin. The relaxation time is a measure of the time it takes for a viscoelastic material to switch from the elastic to the viscous regime. It has been hypothesized to be inversely related to the turnover time of the actin meshwork during treadmilling [101] since the continuous turnover of actin filaments is said to be responsible for the loss of elastic reaction after a continuous application of force. Treadmilling allows the actomyosin network to continuously re-shape itself and adapt to an external deformation (see Fig. 9.1). The faster the turnover time of the actomyosin cortex is, the faster this adaptation happens and the faster the actomyosin cortex displays viscous behavior.

A decrease in relaxation time after Blebbistatin treatment of the cell would indicate an increased turnover time of the actomyosin meshwork. Since the turnover time of the actin network increases with the absence of crosslinkers in the meshwork [102] and myosin II is a crosslinker itself, which is blocked by Blebbistatin in an unattached state [75] [76], an increase in turnover time is not unexpected.

These interpretations are internally consistent with our measurements. However, they remain speculative. Due to the complexity of the actomyosin cortex dynamics and the vast amount of regulatory mechanisms, other explanations are also possible.

(a) Actomyosin cortex before the deformation.

(b) Actomyosin cortex deformed due to external force application. The initial deformation of the network is elastic. In the viscous phase, the actomyosin cortex adapts its shape to the deformation, due to treadmilling. The individual actin filaments adapt their shape to the deformation.

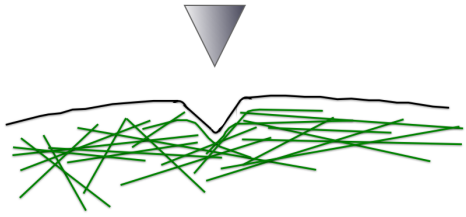

(c) After the force application stops, the actomyosin cortex does not bounce back elastically.

Figure 9.1.: Relaxation time is related to treadmilling

These results also show that the viscoelastic measurements we performed reflect the underlying molecular state and dynamics of an actin cortex; the actin cortex found in migrating cells of the lateral line primordium. However, since the diameter of the used beads was relatively large in comparison to the cell diameter, we could not exclude an attachment of the beads to other cellular structures, e.g. microtubules. Therefore, a partial contribution of the material properties of these structures is probably reflected in our measurements as well.

9.2.3. Measurement of spatial changes in the viscosity in the lateral line primordium

We measured the viscoelastic parameters for cells in the primordium and examined them as a function of their distance from the tip of the primordium.

	mouse fibroblasts [9]	**lateral line primordium**
average k in Pa m	0.01	0.001
average γ_0 in Pa s m	0.03	0.016
average τ in sec	0.1	0.9

Table 9.1.: Comparison of viscoelastic parameters of embryonic cells of the lateral line primordium and of cells in cell culture.

.

Elasticity

In comparison with the measurements done by Bausch et al. [9], our average elasticity parameter k is one order of magnitude smaller (0.001 Pa m vs. 0.01 Pa m) (compare Tbl. 9.1). However, this discrepancy is not surprising, since viscoelastic parameters of cells have been shown to vary over several orders of magnitude in previous studies. Additionally, it is known that cells adapt their stiffness to the stiffness of their environment [103]. Since the measurements of Bausch et al. [9] were performed in a completely different environment (cell culture vs. *in vivo*), a difference in cell elasticity is not surprising.

It has been shown that a substantial part of elasticity corresponds to the presence of motor proteins in the cortex. Specifically myosin II is known to account for up to half of the cells elasticity [104] [79]. In our experiments, blocking of myosin II using Blebbistatin decreased the elastic deflection of the bead by 40% (see also chapter 9.2.2), which shows that myosin II also plays a substantial role towards the elasticity of the cell cortex of the lateral line primordium.

The elasticity parameter varied significantly between cells from the tip of the lateral line primordium towards the back. Starting at the tip and going towards the back of the primordium, k continuously increases (Fig. 8.8) until it peaks at 100 μm distance from the tip. Going further towards the back of the primordium, k decreases rapidly again. Interestingly, this increase in the elasticity parameter k correlates with the change of cell type in the primordium. As described previously, the cells at the tip of the primordium have mesenchymal morphology, while cells in the back of the primordium display traits of epithelial cells (see also chapter 5.5.2). It is known from the literature that different cell types have different mechanical properties. Usually, cells whose main function is to

migrate (like mesenchymal cells or fibroblast) are softer and more elastic than cells that form an epithelium.

Viscosity

It has been proposed that the viscosity of the actin meshwork depends on the numbers of crosslinking proteins present in the mesh. In comparison with [9], our average viscosity parameter γ_0 is in the same order of magnitude (0.03 Pa m vs. 0.016 Pa m) (compare Tbl. 9.1). The viscosity parameter does not vary significantly over the length of the primordium, which indicates that the flow properties of cells in the primordium are not significantly different. However, these measurements are only a read-out for the basic composition of the actin cortex in the lateral line primordium. Different compositions of the same concentration of crosslinking proteins are likely not reflected in the measurement.

Relaxation time

In comparison with the measurements done by Bausch et al. [9], our average relaxation time τ is approximately ten times bigger (0.1 sec vs. 0.9 sec) (compare Tbl. 9.1). It has been hypothesized to be inversely related to the turnover time of the actin meshwork during treadmilling [101] since the continuous turnover of actin filaments is said to be responsible for the loss of elastic reaction after a continuous application of force. Therefore, the presence of actin capping and actin binding proteins will influence the measured relaxation time of the bulk materials. The relaxation time varies significantly over the length of the lateral line primordium. We detect a significant increase of approximately 30%. This change corresponds approximately with the change from mesenchymal like cells to epithelial like cells in the primordium. It suggests an increase in turnover time for filamentous actin in the mesenchymal like tip cells compared with the more static epithelial cells.

The relaxation time is a very interesting viscoelastic parameter, because it might give us a possible time scale for mechanical signaling in the cells. Since the relaxation time is a measurement for the time it takes for a viscoelastic material to switch from the elastic to the viscous state, any forces applied to the cells for much longer than the relaxation

time will result in a viscous behavior of the cell. These forces will dissipate and likely not contribute to any mechanical signaling mechanisms.

Summary

In conclusion, we measured three viscoelastic properties for cells in different positions in the lateral line primordium and discovered three distinct patterns. Compared to the mesenchymal tip cells, both the elasticity parameter k and the relaxation time τ increase in epithelial-like rosette cells, while the viscosity parameter γ_0 does not vary between different cell types. These variances likely reflect differences in molecular composition and molecular dynamics of the actin cortex.

9.2.4. Epithelial differentiation changes the viscoelastic properties of cells in vivo

SU5402 is a small molecule inhibitor of the FGF receptor. It has been previously shown, that FGF signaling is necessary for the formation of rosettes in the primordium [84]. Treatment of a lateral line primordium with SU5402 results in the loss of rosettes and migratory behavior of the primordium. The rosette cells lose their typical clustering and melt into cells with typical mesenchymal shapes.

We wanted to know if this shape change correlates with changes in the viscoelastic parameters as well. Different viscoelastic parameters are affected in different areas of the primordium: The viscosity parameter γ_0 decreased dramatically for cells in the back region of the primordium, while we did not detect a significant change in other regions. When comparing SU5402 treated primodia to untreated control primordia the relaxation time τ decreased in the center region of the primordium, but did not change in the back of the primordium. Finally, the elasticity parameter k decreased dramatically everywhere in the primordium. The characteristic profile of the elasticity in the primordium was lost. This corresponded with a loss of the rosette cells in the primordium.

The FGF receptor fgfr1, which is blocked by the SU5402 is only expressed in the center and back of the primordium [84], which explains why we measure the biggest change in the center and back part of the primordium. FGF has been shown to be the mediator

for epithelial-mesenchymal transitions and mesenchymal-epithelial transitions in many contexts [105] [106] [107]. Since these transitions typically involve a change in cell shape, the actomyosin cortex usually undergoes extensive remodeling during these processes. These dynamic molecular changes in the actomyosin cortex are reflected in our viscoelastic measurements.

We can therefore conclude that the treatment with SU5402 not only leads to morphological changes in the primordium, but it also has an effect on the mechanical properties of the cells. The spatial profiles of all three viscoelastic parameters differ significantly from their untreated counterparts. This change is most pronounced in the back region of the primordium, but it is interesting to note, that the cells in the center region of the primordium behave in the exact same way as untreated cells of the tip region. The rosette cells in the back region behave more like mesenchymal cells. However, the number of measurements of SU5402 treated cells is still rather small, and this needs to be increased.

9.2.5. Conclusions

Previous work has shown that cells in culture display a wide range of mechanical stiffness and elasticity. The mechanical behavior of cells depends on several environmental factors, such as the rigidity of the surrounding environment, as well as on the major influence of the biological state of the cell, namely its protein composition. It has been shown, for example, that different cells types can vastly differ in their tension and elasticity. The actomyosin cortex is responsible for maintaining and adjusting cell shape through a tight regulation of its mechanical properties. Thus, mechanical measurements on cells will often be a read-out for the protein composition and dynamics of the actomyosin cortex.

Our *in vivo* measurements have shown that viscoelastic parameters can differ widely between different cells even within the same discrete tissue. We find a distinct gradient in elasticity in the primordium along the axis of migration. This gradient correlates with changing cell shapes and cell types in the primordium. The leading region of the primordium is softer, while the trailing region is stiffer and less elastically deformable. These results show, that the change in cell type is not only relevant for different cell functions, but also has mechanical consequences for the tissue. Differences in cell elasticity might influence the way intercellular forces are transmitted.

A recent study on collectively migrating cells *in vitro* has shown, that these cells migrate in the opposite direction of an externally applied force [10]. In this study the force was specifically applied to E-cadherin via magnetic tweezers. The cells started migrating within minutes after the force was applied. Weber at al. [10] propose a model in which the directionality of a cell during collective cell migration was determined by the resistance of the adjoining trailing cell (Fig. 9.2).

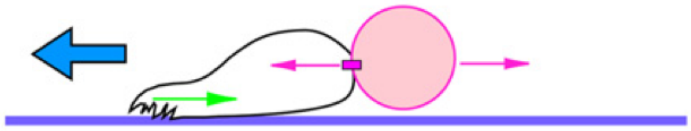

(a) Single cells migrate in the opposite direction of an applied force.

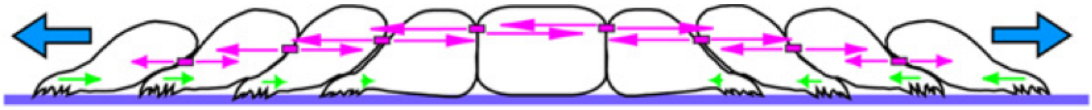

(b) In a cell sheet, cells polarize and migrate in opposite direction from their cell-cell contact.

Figure 9.2.: Figure modified from [10]

It is interesting that this resistance is transmitted via E-cadherin, since this protein complex is also expressed widely by all cells in the primordium. E-cadherin had previously been shown to be a tension sensor of mechanical forces between cells [57] [108]. E-cadherin is connected to f-actin via a protein complex containing α-catenin, which has been shown to be a stretch-activated, tension sensing protein [109] [110]. We therefore speculate that E-cadherin has a similar mechanosensory function in the primordium.

In addition to the phenomenon of cell migration being triggered by resistance, a similar observation has been described before: several studies have shown that collectively migrating cells have a tendency to migrate along the axis of their highest tension. This phenomenon is called plithotaxis [40] [87]. A tension of sufficiently high magnitude seems to be necessary for cells to migrate collectively.

Interestingly, laser-cutting experiments have shown that the primordium also has an intrinsically higher tension in the direction of its migration compared with tension in the perpendicular direction. It is therefore possible that the lateral line primordium could also follow the principles of plithotaxis.

Several different experiments have shown that migration and rosette formation in the lateral line primordium are intrinsically coupled. When the differentiation of mesenchymal cells into epithelial cells is inhibited by drug treatment, the rosette cells lose their cohesion and take a shape similar to the cells in the leading region of the lateral line primordium. They change from a tall, columnar shape towards a flatter shape with less height. At the same time, the migration of the primordium stops and does not resume, until the drug is washed out and the rosettes have re-formed. Laser cutting experiments and the observation of primordium fragments also confirm, that rosette cells and mesenchymal cells have to be present in the primordium for it to migrate successfully.

We showed that after treatment with SU5402 the loss of tissue organization is accompanied by a loss in the spatial distribution of the viscoelasticity of the mechanical properties. Especially the distribution of the elasticity parameter k changed from a pronounced gradient along the tissue axis in the control case to a more even distribution in SU5402 treated primordia. This change was most pronounced for cells that were formerly in the rosette region.

Gradients in general have frequently been discussed in developmental biology. For example, chemokine gradients have been shown to produce a coordinate system for cells. In collective cell migration, traction force gradients have been shown to exist. The traction forces are highest at the leading edge and decrease farther away from the edge [49]. For the migration of the lateral line primordium, the literature mainly focuses on chemokine gradients. The interplay between Cxcr4, Cxcr7 and sdf1 and its role in collective cell migration is the focus of many publications [86] [111] [112] [113] and has been discussed extensively. However, the presence of different cell types in the lateral line primordium is frequently neglected. It is important to note, that cell type differences likely result in differences of mechanical properties, traction forces and cell protrusion activity along the axis of the primordium. The possibility of such gradients are rarely taken into account when investigating the migration of the lateral line primordium.

It is, for example, possible that an elasticity gradient is necessary for the collective cell migration of the primordium. One indicator in favor of this model is the loss of migratory function of the primordium, whenever the rosette cell clusters are lost due to drug treatments or genetic manipulation. Weber et al. [10] have proposed resistance to migration as the mechanism for cell directionality during collective cell migration in a cell sheet with a single cell type.

Similarly, it is possible that cells in the primordium sense their directionality as a result of elasticity differences between the cells. This would require cells to be able to sense the elasticity of the cortex of their neighboring cells, similarly to the way integrins can sense the stiffness/elasticity of the extracellular matrix. E-cadhering, which is widely present in the lateral line primordium, has been demonstrated to be able to transmit force signals to cells [10] and to sense the mechanical properties of their environment [57] [108].

It is therefore possible that the lateral line cells can sense the elasticity difference present in the primordium. This information could be used as a directional signal for cell migration. If this gradient of elasticity is lost, as is the case during the treatment with SU5402, the directional information is lost and the primordium could not migrate anymore. Our measurements have shown, that a defined elasticity gradient along the axis of migration exists. However, our measurements also show the strong variability among cells. Due to the set-up of the experiment, we are not able to directly measure the elasticity difference between two neighboring cells. Instead, we average several measurements on lateral line primordias in random positions. We are therefore unable to say if the elasticity gradient would be pronounced enough to act as a guiding signal for collective cell migration.

10. Materials and Methods

10.1. Fish handling and embryo preparation

Zebrafish (Danio rerio) were raised and staged as previously described [114]. The following mutant and transgenic strains were used: CldnB:lynGFP, SDF1a/medusa and a lifeactGFP line generated by C. Revenu. The CldnB:lynGFP transgenic line was described previously [86]. Early embryos were mounted in 1% low-melting-point agarose. For live imaging at 24 hpf, embryos were anesthetized in 0.01% tricaine and embedded in 1.5% low-melting-point agarose. For force application at 24 hpf, embryos were anesthetized in 0.01% tricaine and mounted on the surface of a drop of 1.5% low-melting-point agarose. Force application experiments were performed using an upright microscope with a water dipping lens under a droplet of standard fish embryo buffer E3 (Calbiochem #572630).

10.2. Bead preparation

Coupling beads to fluorophore

Commercially available Dynabead M-280 superparamagnetic beads with a diameter of 2.8 μm were loaded with a biotin coupled fluorophore (ATTO647 or ATTO561, Attotech) according to the protocol of [115]. The bead surfaces were functionalized with covalently-coupled streptavidin. The beads consisted of superparamagnetic particles (6-12 nm in diameter) embedded into a polymer matrix. Approximately 10 mg of dynabead solution contains 6-7x10^8 beads/mL. 1 mg of pre-coated streptavidin magnetic beads has sufficient affinity to bind up to 650 - 900 pM of free biotin (http://www.dynalbiotech.com). Atto-520 fluorescent-labeled biotin was loaded onto the magnetic beads with the streptavidin via specific ligand-receptor interactions. To load the fluorescent-labeled Atto-520 biotin

with streptavidin magnetic beads, we placed 5 μL of streptavidin-coated magnetic bead solution in a clean eppondorf tube. The bead solution was washed three times with phosphate-buffered saline (PBS) to remove the preservatives. The supernatant of the solution was removed using a micropipette by collecting the magnetic beads at the bottom of the eppondorf tube using a permanent magnet and re-suspending them in 90 μL of water. 1 mg of Atto-520 biotin was diluted in 200 μL of ethanol. 5 μL of diluted fluorophore was mixed with the 90 μL of magnetic bead solution for 10 minutes. Finally, the solution was further washed with PBS buffer several times to remove the biotin surplus by means of magnetic separation and collecting the supernatant using a micropipette.

Bead preparation for injection

Before injection, magnetic beads were washed several times with with phosphate-buffered saline (PBS). The supernatant of the solution was removed using a micropipette by collecting the magnetic beads at the bottom of the eppondorf tube using a permanent magnet

10.3. Force Calibration

Dissolving beads in viscous fluid

Magnetic (Dynabead M-280, Invitrogen) and nonmagnetic beads (Invitrogen) were dissolved in a calibrated viscosity silicone oil (dimethylpolysiloxane, Sigma-Aldrich, St. Louis, Missouri, Cat. No. DMPS1C-1000G). In detail, 20 μL of beads were placed in an eppendorf tube. To avoid bead aggregation, all water was removed from the eppendorf tube containing the bead using speed-vac. 20 μL of a silicone oil with low viscosity (dimethylpolysiloxane, Sigma-Aldrich, St. Louis, Missouri, Cat. No. DMPS1C-10G) was added to the tube. The solution was thoroughly mixed by pipetting this solution up and down for 10 min. 20 μL of the DMPS1c-10G bead solution was dissolved in 5 mL of DMPS-10G and well stirred.

Microscopy

An upright confocal was used for imaging. The bead-DMPS solution was placed under the microscope and the magnetic tip was placed close to a bead. After a few minutes of waiting, to make sure all flows in the DMPS-bead solution was settled, the current was turned on and the movement of the beads was recorded. The movement of the non-magnetic fluorescent beads was used as a control for the absence of other internal flows.

Data analysis

ImageJ was used for the analysis of the data. Beads were tracked using the Particle Detector & Tracker plug-in. The speed of the beads in function of their distance to the electromagnet tip was measured. The force on the bead was calculated using the Stokes equation $F = 6\pi\eta r v$ [1].

10.4. Bead delivery

Early-stage injection

Embryos were injected at the one-cell stage with Magnetic beads (Dynabead M-280, Invitrogen). The next day, recipient embryos were screened for the presence of fluorescent beads cells in the primordium with a Leica MZ10 F fluorescence stereomicroscope.

Late-stage injection

Embryos were injected at the blastula stage with Magnetic beads (Dynabead M-280, Invitrogen). The topmost region of the embryo was targeted. The next day, recipient embryos were screened for the presence of fluorescent beads cells in the primordium with a Leica MZ10 F fluorescence stereomicroscope.

[1] r=1.4 μm; η: viscosity of DMPS

Transplantation

Donor embryos were injected at the one-cell stage with 2.5% Rhodamine-Dextrane (Molecular Probes) and magnetic beads (Dynabeads, 2.8 μm diameter) coupled to a fluorophore (Atto-Tech) and were allowed to develop until the blastula stage. Approximately 20-30 cells were then transplanted into age-matched CldnB::lynGFP- positive host embryos. The next day, recipient embryos were screened for the presence of red cells in the primordium with a Leica MZ10 F fluorescence stereomicroscope.

10.5. External force application on migrating lateral line primordium

Embryos were prepared like described above (Ch.10.1) and placed under the microscope.

Imaging

Imaging was performed with an upright microscope and a water dipping lens with a high working distance. Experiments were performed under a droplet of E3 (Calbiochem #572630). The tip of the electromagnet was placed in close proximity to a bead and a low magnification image containing both the magnetic bead and the tip of the electromagnet was taken. This image was used later to determine the distance between bead and electromagnet tip. Afterwards, an electric current was applied, while the lateral line primordium was recorded with the microscope.

10.6. Speed measurements of primordia containing beads

Embryo preparation

Embryos were injected in the blastula stage with magnetic beads like described above (Ch. 10.4), anesthetized in 0.01% tricaine and embedded in 1.5% low-melting-point

agarose. Uninjected embryos were used as controls and anesthetized in 0.01% tricaine and embedded in 1.5% low-melting-point agarose.

Imaging

Imaging was performed on a spinning disk confocal microscope, using the multi-positioning option to capture the behavior of several embryos at once. A z-stack of the primordium was taken every several times per hour over a time span of four hours.

Data analysis

ImageJ, Fiji and Matlab was used for the analysis of the data. In each embryo the primordium was tracked by hand using the Manual Tracking plug-in in ImageJ. The average speed for primordia labeled with beads and unlabeled primordia were calculated.

10.7. Tracking cells and beads in early embryos

Embryo preparation

Embryos were transplanted with rhodamine dextran filled cells and cells filled with magnetic beads as described in Ch. 10.4. Immediately after transplantation, they were decorionated and mounted in 1% low-melting-point agarose.

Imaging

Mounted embryos were imaged using a spinning disk confocal microscope and a low magnification objective (10X/NA0.3). A z-stack over several hundred micron was taken every 20 minutes over a time span of several hours.

Data analysis

ImageJ, Fiji and Matlab was used for the analysis of the data. Magnetic beads were tracked using he Particle Detector & Tracker plug-in. Rhodamine dextran filled cells were tracked by hand using the Manual Tracking plug-in in ImageJ. The mean square displacement of both tracks were calculated using $MSD(t) =< \Delta r >=< |\vec{r}(t) - \vec{r}(0)| >$.

10.8. Viscoelastic Measurements

Embryo preparation

Embryos were injected with magnetic beads at the blastula stage as described above (Ch. 10.4). The next day, recipient embryos were screened for the presence of fluorescent beads cells in the primordium with a Leica MZ10 F fluorescence stereomicroscope. Embryos were anesthetized in 0.01% tricaine and mounted on the surface of a drop of 1.5% low-melting-point agarose.

Force application

Imaging was performed with an upright microscope and a water dipping lens with a high working distance. Experiments were performed under a droplet of E3. Before force application, a 30 minute long movie was taken of the primordium to ensure it migrates normally. For the application of the force, the tip of the electromagnet was placed in close proximity to a bead and a low magnification image containing both the magnetic bead and the tip of the electromagnet was taken. This image was used later to determine the distance between bead and electromagnet tip and the direction of the force. Afterwards, an electric current of 4A was applied for 10 seconds, while the bead behavior was recorded with a high magnification and time resolution. Beads that showed a strong movement in the z-direction were excluded from the analysis. Beads that were not touching cell boundaries were not measured. Measurements were repeated three to five times for each cell.

Data analysis

Fiji and Matlab was used for the analysis of the data. For each measurement, the movement of the bead was automatically extracted using image segmentation and tracking techniques as described in Ch. 7.1.2. Bead displacement curves were extracted using the directional information from a low magnification image showing both the electromagnet tip and the magnetic bead. The fitting of the model is described in Ch. 7.1.4. It was carried out using the least square method. The resulting fits were additionally inspected and corrected by hand. The elasticity parameter k, the viscosity parameter γ_0 and the relaxation time τ were extracted.

10.9. Drug treatments

Blebbistatin treatment

For blebbistatin treatments, embryos were injected with magnetic beads at the blastula stage as described above (Ch. 10.4). The next day, the embryos were were anesthetized in 0.01% tricaine and mounted on the surface of a drop of 1.5% low-melting-point agarose. For viscosity measurements during drug treatment, a drop of E3 (Calbiochem #572630) containing 20 μM Blebbistatin. Measurements were started after 20 minutes of treatment.

SU5402 treatment

For SU5402 treatments, embryos were injected with magnetic beads at the blastula stage as described above (Ch. 10.4). The next day embryos were dechorionated and incubated for 10-12 hours in 10μM SU5402 in E3 (Calbiochem #572630). For force measurements during drug treatment, pretreated embryos were mounted with agarose and E3 each containing 10 μM SU5402.

11. Appendix

11.1. Statistics Definitions

11.1.1. Mean, Standard deviation and Standard error of the mean

For N measurements, the mean for each parameter α is the arithmetic mean:

$$\overline{\alpha} = \frac{1}{N} \sum_{i}^{N} \alpha_i$$

The variances is defined as:

$$s = \frac{1}{(N-1)} \sum_{i}^{N} (\overline{\alpha} - \alpha_i)^2$$

The standard deviation s is defined as the squareroot of the variance:

$$\sigma = \sqrt{\frac{1}{(N-1)} \sum_{i}^{N} (\overline{\alpha} - \alpha_i)^2}$$

The standard error of the mean (SEM) is defined as:

$$SEM = \sqrt{\frac{1}{N(N-1)} \sum_{i}^{N} (\overline{\alpha} - \alpha_i)^2}$$

11.1.2. Student's t-test, two-tailed, unequal variances

The t-value for the two-tailed student's t-test for unequal sample sizes with unequal variances is defined as:

$$t = \frac{\bar{X_1} - \bar{X_2}}{s_{\bar{X_1} - \bar{X_2}}}$$

with

$$s_{\bar{x_1} - \bar{x_2}} = \sqrt{\frac{s_1^2}{n_1} + \frac{s_2^2}{n_2}}$$

with $\bar{X_1}/\bar{X_2}$ denoting the mean of the two populations respectively, s_1/s_2 denoting the variance, n_1/n_2 being the number of independent measurement and $s_{\bar{X_1} - \bar{X_2}}$ being the standard error of the difference between the two means.

11.1.3. Mann-Whitney U-test

The Mann-Whitney U test is a statistical test for the null hypthesis that two populations are the same. The U-test is more efficient than the t-test on non-normal distributions. For normal distributions it is nearly as efficient [116].

The U-value is given by the smallest of two values U_1 or U_2 with

$$U_1 = n1 * n2 + \frac{n_1(n_1 + 1)}{2} - R_1$$

and

$$U_2 = n1 * n2 + \frac{n_2(n_2 + 1)}{2} - R_2$$

where n_1/n_2 are the sample size for the two populations and $R_1/\ R_2$ are the sum of the ranks for the two populations. To determine the rank for each data point, the two populations are combined in a list, sorting the values from high to low. The ranks for each data point is determined by its position in a list.

11.1.4. Pearson's correlation

The Pearson's correlation between two variables measures the linear correlation between two variables. It is defined as the covariance between two variables divided by the product of their standard deviations.We estimated the popluation Pearsons correlation using the following formula:

$$r = \frac{\sum_{i=1}^{n}(x_i - \bar{x})(y_i - \bar{y})}{\sqrt{\sum_{i=1}^{n}(x_i - \bar{x})^2 \sum(y_i - \bar{y})^2}}$$

with n being the number of measurements, $\bar{x} = \sum_{i=1}^{n} x_i$ and $\bar{y} = \sum_{i=1}^{n} y_i$ being the sample mean, x_i and y_i being the individual measurements.

11.2. Results of viscoelasticity measurements of the untreated lateral line primordium

Table 11.1 and Table 11.2 contain the results for all viscoelastic measurements taken on the untreated lateral line primordium.

	Embryo No.	**Bead No.**	**k in Pa s** $*10^{-6}$	γ_0 **in Pa s m** $*10^{-6}$	τ **in sec**	**Distance bead to tip in** μ**m**
1	1	1	692.66	6247.1	0.84	5
2	1	2	453.34	2584.8	0.43	16.3
3	1	3	380.98	2824.2	0.84	19.5
4	1	4	652.59	11503	1.13	31.7
5	1	5	869.94	8979	0.96	45.6
6	1	6	866.18	8979	0.81	47.9
7	1	7	558.2	13267	0.82	43.3
8	1	8	483.54	18081	0.92	25
9	1	9	443.13	16679	0.7	49
10	2	2	1698	12077	0.41	142
11	2	3	1384.5	15609	0.97	194
12	3	1	1502.8	6253.5	0.7	127
13	4	1	1456.9	27223	0.81	33
14	4	2	1847	20319	0.63	103
15	4	3	5130.6	25086	0.51	141
16	5	2	1192.1	11628	0.73	23
17	6	1	1904.1	18685	0.55	28
18	7	1	563.92	11679	0.64	64.3

Table 11.1.

	Embryo No.	**Bead No.**	**k in Pa s** $*10^{-6}$	γ_0 **in Pa s m** $*10^{-6}$	τ **in sec**	**Distance bead to tip in** μ**m**
19	8	3	1115.5	6256	0.49	56.3
20	8	4	3192.1	29318	0.82	75.8
21	8	5	1667.5	35287	0.71	101
22	8	8	861	10660	0.56	149
23	9	1	1959.8	17111	0.63	132
24	9	4	1947.7	14734	0.49	125
25	9	3	3770.5	41049	0.82	130
26	9	7	2475.4	16307	0.68	115
27	9	12	4013.1	17756	0.8	113
28	9	17	1594.8	15110	0.86	97
29	9	18	1426.3	21717	0.66	77
30	9	19	3586.7	15994	0.74	86
31	10	1	450.85	8265.8	0.99	85
32	10	2	649.25	8817.8	1.05	87.1
33	11	1	1202.7	29580	0.58	84
34	11	3	632.95	7149.4	0.58	151
35	11	2	662.15	9274.1	0.78	145
36	12	1	2458.5	40690	1.04	8
37	12	2	1083.1	20860	0.69	18
38	12	3	1612.8	20847	0.76	31.3
39	12	4	1670	10420	0.43	68.4
40	12	5	3464.4	8535.3	0.69	79.3
41	13	1	781.41	23193	0.99	36
42	13	2	830.66	15521	1.17	47
43	13	3	783.02	14930	0.64	84
44	14	2	2466.6	26343	0.58	140
45	15	3	1947.1	12135	0.69	137
46	16	1	2076.1	26234	0.95	128
47	17	2	3242.5	14281	0.55	90.6
48	17	1	1151.4	12742	0.64	68
49	18	1	831.45	15141	0.47	76.8

Table 11.2.

11.3. Results of viscoelasticity measurements of the lateral line primordium treated with Blebbistatin

Table 11.3 contains the results for all viscoelastic measurements taken on lateral line primordium treated with Blebbistatin (BB) and untreated cells (untr.).

	k in Pa s untr.	**γ_0 in Pa s m untr.**	**τ in s untr.**	**k in Pa s BB**	**γ_0 in Pa s m BB**	**τ in s BB**
1	0.0019877	0.019272	1.352	0.0036	0.092486	0.766
2	0.00077279	0.019322	1.466	0.0014019	0.030876	0.668
3	0.0010429	0.019486	0.84	0.00099836	0.018453	1.032
4	0.00066753	0.0058389	1.2433	0.0012756	0.015454	0.33
5	0.00090873	0.010727	1.266	0.0018988	-0.019094	0.31
6	0.0017614	0.094573	1.9233	0.0013192	0.0073578	0.76667
7	0.0011605	0.0086963	0.84	0.0016604	0.29851	0.13667
8	0.0010101	0.027002	1.1367	0.0028853	0.018703	1.3333

Table 11.3.

11.4. Results of viscoelasticity measurements of the lateral line primordium treated with SU5402

Table 11.4 contains the results for all viscoelastic measurements taken on lateral line primordium treated with SU5402.

	Embryo No.	**Bead No.**	**k in Pa s** $*10^{-6}$	γ_0 **in Pa s m** $*10^{-6}$	τ **in sec**	**Distance bead to tip in** μ**m**
1	1	1	2430.8	29864	0.28	72
2	1	4	2909.5	29931	1.69	80
3	1	2	2545.7	25895	0.78	95
4	1	3	2287.8	30595	0.02	144
5	2	1	2990.4	25668	1.22	50
6	2	2	3685.4	59976	1.43	108
7	3	1	654.57	34317	1.46	80.7
8	3	2	397.23	8456.4	0.43	131
9	4	1	1475.1	7395.8	0.74	58.8
10	4	2	990.95	12897	1.48	81
11	4	3	326.21	4564.6	0.45	153
12	5	1	658.28	6569.8	2.23	74.4
13	5	2	449.54	12385	0.3	141
14	5	3	341.53	3216.1	1.03	180

Table 11.4.

Acknowledgments

There are many people I would like to thank for their help, support, and encouragement during my doctoral work. A heartfelt thank you to those who have advised me and guided me through this process.

I would like to thank Darren Gilmour for giving me the opportunity to work in his lab, introducing me to the world of zebrafish, for his guidance, his enthusiasm and his overall engagement in my project. I would like to thank Lars Hufnagel for supporting me and my project and for taking the time to be part of my TAC committee. I would also like to thank Jan Ellenberg for his helpful advice and guidance. I would like to thank Albrecht Ott for his curiosity in my research and for kindly accepting to be my supervisor at the university. I would like to thank Ewa Paluch, for supervising my master thesis, teaching me all she knows about actin and for all the advice throughout the years.

I am grateful to Uros Krzic for his help with the set-up construction. I would also like to thank Sebastian Streichan for all the engaging discussions we had.

I am gratefult to Marcus Heisler for giving me access to his microscope. I would like to thank the EMBL mechanical workshop, especially Leo Burger and Helmuth Schaar, and the EMBL electronic workshop, especially Georg Ritter, for all the help and advice I received from them.

I would like to thank all the past and present member of the Gilmour lab. Thank you for your support, your friendship, the good time and the many working hours we spent together.

I would like to thank Gulcin, Virginie, Ana and Guillaume for welcoming me into the lab. Thank you to Andreas for introducing me to "mucular biology" and the joys of fishing. Thank you to Andreea for all her work in the fish room and for not getting bored with my repetitive music choices. I would like to thank Christoph for his enthusiasm for

biophysics, for knowing all the Matlab functions by heart and for his poetic rhyming abilities. I would like to thank Li-Kun for scientific discussions and for never getting annoyed with my jokes. I would also like to thank Céline for her help and support, encouragement and all the pub quizzes we lost together. I would like to thank Lionel for being the calm presence throughout the whirlwind of hustle and bustle in the lab. I would also like to thank Erika, for her dedication to science, her seemingly endless energy and her uplifting ability to always end the day in a party. I would like to thank Sevi, for her help with everything fgf and for never being boring.

I would like to thank all the friends I made in Chemnitz, Dresden, Paris and Heidelberg. I am truly grateful for all the help and support I received.

I would also like to thank my family. This work would have never been possible without their support and love.

Bibliography

[1] P. Pullarkat, P. Fernández, and A. Ott, "Rheological properties of the eukaryotic cell cytoskeleton," *Physics reports*, vol. 449, no. 1-3, pp. 29–53, 2007.

[2] F. Crick and A. Hughes, "The physical properties of cytoplasm:: A study by means of the magnetic particle method part i. experimental," *Experimental Cell Research*, vol. 1, no. 1, pp. 37–80, 1950.

[3] S. Smith, L. Finzi, and C. Bustamante, "Direct mechanical measurements of the elasticity of single dna molecules by using magnetic beads," *Science*, vol. 258, no. 5085, pp. 1122–1126, 1992.

[4] F. Schmidt, F. Ziemann, and E. Sackmann, "Shear field mapping in actin networks by using magnetic tweezers," *Eur Biophys J*, vol. 1, Jan 1996.

[5] N. Desprat, W. Supatto, P. Pouille, E. Beaurepaire, and E. Farge, "Tissue deformation modulates twist expression to determine anterior midgut differentiation in drosophila embryos," *Developmental Cell*, vol. 15, pp. 470–477, Sep 2008.

[6] M. Tanase, N. Biais, and M. Sheetz, "Magnetic tweezers in cell biology," *Methods Cell Biol*, vol. 83, pp. 473–93, Jan 2007.

[7] F. Alenghat, "Analysis of cell mechanics in single vinculin-deficient cells using a magnetic tweezer," *Biochemical and Biophysical Research Communications*, vol. 277, pp. 93–99, Oct 2000.

[8] T. R. Strick, J. F. Allemand, D. Bensimon, A. Bensimon, and V. Croquette, "The elasticity of a single supercoiled dna molecule," *Science*, vol. 271, pp. 1835–7, Mar 1996.

[9] A. Bausch, F. Ziemann, A. Boulbitch, K. Jacobson, and E. Sackmann, "Local measurements of viscoelastic parameters of adherent cell surfaces by magnetic bead microrheometry," *Biophysical Journal*, vol. 75, no. 4, pp. 2038–2049, 1998.

[10] G. F. Weber, M. A. Bjerke, and D. W. Desimone, "A mechanoresponsive cadherin-keratin complex directs polarized protrusive behavior and collective cell migration," *Developmental Cell*, vol. 22, pp. 104–115, Oct 2033.

[11] P. Kollmannsberger and B. Fabry, "High-force magnetic tweezers with force feedback for biological applications," *Rev. Sci. Instrum.*, vol. 78, p. 114301, Jan 2007.

[12] C. Gosse and V. Croquette, "Magnetic tweezers: Micromanipulation and force measurement at the molecular level," *Biophysical Journal*, vol. 82, pp. 3314–3329, Oct 2008.

[13] A. Devries, "Micro magnetic tweezers for nanomanipulation inside live cells," *Biophysical Journal*, vol. 88, pp. 2137–2144, Mar 2005.

[14] T. Henighan, A. Chen, G. Vieira, A. Hauser, F. Yang, J. Chalmers, and R. Sooryakumar, "Manipulation of magnetically labeled and unlabeled cells with mobile magnetic traps," *Biophysical Journal*, vol. 98, pp. 412–417, Feb 2010.

[15] C. Haber and D. Wirtz, "Rev. sci. instrum. 2000 haber," *Rev. Sci. Instrum.*, vol. 71, no. 12, p. 8, 2000.

[16] T. R. Strick, J. F. Allemand, D. Bensimon, and V. Croquette, "Behavior of supercoiled dna," *Biophysical Journal*, vol. 74, pp. 2016–28, Apr 1998.

[17] A. Celedon, C. M. Hale, and D. Wirtz, "Magnetic manipulation of nanorods in the nucleus of living cells," *Biophysj*, vol. 101, pp. 1880–1886, Nov 2032.

[18] C. Kittel, "Einführung in die festkörperphysik," 1999.

[19] N. Desprat, W. Supatto, P.-A. Pouille, E. Beaurepaire, and E. Farge, "Tissue deformation modulates twist expression to determine anterior midgut differentiation in drosophila embryos," *Developmental Cell*, vol. 15, pp. 470–7, Sep 2008.

[20] D. Graham, H. Ferreira, and P. Freitas, "Magnetoresistive-based biosensors and biochips," *TRENDS in Biotechnology*, vol. 22, no. 9, pp. 455–462, 2004.

[21] M. Westerfield, "The zebrafish book: A guide for the laboratory use of zebrafish ...," 2007.

[22] J. Wiskirchen, E. F. Grönewäller, F. Heinzelmann, R. Kehlbach, E. Rodegerdts, M. Wittau, H. P. Rodemann, C. D. Claussen, and S. H. Duda, "Human fetal lung fibroblasts: in vitro study of repetitive magnetic field exposure at 0.2, 1.0, and 1.5 t," *Radiology*, vol. 215, pp. 858–62, Jun 2000.

[23] J. Wiskirchen, E. F. Groenewaeller, R. Kehlbach, F. Heinzelmann, M. Wittau, H. P. Rodemann, C. D. Claussen, and S. H. Duda, "Long-term effects of repetitive exposure to a static magnetic field (1.5 t) on proliferation of human fetal lung fibroblasts," *Magn Reson Med*, vol. 41, pp. 464–8, Mar 1999.

[24] S. Pacini, M. Gulisano, B. Peruzzi, E. Sgambati, G. Gheri, S. G. Bryk, S. Vannucchi, G. Polli, and M. Ruggiero, "Effects of 0.2 t static magnetic field on human skin fibroblasts," *Cancer Detect Prev*, vol. 27, pp. 327–32, Jan 2003.

[25] R. R. Raylman, A. C. Clavo, and R. L. Wahl, "Exposure to strong static magnetic field slows the growth of human cancer cells in vitro," *Bioelectromagnetics*, vol. 17, pp. 358–63, Jan 1996.

[26] M. Zmyślony, J. Palus, J. Jajte, E. Dziubaltowska, and E. Rajkowska, "Dna damage in rat lymphocytes treated in vitro with iron cations and exposed to 7 mt magnetic fields (static or 50 hz)," *Mutat Res*, vol. 453, pp. 89–96, Sep 2000.

[27] Y. Shan, S. Ma, L. Nie, X. Shang, X. Hao, Z. Tang, and H. Wang, "Size-dependent endocytosis of single gold nanoparticles," *Chem Commun (Camb)*, vol. 47, pp. 8091–3, Jul 2011.

[28] H. Jin, D. A. Heller, R. Sharma, and M. S. Strano, "Size-dependent cellular uptake and expulsion of single-walled carbon nanotubes: single particle tracking and a generic uptake model for nanoparticles," *ACS Nano*, vol. 3, pp. 149–58, Jan 2009.

[29] T. dos Santos, J. Varela, I. Lynch, A. Salvati, and K. A. Dawson, "Quantitative assessment of the comparative nanoparticle-uptake efficiency of a range of cell lines," *Small*, vol. 7, pp. 3341–9, Dec 2011.

[30] R. E. Serda, S. Ferrati, B. Godin, E. Tasciotti, X. Liu, and M. Ferrari, "Mitotic trafficking of silicon microparticles," *Nanoscale*, vol. 1, p. 250, Jan 2009.

[31] T. Hamasaki, N. Tanaka, N. Kamei, O. Ishida, S. Yanada, K. Nakanishi, K. Nishida, Y. Oishi, S. Kawamata, N. Sakai, and M. Ochi, "Magnetically labeled neural progenitor cells, which are localized by magnetic force, promote axon growth in organotypic cocultures," *Spine*, vol. 32, pp. 2300–5, Oct 2007.

[32] J. Zhang, X. G. Chen, L. Huang, J. T. Han, and X. F. Zhang, "Self-assembled polymeric nanoparticles based on oleic acid-grafted chitosan oligosaccharide: biocompatibility, protein adsorption and cellular uptake," *J Mater Sci Mater Med*, vol. 23, pp. 1775–83, Jul 2012.

[33] P. V. Asharani, Y. Lianwu, Z. Gong, and S. Valiyaveettil, "Comparison of the toxicity of silver, gold and platinum nanoparticles in developing zebrafish embryos," *Nanotoxicology*, vol. 5, pp. 43–54, Mar 2011.

[34] A. Tiwari, G. Punshon, A. Kidane, G. Hamilton, and A. M. Seifalian, "Magnetic beads (dynabead) toxicity to endothelial cells at high bead concentration: implication for tissue engineering of vascular prosthesis," *Cell Biol Toxicol*, vol. 19, pp. 265–72, Oct 2003.

[35] M. Manabe, N. Tatarazako, and M. Kinoshita, "Uptake, excretion and toxicity of nano-sized latex particles on medaka (oryzias latipes) embryos and larvae," *Aquat Toxicol*, vol. 105, pp. 576–81, Oct 2011.

[36] Y. bin Tan, X. ying Wu, J. feng Zhang, and M. ming Zhang, "[magnetic resonance signal detection of superparamagnetic iron oxide nanoparticles and its biological effects on endothelial cells]," *Zhejiang Da Xue Xue Bao Yi Xue Ban*, vol. 39, pp. 118–24, Mar 2010.

[37] O. Ilina and P. Friedl, "Mechanisms of collective cell migration at a glance," *J Cell Sci*, vol. 122, pp. 3203–3208, Sep 2009.

[38] M. Poujade, E. Grasland-Mongrain, A. Hertzog, J. Jouanneau, P. Chavrier, B. Ladoux, A. Buguin, and P. Silberzan, "Collective migration of an epithelial monolayer in response to a model wound," *Proceedings of the National Academy of Sciences*, vol. 104, no. 41, pp. 15988–15993, 2007.

[39] Y. Hegerfeldt, M. Tusch, E.-B. Bröcker, and P. Friedl, "Collective cell movement in primary melanoma explants: plasticity of cell-cell interaction, beta1-integrin function, and migration strategies," *Cancer Research*, vol. 62, pp. 2125–30, Apr 2002.

[40] J. G. Dumortier, S. Martin, D. Meyer, F. M. Rosa, and N. B. David, "Collective mesendoderm migration relies on an intrinsic directionality signal transmitted through cell contacts," *Proceedings of the National Academy of Sciences*, vol. 109, pp. 16945–16950, Oct 2012.

[41] M. Behrndt, G. Salbreux, P. Campinho, R. Hauschild, F. Oswald, J. Roensch, S. W. Grill, and C.-P. Heisenberg, "Forces driving epithelial spreading in zebrafish gastrulation," *Science*, vol. 338, pp. 257–260, Oct 2012.

[42] A. J. Engler, S. Sen, H. L. Sweeney, and D. E. Discher, "Matrix elasticity directs stem cell lineage specification," *Cell*, vol. 126, pp. 677–89, Aug 2006.

[43] X. Trepat, L. Deng, S. S. An, D. Navajas, D. J. Tschumperlin, W. T. Gerthoffer, J. P. Butler, and J. J. Fredberg, "Universal physical responses to stretch in the living cell," *Nature*, vol. 447, pp. 592–595, May 2007.

[44] N. J. Sniadecki, "Minireview: A tiny touch: Activation of cell signaling pathways with magnetic nanoparticles," *Endocrinology*, vol. 151, pp. 451–457, Feb 2010.

[45] T. Wu, T. A. Nieminen, S. Mohanty, J. Miotke, R. L. Meyer, H. Rubinsztein-Dunlop, and M. W. Berns, "A photon-driven micromotor can direct nerve fibre growth," *Nature Photonics*, vol. 6, pp. 62–67, Apr 2011.

[46] M. Krieg, Y. Arboleda-Estudillo, P.-H. Puech, J. Käfer, F. Graner, D. J. Müller, and C.-P. Heisenberg, "Tensile forces govern germ-layer organization in zebrafish," *Nat Cell Biol*, vol. 10, pp. 429–436, Apr 2008.

[47] R. Fernandez-Gonzalez, S. de Matos Simoes, J.-C. Roper, S. Eaton, and J. A. Zallen, "Myosin ii dynamics are regulated by tension in intercalating cells,"

Developmental Cell, vol. 17, pp. 736–743, Nov 2030.

[48] L. Petitjean, M. Reffay, E. Grasland-Mongrain, M. Poujade, B. Ladoux, A. Buguin, and P. Silberzan, "Velocity fields in a collectively migrating epithelium," *Biophysj*, vol. 98, pp. 1790–1800, Oct 2031.

[49] X. Trepat, M. R. Wasserman, T. E. Angelini, E. Millet, D. A. Weitz, J. P. Butler, and J. J. Fredberg, "Physical forces during collective cell migration," *Nature Physics*, vol. 5, pp. 426–430, Mar 2009.

[50] T. E. Angelini, E. Hannezo, X. Trepat, M. Marquez, J. J. Fredberg, and D. A. Weitz, "Glass-like dynamics of collective cell migration," *Proc Natl Acad Sci USA*, vol. 108, pp. 4714–9, Mar 2011.

[51] T. Mammoto and D. E. Ingber, "Mechanical control of tissue and organ development," *Development*, vol. 137, pp. 1407–1420, May 2010.

[52] C. Kung, "A possible unifying principle for mechanosensation," *Nature*, vol. 436, pp. 647–654, Aug 2005.

[53] B. Martinac, "Mechanosensitive ion channels: molecules of mechanotransduction," *J Cell Sci*, vol. 117, pp. 2449–2460, May 2004.

[54] F. van Roy and G. Berx, "The cell-cell adhesion molecule e-cadherin," *Cell. Mol. Life Sci.*, vol. 65, pp. 3756–88, Nov 2008.

[55] N. Borghi, M. Lowndes, V. Maruthamuthu, M. L. Gardel, and W. J. Nelson, "Regulation of cell motile behavior by crosstalk between cadherin- and integrin-mediated adhesions," *Proc Natl Acad Sci USA*, pp. 1–6, Jun 2010.

[56] M. Smutny and A. S. Yap, "Neighborly relations: cadherins and mechanotransduction," *The Journal of Cell Biology*, vol. 189, pp. 1075–7, Jun 2010.

[57] Q. le Duc, Q. Shi, I. Blonk, A. Sonnenberg, N. Wang, D. Leckband, and J. de Rooij, "Vinculin potentiates e-cadherin mechanosensing and is recruited to actin-anchored sites within adherens junctions in a myosin ii-dependent manner," *The Journal of Cell Biology*, vol. 189, pp. 1107–15, Jun 2010.

[58] A. Katsumi, "Integrins in mechanotransduction," *Journal of Biological Chemistry*, vol. 279, pp. 12001–12004, Dec 2003.

[59] N. Q. Balaban, U. S. Schwarz, D. Riveline, P. Goichberg, G. Tzur, I. Sabanay, D. Mahalu, S. Safran, A. Bershadsky, L. Addadi, and B. Geiger, "Force and focal adhesion assembly: a close relationship studied using elastic micropatterned substrates," *Nat Cell Biol*, vol. 3, pp. 466–72, May 2001.

[60] P. W. Oakes, Y. Beckham, J. Stricker, and M. L. Gardel, "Tension is required but not sufficient for focal adhesion maturation without a stress fiber template," *The Journal of Cell Biology*, vol. 196, pp. 363–374, Feb 2012.

[61] W. Goldmann and D. Ingber, "Intact vinculin protein is required for control of cell shape, cell mechanics, and¡ i¿ rac¡/i¿-dependent lamellipodia formation," *Biochemical and biophysical research ...*, Jan 2002.

[62] T. Splettstoesser, K. C. Holmes, F. Noé, and J. C. Smith, "Structural modeling and molecular dynamics simulation of the actin filament," *Proteins*, vol. 79, pp. 2033–43, Jul 2011.

[63] S. Takeda, S. Minakata, R. Koike, I. Kawahata, A. Narita, M. Kitazawa, M. Ota, T. Yamakuni, Y. Maéda, and Y. Nitanai, "Two distinct mechanisms for actin capping protein regulation–steric and allosteric inhibition," *PLoS Biol*, vol. 8, p. e1000416, Jan 2010.

[64] W. Drabikowski and E. Nowak, "The interaction of alpha-actinin with f-actin and its abolition by tropomyosin," *Eur J Biochem*, vol. 5, pp. 209–14, Jul 1968.

[65] J. Vincent, "Structural biomaterials," *Princeton University Press*, pp. 1–28, Jan 2012.

[66] D. Roylance, "Engineering viscoelasticity," *Department of Materials Science and Engineering–Massachusetts Institute of Technology, Cambridge MA*, vol. 2139, pp. 1–37, 2001.

[67] N. Tschoegl, "Time dependence in material properties: an overview," *Mechanics of Time-Dependent Materials*, Jan 1997.

[68] P. Fernández, L. Heymann, A. Ott, N. Aksel, and P. Pullarkat, "Shear rheology of a cell monolayer," *New Journal of Physics*, vol. 9, no. 11, p. 419, 2007.

[69] Y. Fung, "Biomechanics: Mechanical properties of living tissues.," *Springer Verlag, New York.*, 1993.

[70] J. Anderson, K. Leaver, R. Rawlings, and P. Leevers, "Materials science for engineers," *Taylor & Francis*, Jan 2003.

[71] A. R. Bausch, W. Möller, and E. Sackmann, "Measurement of local viscoelasticity and forces in living cells by magnetic tweezers," *Biophysical Journal*, vol. 76, pp. 573–9, Jan 1999.

[72] M. Lorenz and K. C. Holmes, "The actin-myosin interface," *Proc Natl Acad Sci USA*, vol. 107, pp. 12529–34, Jul 2010.

[73] L. C. Gershman, P. Dreizen, and A. Stracher, "Subunit structure of myosin, ii. heavy and light alkali components," *Proc Natl Acad Sci USA*, vol. 56, pp. 966–73, Sep 1966.

[74] R. Niederman and T. D. Pollard, "Human platelet myosin. ii. in vitro assembly and structure of myosin filaments," *The Journal of Cell Biology*, vol. 67, pp. 72–92, Oct 1975.

[75] M. Kovacs, "Mechanism of blebbistatin inhibition of myosin ii," *Journal of Biological Chemistry*, vol. 279, pp. 35557–35563, May 2004.

[76] A. F. Straight, "Dissecting temporal and spatial control of cytokinesis with a myosin ii inhibitor," *Science*, vol. 299, pp. 1743–1747, Mar 2003.

[77] R. Poincloux, O. Collin, F. Lizarraga, M. Romao, M. Debray, M. Piel, and P. Chavrier, "Contractility of the cell rear drives invasion of breast tumor cells in 3d matrigel," *Proc Natl Acad Sci USA*, vol. 108, pp. 1943–1948, Feb 2011.

[78] P. P. A. Fernandez and A. Ott, "A master relation defines the nonlinear viscoelasticity of single fibroblasts," *Biophysical Journal*, vol. 90, pp. 3796–3805, Jan 2006.

[79] V. Swaminathan, K. Mythreye, E. T. O'brien, A. Berchuck, G. C. Blobe, and R. Superfine, "Mechanical stiffness grades metastatic potential in patient tumor cells and in cancer cell lines," *Cancer Research*, vol. 71, pp. 5075–5080, Aug 2011.

[80] P. Pravincumar, D. L. Bader, and M. M. Knight, "Viscoelastic cell mechanics and actin remodelling are dependent on the rate of applied pressure," *PLoS ONE*, vol. 7, p. e43938, Sep 2012.

[81] O. Lieleg, K. M. Schmoller, M. M. A. E. Claessens, and A. R. Bausch, "Cytoskeletal polymer networks: Viscoelastic properties are determined by the microscopic interaction potential of cross-links," *Biophysj*, vol. 96, pp. 4725–4732, Jun 2009.

[82] J. Joanny and J. Prost, "Active gels as a description of the actin myosin cytoskeleton," *HFSP J.*, vol. 3, pp. 94–104, Apr 2009.

[83] P. Friedl and D. Gilmour, "Collective cell migration in morphogenesis, regeneration and cancer," *Nat Rev Mol Cell Biol*, Jan 2009.

[84] V. Lecaudey, G. Cakan-Akdogan, W. H. J. Norton, and D. Gilmour, "Dynamic fgf signaling couples morphogenesis and migration in the zebrafish lateral line primordium," *Development*, vol. 135, pp. 2695–2705, Jul 2008.

[85] G. Valentin, P. Haas, and D. Gilmour, "The chemokine sdf1a coordinates tissue migration through the spatially restricted activation of cxcr7 and cxcr4b," *Curr Biol*, vol. 17, pp. 1026–31, Jun 2007.

[86] P. Haas and D. Gilmour, "Chemokine signaling mediates self-organizing tissue migration in the zebrafish lateral line," *Developmental Cell*, vol. 10, pp. 673–80, May 2006.

[87] X. Trepat and J. J. Fredberg, "Plithotaxis and emergent dynamics in collective cellular migration," *Trends in Cell Biology*, pp. 1–9, Jul 2011.

[88] J. Riedl, A. Crevenna, K. Kessenbrock, and J. Yu. . . , "Lifeact: a versatile marker to visualize f-actin," *Nature . . .*, Jan 2008.

[89] J. Solon, A. Kaya-Copur, J. Colombelli, and D. Brunner, "Pulsed forces timed by a ratchet-like mechanism drive directed tissue movement during dorsal closure," *Cell*, vol. 137, pp. 1331–1342, Jun 2009.

[90] M. Rauzi, P. Verant, T. Lecuit, and P.-F. Lenne, "Nature and anisotropy of cortical forces orienting drosophila tissue morphogenesis," *Nat Cell Biol*, vol. 10, pp. 1401–10, Dec 2008.

[91] L. He, X. Wang, H. L. Tang, and D. J. Montell, "Tissue elongation requires oscillating contractions of a basal actomyosin network," *Nat Cell Biol*, vol. 12, pp. 1133–1142, Dec 2010.

[92] W. Feneberg, M. Aepfelbacher, and E. Sackmann, "Microviscoelasticity of the apical cell surface of human umbilical vein endothelial cells (huvec) within confluent monolayers," *Biophysical Journal*, vol. 87, pp. 1338–1350, Aug 2004.

[93] A. Zidovska and E. Sackmann, "On the mechanical stabilization of filopodia," *Biophysj*, vol. 100, pp. 1428–1437, Mar 2011.

[94] M. Jonas, H. Huang, R. D. Kamm, and P. T. So, "Fast fluorescence laser tracking microrheometry, ii: Quantitative studies of cytoskeletal mechanotransduction," *Biophysical Journal*, vol. 95, pp. 895–909, Jul 2008.

[95] L. Selvaggi, M. Salemme, C. Vaccaro, G. Pesce, G. Rusciano, A. Sasso, C. Campanella, and R. Carotenuto, "Multiple-particle-tracking to investigate viscoelastic properties in living cells," *Methods*, vol. 51, pp. 20–26, May 2010.

[96] O. Chaudhuri, S. H. Parekh, and D. A. Fletcher, "Reversible stress softening of actin networks," *Nature*, vol. 445, pp. 295–298, Jan 2007.

[97] S. Lee, A. Zeiger, J. Maloney, M. Kotecki, K. V. Vliet, and I. Herman, "Pericyte actomyosin-mediated contraction at the cell–material interface can modulate the microvascular niche," *Journal of Physics: Condensed Matter*, vol. 22, no. 19, p. 194115, 2010.

[98] B. A. Filas, P. V. Bayly, and L. A. Taber, "Mechanical stress as a regulator of cytoskeletal contractility and nuclear shape in embryonic epithelia," *Ann Biomed Eng*, vol. 39, pp. 443–454, Jan 2011.

[99] C. M. Hale, S. X. Sun, and D. Wirtz, "Resolving the role of actoymyosin contractility in cell microrheology," *PLoS ONE*, vol. 4, p. e7054, Sep 2009.

[100] M. Balland, A. Richert, and F. Gallet, "The dissipative contribution of myosin ii in the cytoskeleton dynamics of myoblasts," *Eur Biophys J*, vol. 34, pp. 255–261, May 2005.

[101] M. Stachowiak and B. O'Shaughnessy, "Kinetics of stress fibers," *New Journal of Physics*, vol. 10, no. 2, p. 025002, 2008.

[102] D. Laporte, N. Ojkic, D. Vavylonis, and J.-Q. Wu, "-actinin and fimbrin cooperate with myosin ii to organize actomyosin bundles during contractile-ring assembly," *Molecular Biology of the Cell*, vol. 23, pp. 3094–3110, Aug 2012.

[103] A. Besser and U. S. Schwarz, "Hysteresis in the cell response to time-dependent substrate stiffness," *Biophysj*, vol. 99, pp. L10–L12, Jul 2010.

[104] J. D. Mih, A. S. Sharif, F. Liu, A. Marinkovic, M. M. Symer, and D. J. Tschumperlin, "A multiwell platform for studying stiffness-dependent cell biology," *PLoS ONE*, vol. 6, p. e19929, May 2011.

[105] E. Ker, B. Chu, J. Phillippi, B. Gharaibeh, and J. Huard. . . , "Engineering spatial control of multiple differentiation fates within a stem cell population," *Biomaterials*, Jan 2011.

[106] H. Lee and E. Kay, "Fgf-2 induced reorganization and disruption of actin cytoskeleton through pi 3-kinase, rho, and cdc42 in corneal endothelial cells," *Mol Vis*, vol. 9, no. 76-78, pp. 624–634, 2003.

[107] D. Kimelman, J. Abraham, T. Haaparanta, T. Palisi, and M. Kirschner, "The presence of fibroblast growth factor in the frog egg: its role as a natural mesoderm inducer.," *Science*, vol. 242, no. 4881, p. 1053, 1988.

[108] D. Leckband, Q. le Duc, N. Wang, and J. de Rooij, "Mechanotransduction at cadherin-mediated adhesions," *Current Opinion in Cell Biology*, vol. 23, no. 5, pp. 523–530, 2011.

[109] Y. Miyake, N. Inoue, K. Nishimura, N. Kinoshita, H. Hosoya, and S. Yonemura, "Actomyosin tension is required for correct recruitment of adherens junction components and zonula occludens formation," *Experimental Cell Research*, vol. 312, no. 9, pp. 1637–1650, 2006.

[110] S. Yonemura, Y. Wada, T. Watanabe, A. Nagafuchi, and M. Shibata, "alpha-catenin as a tension transducer that induces adherens junction development," *Nat Cell Biol*, vol. 12, no. 6, pp. 533–542, 2010.

[111] V. Lecaudey, G. Cakan-Akdogan, W. H. J. Norton, and D. Gilmour, "Dynamic fgf signaling couples morphogenesis and migration in the zebrafish lateral line primordium," *Development*, vol. 135, pp. 2695–2705, Jul 2008.

[112] L. Gamba, N. Cubedo, A. Ghysen, G. Lutfalla, and C. Dambly-Chaudiere, "Estrogen receptor esr1 controls cell migration by repressing chemokine receptor cxcr4 in the zebrafish posterior lateral line system," *Proc Natl Acad Sci USA*, vol. 107, pp. 6358–6363, Apr 2010.

[113] L. E. Valdivia, R. M. Young, T. A. Hawkins, H. L. Stickney, F. Cavodeassi, Q. Schwarz, L. M. Pullin, R. Villegas, E. Moro, F. Argenton, M. L. Allende, and S. W. Wilson, "Lef1-dependent wnt/ -catenin signalling drives the proliferative engine that maintains tissue homeostasis during lateral line development," *Development*, vol. 138, pp. 3931–3941, Sep 2011.

[114] M. Westerfield, "The zebrafish book: A guide for the laboratory use of zebrafish ...," *Eugene, OR: University of Oregon Press.*, 1994.

[115] S. Anandakumar, V. S. Rani, S. Oh, B. Sinha, M. Takahashi, and C. Kim, "Translocation of bio-functionalized magnetic beads using smart magnetophoresis," *Biosensors and Bioelectronics*, vol. 26, pp. 1755–1758, Dec 2010.

[116] W. J. Conover, *Practical Nonparametric Statistics*.
John Wiley and Sons, 1980.